Quantum Phase Transitions in d-wave Superconductors and Antiferromagnetic Kagome Lattices

A dissertation presented
by

Yejin Huh

to
The Department of Physics
in partial fulfillment of the requirements
for the degree of
Doctor of Philosophy
in the subject of

Physics

Harvard University
Cambridge, Massachusetts
August 2011

Thesis advisor
Subir Sachdev

Author
Yejin Huh

Quantum Phase Transitions in d-wave Superconductors and Antiferromagnetic Kagome Lattices

Abstract

Strongly correlated systems are of interest due to their exotic collective behavior. In this thesis we study low energy effective theory and quantum phase transitions of d-wave superconductors and spin liquids.

First we examine the quantum theory of the spontaneous breaking of lattice rotation symmetry in d-wave superconductors on the square lattice. This is described by a field theory of an Ising nematic order parameter coupled to the gapless fermionic quasiparticles. We determine the structure of the renormalization group to all orders in a $1/N_f$ expansion, where N_f is the number of fermion spin components. Asymptotically exact results are obtained for the quantum critical theory in which, as in the large N_f theory, the nematic order has a large anomalous dimension, and the fermion spectral functions are highly anisotropic.

Next we study quantum phase transitions in antiferromagnetic kagome lattices. Due to the high geometric frustration, this system poses as a good candidate for a spin liquid with exotic excitations. Here we look at physics of the spinon and vison sector.

In the spinon sector, we investigate the zero-temperature phase diagram of the nearest-neighbor kagome antiferromagnet in the presence of Dzyaloshinksii-Moriya interaction. We develop a theory for the transition between Z_2 spin liquids with bosonic spinons and a phase with antiferromagnetic long-range order. Connections to recent numerical studies and experiments are discussed.

Finally in the vison sector, we present a projective symmetry group (PSG) analysis of the spinless excitations of $\mathbb{Z}_2$ spin liquids on the kagome lattice. In the simplest case, vortices carrying $\mathbb{Z}_2$ magnetic flux ('visons') are shown to transform under the

48 element group $\mathrm{GL}(2,\mathbb{Z}_3)$. Alternative exchange couplings can also lead to a second case with visons transforming under 288 element group $\mathrm{GL}(2,\mathbb{Z}_3)\times \mathrm{D}_3$. We study the quantum phase transition in which visons condense into confining states with valence bond solid order. The critical field theories and confining states are classified using the vison PSGs.

Contents

Citations to Previously Published Work

Chapter 2 has been previously published as

> "Renormalization group theory of nematic ordering in d -wave superconductors", Yejin Huh and Subir Sachdev, Phys. Rev. B, **78**, 064512 (2008), `arXiv:0806.0002`.

Chapter 3 has been previously published as

> "Quantum criticality of the kagome antiferromagnet with Dzyaloshinskii-Moriya interactions", Yejin Huh and Lars Fritz and Subir Sachdev, Phys. Rev. B, **81**, 144432 (2010), `arXiv:1003.0891`.

Chapter 4 has been previously published as

> "Vison states and confinement transitions of Z2 spin liquids on the kagome lattice", Yejin Huh and Matthias Punk and Subir Sachdev, `arXiv:1106.3330`.

Electronic preprints (shown in `typewriter font`) are available on the Internet at the following URL:

> `http://arXiv.org`

Acknowledgments

It is a pleasure to thank the many people who have made this thesis possible.

I would like to start by expressing my sincere gratitude to my advisor, Professor Subir Sachdev. Since first meeting him as a sophomore at Yale, I've learned everything from quantum mechanics, statistical mechanics, to quantum phase transitions from him. More importantly, I've been inspired by his depth of understanding and flow of ideas. His guidance has helped me in the research and it has been an honor working with him.

I would also like to thank Professor Jenny Hoffman and Professor Eugene Demler for serving on my committee along with my advisor. I deeply appreciate all the advice, insightful comments, and kind words they have given me.

It has been a great experience learning from talented postdocs at Harvard. I am especially grateful to Lars Fritz and Matthias Punk. I have collaborated with Lars on a project which became Chapter 3, and with Matthias on what became Chapter 4. I have enjoyed working with them and learned a lot from each of them. The exchanges have always been inspiring and stimulating. I would also like to thank Markus Mueller, Cenke Xu, Erez Berg, and Philipp Strack for the discussions and advice.

I have appreciated the camaraderie of my fellow students in Subir's group, Adrian Del Maestro, Yang Qi, Rudro Biswas, Max Metlitski, Eun Gook Moon and Susanne Pielawa, all of whom I have become great friends with. I have benefited a great amount from discussions with them. I'd like to thank Adrian for advice when I first started out. I would like to especially thank Max for educating me on a lot of field theory, and Eun Gook for being a wonderful officemate as well as for the great many discussions and advice.

Sheila Ferguson, William Walker and Heidi Kaye have helped me navigate through the system. I am grateful for their assistance, which has let me focus on my studies and research.

I would also like to take this opportunity to thank some wonderful friends I have made here at Harvard. Jung Ook Hong, Eunmi Chae, Junhyun Lee, Seung-Yeon Kang, and Jaehoon Lee have all been immense support through my time at Harvard.

Finally I would like to thank my parents Ick-Ryol Huh and Myoung Soon Kim for always loving me, supporting me and being my role models. I would like to thank my sister and best friend, Yesol Huh, for always being someone I can count on.

Dedicated to my father Ick Ryol Huh,
my mother Myoung Soon Kim,
and my sister Yesol Huh.

Chapter 1

Introduction

Classifying quantum phases and studying the quantum phase transitions between them are powerful tools for studying the collective behavior of strongly correlated materials. Continuous quantum phase transitions are usually associated with a vanishing order parameter and diverging physical quantities at the critical point. The low energy effective theory and exponents for the power law divergence are characteristics of the transition. While quantum phase transitions occur strictly at 0K, which is experimentally not attainable, they do influence the $T > 0$ region as well. In fact, there is a fan-like region in the phase diagram called the quantum critical region characterized by its large critical fluctuations. Its universal properties are controlled by the quantum critical point which lies at 0K. (Sachdev, 1999)

Various methods are used to study these quantum phases. In this thesis we will encounter renormalization group method, mean field theory, projective symmetry group analysis, and Ginzburg-Landau-Wilson type functionals. Systems that are studied are *d*-wave superconductors and antiferromagnetic kagome lattices.

1.1 *d*-wave Superconductivity and Nematic Ordering

Since its discovery in 1986, many different families of cuprates have been discovered. Some examples are LSCO ($La_{2-x}Sr_xCuO_2$), BSCCO ($Bi_2Sr_2Ca_nCu_{n+1}O_{2n+6}$), and YBCO ($YBa_2Cu_3O_{6+x}$). Structurally all these materials have Copper oxide layers in common, and it is believed that these CuO_2 planes are responsible for the physics of superconductivity. Electronic states near the Fermi level of high T_c cuprates derive from the hybridized d and p orbitals of copper and oxygen. Layers of Copper oxide are only very weakly coupled due to the large c/a ratio of the cuprate unit cell. This in turn means that the size of the Brillouin zone in the k_z direction is very small and that a cuprate is a quasi-2 dimensional system with the symmetry properties of a square lattice. In undoped parent materials of the cuprate, $\frac{1}{2}$ spins are located at the sites of copper, forming a square lattice of spin $\frac{1}{2}$s. The ground state of this material is an antiferromagnetic Mott Insulator. Similarities between the antiferromagnetic low-temperature state of the undoped materials and the superconducting state that emerges upon doping, primarily the $d_{x_2-y_2}$ orbital state of the Cu^{2+} ions, suggest that electron-electron interactions are more significant than electron-phonon interactions in cuprates, making the superconductivity unconventional. The Fermi surface of these materials is shown in Fig 1.1. d-wave superconductors have an order parameter, or the superconducting gap, proportional to $\cos k_x - \cos k_y$ which vanish along $k_x = \pm k_y$. On the Fermi surface, there are four special points where the gap vanishes. At these four nodal points of the Fermi surface, we can have excitations with arbitrarily low energies.

Neutron scattering experiments on under-doped $YBa_2Cu_3O_{6.45}$ (T_c=35K) Hinkov et al. (2004, 2007, 2008) suggest nematic ordering. Upon measuring the spin-spin correlation function, they have observed spontaneous onset of one dimensional order below 150K. The anisotropy increased at lower temperatures and with decreasing excitation energy. Spin excitation spectra are shown in Fig. 1.2. It can be seen that the anisotropy comes from incommensurate peaks symmetrically displacing from Neel

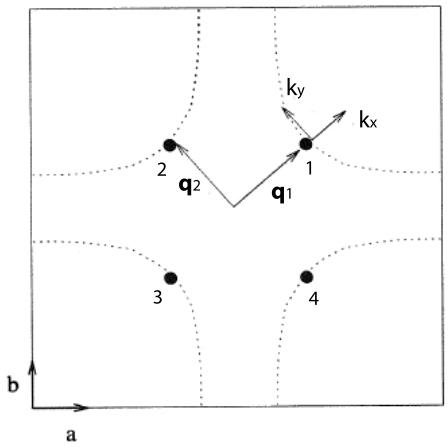

Figure 1.1: Fermi surface and nodal points of a d-wave superconductor. A typical large fermi surface is illustrated. The superconducting gap, $\Delta(k) = \Delta_0(\cos k_x - \cos k_y)$, vanishes at four nodal points on the fermi surface. Excitations with arbitrarily low energies are allowed and thus these nodal points play an important role in the low energy physics.

order wave vector $Q_{\rm AF} = (\pi, \pi)$.

This was not recognized in previous experiments due to crystal twinning. In cuprates, subtle crystallographic distortions can serve as aligning fields for symmetry-broken electronic phases, which will otherwise be averaged out. YBCO has natural slight anisotropy which serves as the aligning field. The parent material of YBCO is $YBa_2Cu_3O_6$ which is a Mott insulator which can be hole-doped by adding oxygen atoms interstitially. This creates CuO chains only in the b direction which is unique to this type of cuprate. Thus the a and b axes are no longer equivalent. This leads to slightly, about 1%, different lattice constants. Usually YBCO is twinned when doped, which means that there are patches with a in x axis and b in the y axis and patches rotated by 90 degrees. In Hinkov et al. (2004, 2007, 2008) experiments, they detwinned the material to observe the anisotropy. (by applying mechanical uniaxial mechanical stress while flowing oxygen.)

Vojta *et al.* (Vojta et al., 2000c,b, 2008) have studied possible ordering that could occur from a d-wave superconductor. Seven inequivalent order parameters were

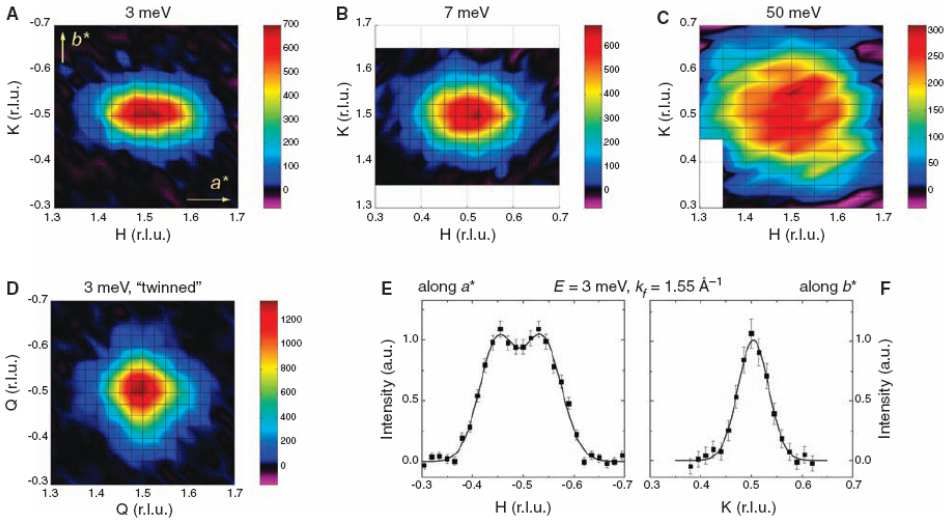

Figure 1.2: (Hinkov et al., 2008) Spin excitation spectra at T = 5K at 3, 7, and 50meV (energy transfer) are plotted and wave vectors are in reciprocal lattice units. Here we can see that spin excitations occur near Neel order wave vector $Q_{\mathrm{AF}} = (\pi, \pi)$. At high excitation energies the spectrum is isotropic while at lower excitation energies, anisotropy increases with decreasing energy. D shows the spectrum that would been measured in the presence of crystal twinning. Previously the anisotropy had not been measured due to crystal twinning. E shows intensity plots along two different axes a and b. Along a, there are two incommensurate peaks symmetrically displaced from Q_{AF}, while along b, the distribution is commensurate.

found, involving charge density waves and various subsidiary ordering, shifting the four nodal points. In some cases the C_4 symmtry was broken. In this thesis, we will focus on the appearance of nematic ordering, in which the four-fold rotation breaks into a two-fold rotation symmetry. This is the appearance of s-wave pairing. Initial renormalization group analysis by Vojta et al. (2000c,b, 2008) of nematic ordering at $T = 0$ found runaway flow to strong coupling in a computation based on an expansion in $(3 - d)$, where d is the spatial dimensionality. More recently, Kim et al. (2008) argued that a second-order quantum phase transition existed in the limit of large N_f, where N_f is the number of spin components. The physical case corresponding to $N_f = 2$. In Chapter 2 we will present a different RG analysis using the framework of the $\frac{1}{N_f}$ expansion. We will find a fixed point that does indeed exist at the order $\frac{1}{N_f}$, describing a second order transition.

1.2 Phase Transitions in Kagome Lattice Z_2 Spin Liquids

Frustrated magnets are consisted of localized magnetic moments, or spins, interacting with competing exchange interactions that cannot be simultaneously satisfied. A well-known simple example of a geometrically frustrated magnet is a triangle of antiferromagnetic Ising spins, which exhibits frustration even at the level of three sites. It can be easily verified that there is no way of satisfying all three bonds, and that there are six ground states, each with two satisfied bonds and one frustrated bond.

Macroscopic number of ground states in a lattice leads to strong fluctuations in these systems. Both classical and quantum fluctuations may be present. Unlike classical fluctuations which at lower temperatures become more sluggish, eventually freezing out of equilibrium, quantum fluctuations persist down to 0K. In this thesis we will focus on systems with spin $S = \frac{1}{2}$ that have strong quantum fluctuations which connect different ground states.

Interest in frustrated magnets are largely connected to spin liquids. Quantum

spin liquids have such strong quantum fluctuations that it has no magnetic order down to 0K. It has a non-magnetic ground state although it is built from local moments. Valance bonds, having the same property, is a good example of building blocks that may describe the system. Resonating valance bonds (RVB) were first proposed by Anderson (1973) as ground state wave functions for spin liquids. RVB state is a superposition of electron pairs that form singlet bonds. This is a liquid-like state that does not break spin rotation symmetry or any lattice symmetry. If the RVB state is frozen into a specific configuration that breaks lattice symmetry, it is a valance bond solid (VBS).

Candidates for spin liquids include geometrically frustrated lattices such as triangular, kagome, and pyrocloro lattices. Some examples of specific systems are organic compounds $EtMe_3Sb[Pd(dmit)_2]_2$ (triangular) and κ-(BEDT-TTF)$_2Cu_2(CN)_3$ (triangular), non-organic compounds herbertsmithite (kagome) and $Na_4Ir_3O_8$ (hyper-kagome).

Unlike organic materials which have a small charge gap, kagome antiferromagnets have a large charge gap. Charges are well localized and therefore the Heisenberg Hamiltonian is a good description of the system. Herbertsmithite is known to evade ordering down to temperatures of 35 mK. The material does not show signs of structural distortions or anisotropy. (Helton et al., 2007; Ofer et al., 2006; Mendels et al., 2007; Imai et al., 2008) Substitutional disorder and Dzyaloshinski-Moriya interactions are present. (Olariu et al., 2008; Gregor and Motrunich, 2008; Rozenberg and Chitra, 2008; Lee et al., 2007; Rigol and Singh, 2007; Zorko et al., 2008; Ofer and Keren, 2009) Effect of Dzyaloshinski-Moriya interactions on quantum phases of kagome antiferromagents are the focus of Chapter 3.

On the theoretical side, the most recent evidence (Nikolic and Senthil, 2003; Singh and Huse, 2007; Jiang et al., 2008; Evenbly and Vidal, 2010; Poilblanc et al., 2010; Schwandt et al., 2010) on the nearest-neighbor antiferromagnet points consistently to a ground state with a spin gap of $0.05J$ and VBS order. The pattern of the VBS order is quite complex with a large unit cell, but was anticipated by Marston and Zeng (Marston and Zeng, 1991) by an application of the VBS selection mechanism

described in the $1/N$ expansion of the SU(N) antiferromagnet. (Read and Sachdev, 1989a)

Below I will briefly present some theoretical tools that are useful in studying Z_2 spin liquids. I will start with the reviewing the Schwinger boson method, discussing the emergent Z_2 gauge field, and will outline a mapping between a frustrated magnet and a fully frustrated Ising model on the dual lattice. These will be used in Chapters 3 and 4.

1.2.1 Schwinger Boson

The Hamiltonians we are interested are the standard antiferromagnetic Heisenberg Hamiltonian,

$$\mathcal{H} = \sum_{ij} J_{ij} \mathbf{S}_i \cdot \mathbf{S}_j \tag{1.1}$$

where J_{ij} are nearest neighbor antiferromagnetic exchange interaction between spin S quantum spins $\mathbf{S}_i$ and $\mathbf{S}_j$, each located at sites i and j. We describe SU(2) states using spin $\frac{1}{2}$ Schwinger bosons created by operators $b^\dagger_{i\alpha}$, with $\alpha = \uparrow / \downarrow$. (Arovas and Auerbach, 1988; Auerbach and Arovas, 1988)

$$|S, m\rangle \equiv \frac{1}{\sqrt{(S+m)!(S-m)!}} (b^\dagger_{i\uparrow})^{S+m} (b^\dagger_{i\downarrow})^{S-m} |0\rangle \tag{1.2}$$

It follows that

$$\begin{aligned} b^\dagger_{i\alpha} b^\alpha_i &= n_b = 2S \\ S_{ia} &= \frac{1}{2} b^\dagger_{i\alpha} \sigma^{a\alpha}_\beta b^\beta_i. \end{aligned} \tag{1.3}$$

Here we define a singlet operator between sites i and j as

$$Q_{ij} = \sum_{\sigma\sigma'} \epsilon_{\sigma\sigma'} b_{i\sigma} b_{j\sigma'} \tag{1.4}$$

with ϵ a fully anti-symmetric tensor.

$$\epsilon = \begin{pmatrix} 0 & 1 \\ -1 & 0 \end{pmatrix} \tag{1.5}$$

We can describe the Hamiltonian as

$$\mathcal{H} = -\frac{J}{2}\sum_{<ij>}(Q_{ij}^{\dagger}Q_{ij} - 2S^2) \tag{1.6}$$

where $J = J_{ij} > 0$ for nearest neighbors i and j.
In the next step we generalize the fields to N flavors. SU($2N$) turns out to be too large and there is no generalization for the antisymmetric tensor ϵ for $N > 1$. Sp(N) is the correct generalization which preserves the singlet formation. (Read and Sachdev, 1991) This leads to

$$\begin{aligned} Q_{ij} &= \frac{1}{N}\sum_{m,\sigma,\sigma'}\epsilon_{\sigma\sigma'}b_{i\sigma}^{m}b_{j\sigma'}^{m} \\ \mathcal{H} &= -\frac{J}{2N}\sum_{<ij>}(\mathbb{J}^{\alpha\beta}b_{i\alpha}^{\dagger}b_{j\beta}^{\dagger})(\mathbb{J}_{\gamma\delta}b_{i\gamma}b_{j\delta}) \end{aligned} \tag{1.7}$$

up to an additive constant, where $\mathbb{J}$ is the Sp(N) generalization of ϵ.
In Chapter 3 we are interested in the the limit of $N \to \infty$ while keeping the ratio

$$\kappa = \frac{n_b}{N} \tag{1.8}$$

fixed. We will study phase transitions occuring while tuning κ.

1.2.2 Z_2 Spin Liquid

In the following I will motivate the Z_2 spin liquid starting from the Schwinger boson Hamiltonian discussed in section 1.2.1 using projective symmetry group (PSG) analysis following Wang and Vishwanath (2006). The mean field Hamiltonian is

$$\mathcal{H}_{MF} = -\frac{J}{2}\sum_{<ij>}(q_{ij}^{\dagger}Q_{ij} + Q_{ij}^{\dagger}q_{ij} - q_{ij}^{*}q_{ij}). \tag{1.9}$$

In the Schwinger boson description of spins there is a local $U(1)$ transformation,

$$b_{r\sigma} \to e^{i\phi(r)}b_{r\sigma}, \tag{1.10}$$

which leaves all the observables invariant as can be seen in Eq. 1.3. The mean-field ansatz transforms as,

$$q_{ij} \to e^{-i\phi(i)-i\phi(j)}q_{ij}. \tag{1.11}$$

As defined by Wen (2002), invariant gauge group (IGG) is the subgroup of PSG which keeps the ansatz invariant. This is an artificial gauge symmetry that rises from defining fractionalized particles. These do not have a corresponding physical symmetry and describe the low energy gauge group. Assuming a non-zero q_{ij}, for bipartite lattices a transformation of $b_{r\sigma} \rightarrow e^{\pm i\phi} b_{r\sigma}$ with opposite signs on different sublattices, keeps the ansatz invariant and therefore the IGG is U(1). However, for non-bipartite frustrated lattices, such as the antiferromagnetic kagome lattice, the only transformations that satisfy this condition are the identity operation and $b_{r\sigma} \rightarrow -b_{r\sigma}$. The IGG is Z_2. Therefore the low energy effective theory (fluctuations about the mean field state) of an antiferromagnetic kagome lattice will be described by an emergent Z_2 gauge field.

Another approach we can take is to realize that the frustration introduces a charge -2 Higgs scalar, coming from the non-collinear wave vector which minimizes the energy (coplanar critical mode), which reduces the U(1) gauge symmetry down to Z_2. (Sachdev, 2010) In the case with large spin gap, we may integrate out the spin degrees of freedom and we will be left with a pure Z_2 gauge degree of freedom.

1.2.3 Quantum Dimer Model

Low energy singlet excitations of a quantum paramagnet can be captured using a quantum dimer model. RVB states that involve only nearest neighbor pairing are described using a quantum dimer model. A quantum dimer model on a square lattice can be written by

$$\mathcal{H}_{\mathrm{QDM}} = -t\hat{T} + v\hat{V} = \sum_{\square} \left(-t(|=\rangle\langle\| \; | + | \; \|\rangle\langle= |) + v(|=\rangle\langle= | + | \; \|\rangle\langle\| \; |)\right). \quad (1.12)$$

$\hat{V}$ is the potential term while $\hat{T}$ describes the motion. The kinetic term flips the dimers from one configuration to another. Only flippable even loops, square plaquettes in the square lattice and hexagons, diamonds, and stars etc. for kagome lattices are allowed. (for a full classification of of flippable loops on kagome lattices, see Nikolic and Senthil (2003))

This quantum dimer model can be derived as a perturbation expansion of the SU(2) Heisenberg magnet where orthonormalized dimer coverings form a basis and overlaps between dimer coverings give rise to the kinetic term. (Rokhsar and Kivelson, 1988) Another method is to start from the Schwinger boson method discussed in Section 1.2.1. Instead of keeping κ fixed, we can fix n_b and take the $N \to \infty$ limit. This gives rise to the quantum dimer model with hard core constraint. Dimer resonance term comes in order $\frac{1}{N}$. (Affleck and Marston, 1988)

1.2.4 Ising Gauge Theory

Since the low energy theory is an Ising gauge theory, we can write the effective Hamiltonian as

$$\mathcal{H}_{\mathrm{GDM}} = \Gamma \sum_{-} \sigma^x - \kappa \sum_{\square} \prod_{\square} \sigma^z \tag{1.13}$$

where Ising gauge fields σ live on the links of the lattice, $\sum_{-}$ is a sum over all links and $\sum_{\square}$ sums over closed loops. All loops are allowed due to gauge symmetry, although the shorter loops are more important. In the case of the kagome lattice,

$$\mathcal{H} = \Gamma \sum_{-} \sigma^x - \kappa_3 \sum_{\triangle} \prod_{\triangle} \sigma^z - \kappa_6 \sum_{\hexagon} \prod_{\hexagon} \sigma^z \tag{1.14}$$

This Hamiltonian has a gauge invariance under flipping all spins in the σ^z basis emanating from a site. The transformation that generates this is

$$G_{\mathrm{IGT}} = \prod_{+} \sigma^x \tag{1.15}$$

Ising gauge theory Eq. 1.13 exhibits a confined phase at $\Gamma \gg \kappa$, in which the low energy excitations are elementary loops of $\sigma^x = 1$ that cost energy 2Γ per length of the loop. On the other hand, when $\Gamma \ll \kappa$, the loops proliferate with no tension and drives deconfinement.

We can map the above Ising gauge theory to a quantum dimer model under a certain limit following Moessner et al. (2001). We start by interpreting link variables (gauge fields) $\sigma^x = \pm 1$ as the presence/absense of dimer on the link. σ^z flips between $\sigma^x = \pm 1$ states. Then we can see that the σ^x term is the potential term while σ^z acts

as the kinetic term of the dimers. Only flippable loops are allowed in summation for the dimer model. In a kagome lattice these are even loops containing one hexagon, such as hexagons, diamonds, which may have different κ values. We can break up these loops into elementary plaquettes which are hexagons and triangles. It can be easily seen that flipping each flippable plaquette can be written as flipping a hexagon and even number of bond-sharing triangles. Here we will treat hexagons and triangles as independent plaquettes that we may flip and project out the states that are not allowed.

Assuming that even number of links emanate from a site, we need $G_{\rm IGT} = 1$ for cases where we have an even number of dimers on each site, while we should impose $G_{\rm IGT} = -1$ for odd number of dimers. Since we are interested in the case where there is one dimer emanating from all the sites, we will focus on $G_{\rm IGT} = -1$. To complete the mapping to the QDM, we need to project out the cases where there are more than one dimer (such as 3 or 5) from any site. We can reach this by taking the limit $\Gamma \to \infty$. Therefore we can see that the Ising gauge theory maps exactly on to the QDM deep in the confined phase. This mapping will be used in Chapter 4 to describe different confined phases that appear.

1.2.5 Duality of Ising Gauge Theory and Ising Model in d=2+1

Here I will review the duality mapping of 2+1d IGT to Ising model. (For an in depth review, see Kogut (1979).) Define at the center of plaquettes (p),

$$\mu_p^x \equiv \prod_p \sigma^z, \quad \mu_p^z \equiv -\prod_{\sim p} \epsilon\sigma^x, \quad \mu_p^y \equiv i\mu^x\mu^z, \quad \prod_\diamond \epsilon = -1, \tag{1.16}$$

where $\prod_p$ is the product of the σ's around the plaquette p and $\prod_{\sim p}$ is the product of σ's intersecting any path from infinity to p. ϵ is the external gauge defined on the dual lattice. Notice that without ϵ defined as above the definition of μ^z is path-dependent where the phase acquired in a loop $\mathcal{C}$ is $\pi\times$(direct sites enclosed in loop $\mathcal{C}$). This condition comes from the requirement $G_{\rm IGT} = -1$ and in the case of $G_{\rm IGT} = 1$ we do not need ϵ.

It can be easily checked that the μ's satisfy the usual commutation relation of Pauli matrices. Using this definition we can express the Hamiltonian in Eq. 1.14 as

$$\begin{aligned} \mathcal{H}_{dual} &= -\Gamma \sum_{p,p'} \epsilon_{pp'} \mu^z_p \mu^z_{p'} - \kappa_3 \sum_3 \mu^x_p - \kappa_6 \sum_6 \mu^x_p \\ &= -\sum_{<ij>} J_{ij} \mu^z_p \mu^z_{p'} - \kappa_3 \sum_3 \mu^x_p - \kappa_6 \sum_6 \mu^x_p \end{aligned} \tag{1.17}$$

where the product of the bonds around each elementary plaquette is negative.

$$\prod_{\diamond} \mathrm{sgn}(J_{ij}) = -1. \tag{1.18}$$

This is a fully frustrated Ising model in the dual dice lattice. μ defined on the dual lattice are vortices in the Z_2 gauge field called visons. μ^z_p has the physical interpretation of creating/annhilating a vison at dual site p, while the transverse field term serves as the kinetic term which interchanges frustrated bonds ($-J\mu\mu > 0$) and satisfied bonds ($-J\mu\mu < 0$) emanating from the site.

Visons have minimal long range coupling with spinons and chagons such that the spinon (or chargon) gains a phase π when it goes around a vison. We will see the case of the phase gain of spinon around a vison explicitly in Chapter 4. Thus when the visons are gapped, spinons and chargons are deconfined and may propagate freely. This is the fractionalized state. However when the visons condense, they drive confinement, such that spinons and chargons are no longer well defined quasi-particles.

1.3 Organization of the thesis

In Chapter 2 we examine the quantum theory of the spontaneous breaking of lattice rotation symmetry in d-wave superconductors on the square lattice. This is described by a field theory of an Ising nematic order parameter coupled to the gapless fermionic quasiparticles. We determine the structure of the renormalization group to all orders in a $1/N_f$ expansion, where N_f is the number of fermion spin components. Asymptotically exact results are obtained for the quantum critical theory in which, as in the large N_f theory, the nematic order has a large anomalous dimension, and the fermion spectral functions are highly anisotropic.

In Chapter 3 we investigate the zero-temperature phase diagram of the nearest-neighbor kagome antiferromagnet in the presence of Dzyaloshinksii-Moriya interaction. We develop a theory for the transition between Z_2 spin liquids with bosonic spinons and a phase with antiferromagnetic long-range order. Connections to recent numerical studies and experiments are discussed.

In Chapter 4 we present a projective symmetry group (PSG) analysis of the spinless excitations of $\mathbb{Z}_2$ spin liquids on the kagome lattice. In the simplest case, vortices carrying $\mathbb{Z}_2$ magnetic flux (visons) are shown to transform under the 48 element group $\mathrm{GL}(2,\mathbb{Z}_3)$. Alternative exchange couplings can also lead to a second case with visons transforming under 288 element group $\mathrm{GL}(2,\mathbb{Z}_3)\times \mathrm{D}_3$. We study the quantum phase transition in which visons condense into confining states with valence bond solid order. The critical field theories and confining states are classified using the vison PSGs.

Chapter 2

Renormalization group theory of nematic ordering in d-wave superconductors

2.1 Introduction

There has been a great deal of research on the onset of a variety of competing orders in the hole-doped cuprate superconductors. In Ref. Vojta et al. (2000c,b, 2008), a classification of spin-singlet order parameters at zero momentum was presented: such orders are able to couple efficiently to the gapless nodal quasiparticle excitations of a d-wave superconductor. Our focus in the present paper will be on one such order parameter: 'nematic' ordering in which the square lattice (tetragonal) symmetry of the d-wave superconductor is spontaneously reduced to rectangular (orthorhombic) symmetry (Kivelson et al., 1998). This transition is characterized by an Ising order parameter, but the quantum phase transition is not in the usual Ising universality class (Vojta et al., 2000c,b, 2008) because the coupling to the gapless fermionic quasiparticles changes the nature of the quantum critical fluctuations. Our work is motivated by recent neutron scattering observations (Hinkov et al., 2004, 2007, 2008) of a strongly temperature (T) dependent susceptibility to nematic ordering in

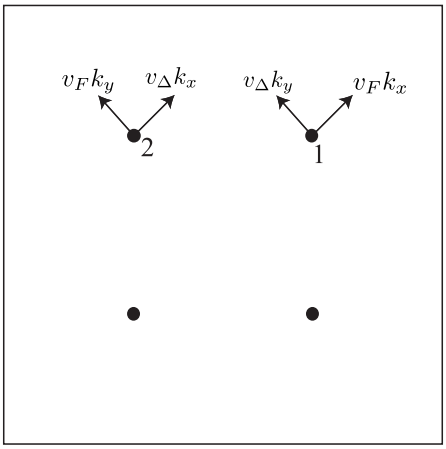

Figure 2.1: Nodal points of the d-wave superconductor in the square lattice Brillouin zone. The 2-component $\Psi_{1,2}$ fermions are in the vicinity of the labelled nodal points and their partners at diagonally opposite points.

detwinned crystals of $YBa_2Cu_3O_{6.45}$.

An initial renormalization group (RG) analysis (Vojta et al., 2000c,b, 2008) of nematic ordering at $T = 0$ found runaway flow to strong-coupling in a computation based on an expansion in $(3-d)$ where d is the spatial dimensionality. More recently, Ref. Kim et al. (2008) argued that a second-order quantum phase transition existed in the limit of large N_f, where N_f is the number of spin components (the physical case corresponding to $N_f = 2$). We refer the reader to Ref. Kim et al. (2008) for further discussion on the physical importance and experimental relevance of nematic ordering in d-wave superconductors.

Here we will present a RG analysis using the framework of the $1/N_f$ expansion. We will find that a fixed point does indeed exist at order $1/N_f$, describing a second-order quantum transition associated with the onset of long-range nematic order. However, the scaling properties near the fixed point have a number of unusual properties, controlled by the marginal flow of a "dangerously" irrelevant parameter. This parameter is v_Δ/v_F, where v_Δ and v_F are the velocities of the nodal fermions parallel and perpendicular to the Fermi surface (see Fig. 2.1). We will show that the fixed point has $(v_\Delta/v_F)^* = 0$ and so the transition is described by an "infinite anisotropy" away

from the "relativistic" fixed points found for other competing orders (Vojta et al., 2000c,b, 2008). It is important to note, however, that even though the fixed point has $(v_\Delta/v_F)^* = 0$, it is not described by an effectively one-dimensional theory of a straight Fermi surface; a fully two-dimensional theory is needed as is discussed in more detail in Section 2.4. The approach to this fixed point is logarithmically slow, and physical properties have to be computed at finite v_Δ/v_F. Our main results for the RG flow of the velocities are in Eqs. (2.25) and (2.26), where $C_{1,2,3}$ are functions only of v_Δ/v_F which are specified in Eq. (2.35); for $v_\Delta/v_F \ll 1$, the equations reduce to the explicit forms in Eqs. (2.39-2.41). These (and related) equations can be integrated in a standard manner to yield the dependence of observables on temperature and deviation from the nematic critical point, and the results are in Figs. 2.6, 2.7, and 2.8.

The existence of a fixed point at $(v_\Delta/v_F)^* = 0$ suggests that we analyze the theory directly in the limit of small v_Δ/v_F, without an appeal to an expansion in powers of $1/N_f$. The nature of the small v_Δ/v_F limit is quite subtle, and has to be taken with care: it will be described in Section 2.4. We argue there that the fluctuations of the nematic order are controlled by a small parameter which is $\sim v_\Delta/(N_f v_F)$, and not $1/N_f$ alone. Consequently, we believe our computations are controlled in the limit of small v_Δ/v_F even for $N_f = 2$. Indeed, the results in Eqs. (2.39-2.41), and many other related results, are expected to be exact as we approach the quantum critical point.

The outline of the remainder of this paper is as follows. The field theory for the nematic ordering transition will be reviewed in Section 2.2, along with a discussion of the $1/N_f$ expansion. The RG analysis to order $1/N_f$ will be presented in Section 2.3. Finally, higher order corrections in $1/N_f$, and the nature of the small v_Δ/v_F limit will be discussed in Section 2.4

2.2 Field theory

We begin by review the field theory for the nematic ordering transition introduced in Ref. Vojta et al. (2000c,b, 2008).

The action for the field theory, S, has three components

$$S = S_\Psi + S_\phi^0 + S_{\Psi\phi}. \tag{2.1}$$

The first term in the action, S_Ψ, is simply that for the low energy fermionic excitations in the $d_{x^2-y^2}$ superconductor. We begin with the electron annihilation operator $c_{\mathbf{q}a}$ at momentum $\mathbf{q}$ and spin $a =\uparrow,\downarrow$. We will shortly generalize the theory to one in which $a = 1 \ldots N_f$, with N_f an arbitrary integer. We denote the $c_{\mathbf{q}a}$ operators in the vicinity of the four nodal points $\mathbf{q} = (\pm K, \pm K)$ by (anti-clockwise) f_{1a}, f_{2a}, f_{3a}, f_{4a}. Now introduce the 2-component Nambu spinors $\Psi_{1a} = (f_{1a}, \varepsilon_{ab} f_{3b}^\dagger)$ and $\Psi_{2a} = (f_{2a}, \varepsilon_{ab} f_{4b}^\dagger)$ where $\varepsilon_{ab} = -\varepsilon_{ba}$ and $\varepsilon_{\uparrow\downarrow} = 1$ [we will follow the convention of writing out spin indices (a, b) explicitly, while indices in Nambu space will be implicit]. Expanding to linear order in gradients from the nodal points, the Bogoliubov action for the fermionic excitations of a d-wave superconductors can be written as (see Fig. 2.1)

$$\begin{aligned} S_\Psi &= \int \frac{d^2k}{(2\pi)^2} T \sum_{\omega_n} \sum_{a=1}^{N_f} \Psi_{1a}^\dagger \left(-i\omega_n + v_F k_x \tau^z + v_\Delta k_y \tau^x \right) \Psi_{1a} \\ &+ \int \frac{d^2k}{(2\pi)^2} T \sum_{\omega_n} \sum_{a=1}^{N_f} \Psi_{2a}^\dagger \left(-i\omega_n + v_F k_y \tau^z + v_\Delta k_x \tau^x \right) \Psi_{2a}. \end{aligned} \tag{2.2}$$

Here ω_n is a Matsubara frequency, τ^α are Pauli matrices which act in the fermionic particle-hole space, $k_{x,y}$ measure the wavevector from the nodal points and have been rotated by 45 degrees from $q_{x,y}$ co-ordinates, and v_F, v_Δ are velocities. The sum over a in Eq. (2.2) can be considered to extend over an arbitrary number N_f.

The second term, S_ϕ^0 describes the effective action for the Ising nematic order parameter, which we represent as a real field ϕ. Considering only the contribution to its action generated by high energy electronic excitations, we obtain only the analytic terms present in the quantum Ising model:

$$S_\phi^0 = \int d^2x d\tau \Big[\frac{1}{2} (\partial_\tau \phi)^2 + \frac{c^2}{2} (\nabla \phi)^2 + \frac{r}{2} \phi^2 + \frac{u_0}{24} \phi^4 \Big]; \tag{2.3}$$

here τ is imaginary time, c is a velocity, r tunes the system across the quantum critical point, and u_0 is a quartic self-interaction.

The final term in the action, $S_{\Psi\phi}$ couples the Ising nematic order, ϕ, to the nodal fermions, Ψ_{1a}, Ψ_{2a}. This can be deduced by a symmetry analysis (Vojta et al., 2000c,b, 2008), and the important term is a trilinear "Yukawa" coupling

$$S_{\Psi\phi} = \int d^2x d\tau \Big[\lambda_0 \phi \sum_{a=1}^{N_f} \Big(\Psi_{1a}^\dagger \tau^x \Psi_{1a} + \Psi_{2a}^\dagger \tau^x \Psi_{2a} \Big) \Big], \tag{2.4}$$

where λ_0 is a coupling constant.

We can now see that the action S describes the couplings between the ϕ bosons and the Ψ fermions, both of which have a 'relativistic' dispersion spectrum. However, the velocity of 'light' in their dispersion spectrums, c, v_F, v_Δ, are not all equal. If we choose equal velocities with $v_F = v_\Delta = c$, then the decoupled theory $S_\Psi + S_\phi^0$ does have a relativistically invariant form. However, even in this case, the fermion-boson coupling $S_{\Psi\phi}$ is *not* relativistically invariant: the coupling matrix τ^x in Eq. (2.4) breaks Lorentz symmetry, and this feature will be crucial for our analysis. If we replace τ^x by τ^y in Eq. (2.4), then we obtain an interacting relativistically invariant theory for the equal velocity case, which was studied in Ref. Vojta et al. (2000c,b, 2008) as a description of the transition from a $d_{x^2-y^2}$ to a $d_{x^2-y^2}+id_{xy}$ superconductor.

A renormalization group analysis of the above action has been presented previously (Vojta et al., 2000c,b, 2008) in an expansion in $(3-d)$. No fixed point describing the onset of nematic order was found, with the couplings u_0 and λ_0 flowing away to infinity. This runaway flow was closely connected to the non-Lorentz-invariant structure of $S_{\Psi\phi}$ and the resulting flow of the velocities away from each other. In contrast, for the transition to a $d_{x^2-y^2} + id_{xy}$ superconductor, a stable fixed point was found at which the velocities flowed to equal values at long scales (Vojta et al., 2000c,b, 2008). Similar relativistically-invariant fixed points are also found in other cases involving the onset of spin or charge density wave orders at wavevectors which nest the separation between nodal points (Balents et al., 1998; Vojta et al., 2000a).

2.2.1 Large N_f expansion

We will analyze S in the context of the $1/N_f$ expansion. Formally, this involves integrating out the $\Psi_{1,2}$ fermions, and obtaining the resulting non-local effective action

for ϕ. Near the potential quantum critical point, the non-local terms so generated are more important in the infrared than the terms S_ϕ^0 in Eq. (2.3), apart from the "mass" term r. So we can drop the remaining terms in S_ϕ^0; also for convenience we rescale $\phi \to \phi/\lambda_0$ and $r \to N_f r \lambda_0^2$, and obtain the local field theory

$$S = S_\Psi + \int d^2x d\tau \left[\frac{N_f r}{2} \phi^2 + \phi \sum_{a=1}^{N_f} \left(\Psi_{1a}^\dagger \tau^x \Psi_{1a} + \Psi_{2a}^\dagger \tau^x \Psi_{2a} \right) \right]. \tag{2.5}$$

This local field theory will form the basis of all our RG analysis. Note that this field theory has only 3 parameters: r, v_F, and v_Δ. So any RG equations can be expressed only in terms of these parameters, as will be presented in the following section.

The large N_f expansion proceeds by integrating out the Ψ fermions, yielding an effective action S_ϕ for the nematic order ϕ. It is important to note that S_ϕ is a complicated non-local functional of ϕ, which however depends upon only r, v_F, and v_Δ. Also, in writing out explicit forms for S_ϕ it is essential to keep subtle issues on orders of limits in mind. In particular, for the large N_f phase diagram, we need the effective potential for ϕ at zero k and ω. Thus we need an expansion of the effective potential in the regime $|\phi| \gg |k|, |\omega|$ — the structure of this was discussed in Ref. Kim et al. (2008), and yielded a second-order transition in the limit of large N_f. In contrast, for our RG analysis here, we will work in the quantum critical region, where $\langle \phi \rangle = 0$, and so we need the functional for $|\phi| \ll |k|, |\omega|$. In this case, we can expand S_ϕ in powers of ϕ to yield the formal result

$$\begin{aligned} \frac{S_\phi}{N_f} &= \frac{1}{2} \int_K \left(r + \Gamma_2(K) \right) |\phi(K)|^2 \\ &\quad + \frac{1}{4} \prod_{i=1}^4 \int_{K_i} \delta \left(\sum_i K_i \right) \Gamma_4(K_1, K_2, K_3, K_4) \phi(K_1) \phi(K_2) \phi(K_3) \phi(K_4) + \ldots \end{aligned} \tag{2.6}$$

Here the $K_i \equiv (k_i, \omega_i)$ are 3-momenta. The functions Γ_i are all given by one fermion loop Feynman graphs with i insertions of the external ϕ vertices, as shown in Fig. 2.2; we denote the external momenta of these vertices, K_i, clockwise around the fermion loop. The Feynman loop integrals are quite tedious to evaluate, especially for large

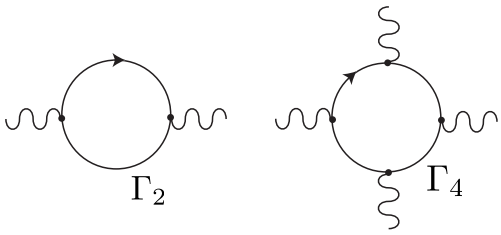

Figure 2.2: Feynman graph expansion for the effective action S_ϕ. The full lines are fermion propagators, while the wavy lines are ϕ insertions.

i, and so below we only present explicit expressions for the needed low order terms. However, all the Γ_i are universal functions of only the momenta and v_F and v_Δ

Our analysis will require the explicit form of $\Gamma_2(K)$. This can be written as

$$\Gamma_2(K) = \Pi_2(k_x, k_y, \omega) + \Pi_2(k_y, k_x, \omega) \tag{2.7}$$

with the 2 terms representing the contributions of the Ψ_1 and Ψ_2 fermions respectively. The one fermion loop diagram yields

$$\begin{aligned}\Pi_2(k_x, k_y, \omega) &= \int \frac{d^2p}{4\pi^2} \int \frac{d\Omega}{2\pi} \mathrm{Tr}\Big[\tau^x \left(-i(\Omega+\omega) + v_F(p_x+k_x)\tau^z + v_\Delta(p_y+k_y)\tau^x\right)^{-1} \\ &\qquad \times \tau^x \left(-i\Omega + v_F p_x \tau^z + v_\Delta p_y \tau^x\right)^{-1}\Big] \\ &= \frac{1}{16 v_F v_\Delta} \frac{(\omega^2 + v_F^2 k_x^2)}{(\omega^2 + v_F^2 k_x^2 + v_\Delta^2 k_y^2)^{1/2}}\end{aligned} \tag{2.8}$$

Here, we have subtracted out a constant which shifts the position of the critical point.

For Γ_4 we will only need the cases where 2 of the four external 3-momenta vanish. The first is

$$\Gamma_4(K, -K, 0, 0) = \Pi_{4a}(k_x, k_y, \omega) + \Pi_{4a}(k_y, k_x, \omega) \tag{2.9}$$

where

$$\begin{aligned}\Pi_{4a}(k_x,k_y,\omega) &= \int \frac{d^2p}{4\pi^2}\int\frac{d\Omega}{2\pi}\mathrm{Tr}\Big[\tau^x\left(-i\Omega+v_F p_x\tau^z+v_\Delta p_y\tau^x\right)^{-1}\\ &\qquad\times\left\{\tau^x\left(-i(\Omega+\omega)+v_F(p_x+k_x)\tau^z+v_\Delta(p_y+k_y)\tau^x\right)^{-1}\right\}^3\Big]\\ &= \frac{1}{2v_\Delta^2}\frac{\partial^2\Pi_2(k_x,k_y,\omega)}{\partial k_y^2}\\ &= -\frac{1}{32v_Fv_\Delta}\frac{(\omega^2+v_F^2k_x^2)(\omega^2+v_F^2k_x^2-2v_\Delta^2k_y^2)}{(\omega^2+v_F^2k_x^2+v_\Delta^2k_y^2)^{5/2}}. \end{aligned} \tag{2.10}$$

The other case with 2 vanishing 3-momenta is

$$\Gamma_4(K,0,-K,0)=\Pi_{4b}(k_x,k_y,\omega)+\Pi_{4b}(k_y,k_x,\omega) \tag{2.11}$$

where

$$\begin{aligned}\Pi_{4b}(k_x,k_y,\omega) &= \int \frac{d^2p}{4\pi^2}\int\frac{d\Omega}{2\pi}\mathrm{Tr}\Big[\left\{\tau^x\left(-i\Omega+v_F p_x\tau^z+v_\Delta p_y\tau^x\right)^{-1}\right\}^2\\ &\qquad\times\left\{\tau^x\left(-i(\Omega+\omega)+v_F(p_x+k_x)\tau^z+v_\Delta(p_y+k_y)\tau^x\right)^{-1}\right\}^2\Big]\\ &= \frac{1}{16v_Fv_\Delta}\frac{(\omega^2+v_F^2k_x^2)(\omega^2+v_F^2k_x^2-2v_\Delta^2k_y^2)}{(\omega^2+v_F^2k_x^2+v_\Delta^2k_y^2)^{5/2}}. \end{aligned} \tag{2.12}$$

From the effective action S_ϕ in (2.6), we can obtain the $1/N_f$ corrections to various observable quantities.

For the nematic susceptibility, χ_ϕ, we have

$$\chi_\phi^{-1}=r+\frac{1}{N_f}\int_K\frac{2\Gamma_4(K,-K,0,0)+\Gamma_4(K,0,-K,0)}{\Gamma_2(K)+r}. \tag{2.13}$$

Using the values in Eq. (2.10) and (2.12), we observe that the $1/N_f$ correction is identically zero. This can be traced to the arguments in Ref. Kim et al. (2008) (based upon gauge invariance and the fact that the coupling in Eq. (2.4) is to a globally conserved fermion current) that the effective potential for the field ϕ is unrenormalized by the low energy fermion action. Indeed, this argument implies that all higher order terms in $1/N_f$ also vanish, and that $\chi_\phi^{-1}=r$ exactly in the present continuum field theory. So we may conclude that the susceptibility exponent, γ, for the nematic order parameter has the exact value

$$\gamma=1. \tag{2.14}$$

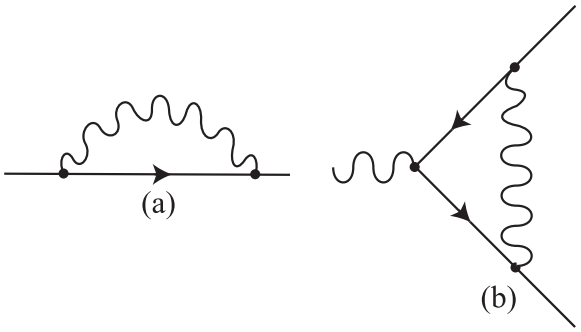

Figure 2.3: Order $1/N_f$ contributions to the (a) self energy Σ_1 of Ψ_1 fermions and (b) the vertex Ξ.

Note that there are $1/N_f$ corrections to the momentum and frequency dependence of the nematic susceptibility, and these will appear in our RG analysis below.

Turning to the $1/N_f$ expansion for the Ψ_1 Green's function, we write this as

$$G_{\Psi_1}^{-1}(k,\omega) = -i\omega + v_F k_x \tau^z + v_\Delta k_y \tau^x - \Sigma_1(k,\omega), \tag{2.15}$$

the self-energy is given by the Feynman graph in Fig. 2.3:

$$\begin{aligned}\Sigma_1(k,\omega) &= \frac{1}{N_f}\int \frac{d^2p}{4\pi^2}\int \frac{d\Omega}{2\pi}\frac{[i(\Omega+\omega) - v_F(p_x+k_x)\tau^z + v_\Delta(p_y+k_y)\tau^x]}{(\Omega+\omega)^2 + v_F^2(p_x+k_x)^2 + v_\Delta^2(p_y+k_y)^2} \\ &\quad \times \frac{1}{\Gamma_2(p,\Omega)+r}.\end{aligned} \tag{2.16}$$

Finally, we will also need the $1/N_f$ correction to the boson-fermion vertex (the Yukawa couping) in Eq. (2.4). At zero external momenta and frequencies, this vertex is renormalized by Fig. 2.3 to

$$\begin{aligned}\Xi &= \tau^x + \frac{1}{N_f}\int \frac{d^2p}{4\pi^2}\int \frac{d\Omega}{2\pi}\Big[\tau^x\left(-i\Omega + v_F p_x\tau^z + v_\Delta p_y \tau^x\right)^{-1} \\ &\quad \times \tau^x\left(-i\Omega + v_F p_x\tau^z + v_\Delta p_y \tau^x\right)^{-1}\tau^x \frac{1}{\Gamma_2(p,\Omega)+r}\Big]\end{aligned} \tag{2.17}$$

The RG equations will be obtained in the next section from Eqs. (2.13), (2.16) and (2.17).

2.3 Renormalization group analysis

We begin our discussion of the RG by describing the general structure which applies to *all* orders in the $1/N_f$ expansion. The RG will be based upon a consideration of the renormalization of the local field theory S in Eq. (2.5). We are interested in the behavior of this field theory under the rescaling transformation

$$\begin{aligned} k &= k' e^{-\ell} \\ \omega &= \omega' e^{-\ell}. \end{aligned} \tag{2.18}$$

Note that we have not introduced a dynamic critical exponent z for the rescaling of the frequency. This is because we will allow both velocities v_F and v_Δ to flow, and this flow will effectively account for any anomalous dynamic scaling. Under this spacetime rescaling, we also have a rescaling of the fermion and boson fields

$$\begin{aligned} \Psi_{1,2}(k,\omega) &= \Psi'_{1,2}(k',\omega') \exp\left(\frac{1}{2}\int_0^\ell d\ell(4-\eta_f)\right) \\ \phi(k,\omega) &= \phi'(k',\omega') \exp\left(\frac{1}{2}\int_0^\ell d\ell(5-\eta_b)\right). \end{aligned} \tag{2.19}$$

Here we have allowed the anomalous dimensions $\eta_{b,f}$ to be scale-dependent, as that will be the case below. To implement these field rescalings, we have to determine how the field scales are defined. For the fermions, as is conventional, we set the scale of $\Psi_{1,2}$ so that the co-effecients of the time derivative terms in S_Ψ remain unity. For the nematic order parameter, ϕ, there is no "kinetic energy" term in Eq. (2.5), and so we cannot use the conventional method. Instead, recall that the "Yukawa" coupling λ_0 was absorbed into the overall scale of ϕ in Eq. (2.5). Therefore it is natural to set the scale of ϕ so that the boson-fermion vertex in Eq. (2.5) remains fixed at unity. This is also consonant with the fact that the boson "kinetic energy" comes entirely from the fermion loops.

The RG equations now follow from the low frequency forms of the fermion self energy Σ_1 and the vertex Ξ. These will have a dependence upon an ultraviolet cutoff, Λ. We will discuss below an explicit method of applying this cutoff. For now, we note that for the RG we only need the logarithmic derivative of the self energy and

the vertex. Thus let us write

$$\begin{aligned} \Lambda\frac{d}{d\Lambda}\Sigma_1(k,\omega) &= C_1(-i\omega) + C_2 v_F k_x \tau^z + C_3 v_\Delta k_y \tau^x \\ \Lambda\frac{d}{d\Lambda}\Xi &= C_4\tau^x. \end{aligned} \tag{2.20}$$

On the right hand side, we assume (as in the usual field-theoretic RG) that the limit $\Lambda \to \infty$ can be safely taken. Then a simple dimensional analysis shows that the C_{1-4} are all universal dimensionless functions of the velocity ratio v_Δ/v_F. In principle, the above method can be generalized to any needed order in the $1/N_f$ expansion by taking the appropriate logarithmic cutoff derivative of the self energy Σ_1 and the vertex Ξ, as reviewed in Ref. Brézin et al. (1976).

With the results in Eq. (2.20), we can set the scaling dimensions of the fields. Considering the renormalization of the $-i\omega$ term in S_Ψ, we obtain

$$\eta_f = -C_1. \tag{2.21}$$

Imposing the unit value of the Yukawa coupling in Eq. (2.5) we obtain

$$\eta_b = 1 + 2C_4 - 2\eta_f = 1 + 2C_4 + 2C_1 \tag{2.22}$$

Note the large value of η_b in the large N_f theory. This is a consequence of the fact that the ϕ kinetic energy is tied to the non-analytic fermion loop contribution. We can now also use the non-renormalization of the ϕ^2 term in Eq. (2.5), as noted in Eq. (2.14), to determine the flow equation for the "mass" r. This defines the correlation length exponent ν by the RG equation

$$\frac{dr}{d\ell} = \frac{1}{\nu} r \tag{2.23}$$

for small r, and we have the non-mean-field value

$$\nu = \frac{1}{2 - \eta_b}. \tag{2.24}$$

The results in Eq. (2.20) also yield the flow equations for the velocities. By considering the renormalization of the k-dependent terms in S_Ψ we determine that the velocity v_F flows according

$$\frac{dv_F}{d\ell} = (-\eta_f - C_2)v_F = (C_1 - C_2)v_F, \tag{2.25}$$

while the velocity v_Δ obeys

$$\frac{dv_\Delta}{d\ell} = (-\eta_f - C_3)v_\Delta = (C_1 - C_3)v_\Delta. \tag{2.26}$$

Clearly, the ratios of the velocity obeys

$$\frac{d(v_\Delta/v_F)}{d\ell} = (C_2 - C_3)(v_\Delta/v_F). \tag{2.27}$$

All that remains now is to determine the C_{1-4} as a function of v_Δ/v_F. These functions also depend upon the "mass" r, but we will henceforth restrict ourselves to the vicinity of the critical point by setting $r = 0$. We reiterate that, in principle, our method allows us to obtain these functions to any needed order in the $1/N_f$ expansion. However, we will only obtain explicit results below to first order $1/N_f$.

The computation of C_{1-4} requires the imposition of a ultraviolet momentum cutoff. We implement this (Vojta et al., 2000c,b, 2008) by multiplying both the Fermi and Bose propagators by a smooth cutoff function $\mathcal{K}(k^2/\Lambda^2)$. Here $\mathcal{K}(y)$ is an arbitrary function with $\mathcal{K}(0) = 1$ and which falls off rapidly with y at $y \sim 1$ *e.g.* $\mathcal{K}(y) = e^{-y}$. We will show below that the RG equations are independent of the particular choice of $\mathcal{K}(y)$.

Let us now discuss the evaluation of C_{1-3}. Schematically, we can write for the fermion self energy

$$\Sigma_1(K) = \int \frac{d^3P}{8\pi^3} F(P+K)G(P)\mathcal{K}\left(\frac{(p+k)^2}{\Lambda^2}\right)\mathcal{K}\left(\frac{p^2}{\Lambda^2}\right) \tag{2.28}$$

where $K \equiv (k, \omega)$ and $P \equiv (p, \Omega)$ are 3-momenta, and F and G are functions which can be obtained by comparing this expression to Eq. (2.16). Also notice that (at $r = 0$) F and G are both homogenous functions of 3-momenta of degree -1. Expanding to first order in K_μ (μ is a spacetime index) we have

$$\Sigma_1(K) \approx K_\mu \int \frac{d^3P}{8\pi^3}\left[\frac{\partial F(P)}{\partial P_\mu}G(P)\mathcal{K}^2\left(\frac{p^2}{\Lambda^2}\right) + F(P)G(P)\mathcal{K}\left(\frac{p^2}{\Lambda^2}\right)\frac{2p_\mu}{\Lambda^2}\mathcal{K}'\left(\frac{p^2}{\Lambda^2}\right)\right] \tag{2.29}$$

where p_μ is the three vector $(0, p_x, p_y)$ (while $P_\mu = (\Omega, p_x, p_y)$). Now taking the Λ

derivative

$$\Lambda\frac{d}{d\Lambda}\Sigma_1(K) \approx K_\mu\int\frac{d^3P}{8\pi^3}\left[\left\{-\frac{4p^2}{\Lambda^2}\frac{\partial F(P)}{\partial P_\mu}-4F(P)\frac{p_\mu}{\Lambda^2}\right\}G(P)\mathcal{K}\left(\frac{p^2}{\Lambda^2}\right)\mathcal{K}'\left(\frac{p^2}{\Lambda^2}\right)\right.$$
$$\left.-\frac{4p^2p_\mu}{\Lambda^4}F(P)G(P)\left\{\mathcal{K}\left(\frac{p^2}{\Lambda^2}\right)\mathcal{K}''\left(\frac{p^2}{\Lambda^2}\right)+\mathcal{K}'^2\left(\frac{p^2}{\Lambda^2}\right)\right\}\right] \quad (2.30)$$

Now we convert to cylindrical co-ordinates in spacetime by writing $P_\mu = y\Lambda(v_F x, \cos\theta, \sin\theta)$ and integrate over y, x, and θ. Also, let us define $\hat{P}_\mu = (v_F x, \cos\theta, \sin\theta)$ and $\hat{p}_\mu = (0, \cos\theta, \sin\theta)$. We use the homogeneity properties of the functions F and G to obtain

$$\Lambda\frac{d}{d\Lambda}\Sigma_1(K) \approx \frac{v_F K_\mu}{8\pi^3}\int_{-\infty}^{\infty}dx\int_0^{2\pi}d\theta\left[\left\{-4\frac{\partial F(\hat{P})}{\partial P_\mu}-4\hat{p}_\mu F(\hat{P})\right\}G(\hat{P})\int_0^\infty ydy\mathcal{K}(y^2)\mathcal{K}'(y^2)\right.$$
$$\left.-4\hat{p}_\mu F(\hat{P})G(\hat{P})\int_0^\infty y^3dy\left\{\mathcal{K}\left(y^2\right)\mathcal{K}''\left(y^2\right)+\mathcal{K}'^2\left(y^2\right)\right\}\right] \quad (2.31)$$

Now the integrals over y can be evaluated exactly by integration by parts, and the final result is *independent* of the precise form of $\mathcal{K}(y)$:

$$\Lambda\frac{d}{d\Lambda}\Sigma_1(K) = \frac{v_F K_\mu}{8\pi^3}\int_{-\infty}^{\infty}dx\int_0^{2\pi}d\theta\frac{\partial F(\hat{P})}{\partial P_\mu}G(\hat{P}) \quad (2.32)$$

In a similar manner, we can write the result for the vertex Ξ in Eq. (2.17) in the schematic form

$$\Xi = \tau^x + \int\frac{d^3P}{8\pi^3}H(P)\mathcal{K}^3\left(\frac{p^2}{\Lambda^2}\right), \quad (2.33)$$

where $H(P)$ is a homogenous function of P of degree -3. Proceeding as above we obtain the analog of Eq. (2.32)

$$\Lambda\frac{d}{d\Lambda}\Xi = \frac{v_F}{8\pi^3}\int_{-\infty}^{\infty}dx\int_0^{2\pi}d\theta H(\hat{P}). \quad (2.34)$$

We can now use the above expressions to obtain explicit results for the constants C_{1-4} at order $1/N_f$. For C_{1-3} we combine Eqs. (2.16), (2.20), (2.28), and (2.32) to obtain

$$C_1 = \frac{2(v_\Delta/v_F)}{\pi^3 N_f}\int_{-\infty}^{\infty}dx\int_0^{2\pi}d\theta\frac{(x^2-\cos^2\theta-(v_\Delta/v_F)^2\sin^2\theta)}{(x^2+\cos^2\theta+(v_\Delta/v_F)^2\sin^2\theta)^2}\mathcal{G}(x,\theta)$$
$$C_2 = \frac{2(v_\Delta/v_F)}{\pi^3 N_f}\int_{-\infty}^{\infty}dx\int_0^{2\pi}d\theta\frac{(-x^2+\cos^2\theta-(v_\Delta/v_F)^2\sin^2\theta)}{(x^2+\cos^2\theta+(v_\Delta/v_F)^2\sin^2\theta)^2}\mathcal{G}(x,\theta)$$
$$C_3 = \frac{2(v_\Delta/v_F)}{\pi^3 N_f}\int_{-\infty}^{\infty}dx\int_0^{2\pi}d\theta\frac{(x^2+\cos^2\theta-(v_\Delta/v_F)^2\sin^2\theta)}{(x^2+\cos^2\theta+(v_\Delta/v_F)^2\sin^2\theta)^2}\mathcal{G}(x,\theta) \quad (2.35)$$

where

$$\mathcal{G}^{-1}(x,\theta) = \frac{x^2+\sin^2\theta}{\sqrt{x^2+(v_\Delta/v_F)^2\cos^2\theta+\sin^2\theta}} + \frac{x^2+\cos^2\theta}{\sqrt{x^2+\cos^2\theta+(v_\Delta/v_F)^2\sin^2\theta}} \quad (2.36)$$

is the ϕ propagator inverse. All the integrals in Eqs. (2.35) are well-defined and convergent for all non-zero v_Δ/v_F, and have to be evaluated numerically. It is also evident that the results are functions only of v_Δ/v_F. The results of a numerical evaluation are shown in Fig. 2.4.

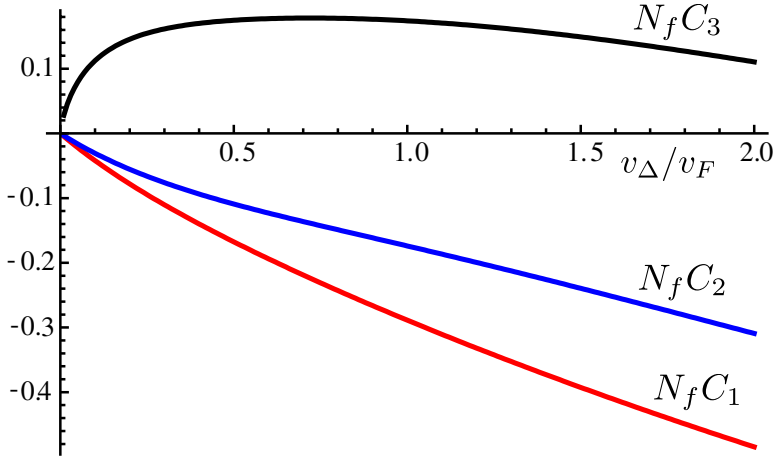

Figure 2.4: Plots of the functions C_{1-3} in Eq. (2.35).

Similarly, we can combine Eqs. (2.17), (2.20), (2.33), and (2.34) to deduce that

$$C_4 = -C_3, \quad (2.37)$$

at leading order in the $1/N_f$ expansion.

With the values in Eq. (2.35), we are now in a position to numerically solve the RG flow for the velocity ratio v_Δ/v_F in Eq. (2.27). We plot the right-hand-side of this flow equation in Fig. 2.5. Note that the only zero of the flow equation is at $v_\Delta/v_F = 0$, and that this fixed point is attractive in the infrared. So for all starting values of the parameter v_Δ/v_F, the flow is towards $v_\Delta/v_F \to 0$ for large ℓ. At large enough scales, it is always possible to approximate the constants C_{1-3} in Eqs. (2.35)

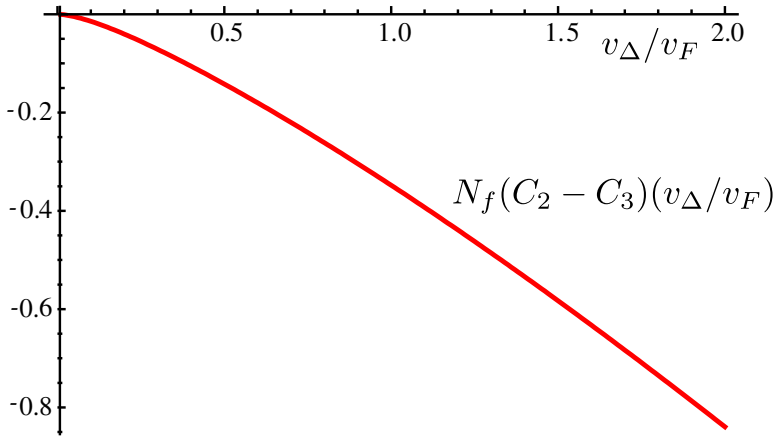

Figure 2.5: Right-hand-side of the RG flow equation Eq. (2.27) for v_Δ/v_F.

by their limiting values for small v_Δ/v_F. Evaluating the integrals in Eq. (2.35) in this limit, we obtain

$$\begin{aligned} C_1 &= -0.4627\frac{(v_\Delta/v_F)}{N_f} + \mathcal{O}\left((v_\Delta/v_F)^3\right) \\ C_2 &= -0.3479\frac{(v_\Delta/v_F)}{N_f} + \mathcal{O}\left((v_\Delta/v_F)^3\right) \\ C_3 &= \left(\frac{8}{\pi^2}\ln(v_F/v_\Delta) - 0.9601\right)\frac{(v_\Delta/v_F)}{N_f} + \mathcal{O}\left((v_\Delta/v_F)^3\right). \end{aligned} \tag{2.38}$$

The logarithmic dependence on v_Δ/v_F arises from a singularity in the integrand at $x = 0$ and $\theta = \pm\pi/2$: this corresponds to an integral across the underlying Fermi surface over ω and k_x where the inverse fermion propagator $\sim -i\omega + v_F k_x \tau^z$. Inserting these values into the flow equations (2.25), (2.26), and (2.27) we obtain an explicit form of the RG flow for small v_Δ/v_F:

$$\frac{dv_\Delta}{d\ell} = -\left(\frac{8}{\pi^2}\ln\left(v_F/v_\Delta\right) - 0.4974\right)\frac{v_\Delta^2}{N_f v_F} \tag{2.39}$$

$$\frac{dv_F}{d\ell} = -0.1148\frac{v_\Delta}{N_f} \tag{2.40}$$

$$\frac{d(v_\Delta/v_F)}{d\ell} = -\left(\frac{8}{\pi^2}\ln\left(v_F/v_\Delta\right) - 0.6122\right)\frac{(v_\Delta/v_F)^2}{N_f}. \tag{2.41}$$

The right-hand-side of Eq. (2.41) has a zero for $v_\Delta/v_F \approx 2$; this is spurious as this equation is valid only for $v_\Delta/v_F \ll 1$. The full expression for the right-hand-side,

valid for arbitrary v_Δ/v_F, is plotted in Fig. 2.5, and this makes it clear that the only zero of the beta function is at $v_\Delta/v_F = 0$.

The results of a numerical integration of Eqs. (2.25), (2.26) and (2.27) are shown in Figs. 2.6, 2.7, and 2.8. We start the RG integration at $\ell = 0$ corresponding to a

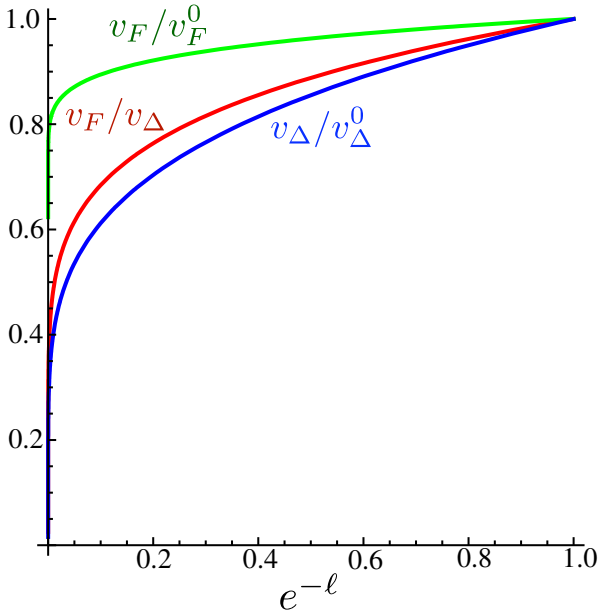

Figure 2.6: Integration of Eqs. (2.25), (2.26) and (2.27) from $\ll = 0$ to ℓ for $N_f = 2$, starting from the velocities v_F^0 and v_Δ^0. Results above are for $v_\Delta^0/v_F^0 = 1$.

temperature $T = T_0$ at the nematic critical point, at which point the velocities have the values v_F^0 and v_Δ^0. Integrating to the scale ℓ yields the velocities $v_F(\ell)$ and $v_\Delta(\ell)$ at a temperature $T = T_0 e^{-\ell}$. The results depend upon the initial value of the velocity ratio, v_Δ^0/v_F^0, and are shown in the figures for $v_\Delta^0/v_F^0 = 1, 0.1, 0.05$. These results can also be converted into dependence on the deviation from the nematic critical point, r, by integrating Eq. (2.23).

In the asymptotic low temperature regime ($\ell \to \infty$), we have $v_\Delta/v_F \to 0$, and so we can integrate the asymptotic expression in Eq. (2.41). This yields

$$\frac{v_\Delta}{v_F} = \frac{\pi^2 N_f}{8} \frac{1}{\ell} \frac{1}{\ln[0.3809\, \ell/N_f]} \tag{2.42}$$

The T dependence follows by using $\ell = \ln(T_0/T)$. Using the result for v_Δ/v_F in

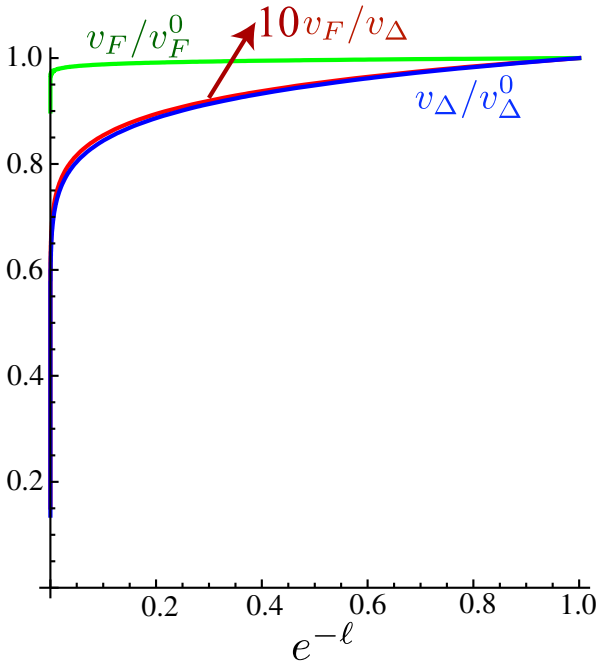

Figure 2.7: As in Fig. 2.6 but for $v_\Delta^0/v_F^0 = 0.1$.

Eq. (2.42) and integrating Eq. (2.40), we find that v_F only has a finite renormalization from its bare value as $\ell \to \infty$. So the decrease in v_Δ/v_F as $\ell \to \infty$ (*i.e.* as $T \to 0$) comes primarily from the decrease in v_Δ. This is also clear from the plots in Figs. 2.6-2.8.

We can also apply these results to obtain the $T = 0$ evolution of the velocities as a function of the tuning parameter, r, across the nematic ordering transition. In this case we use Eq. (2.23), along with the fact that $\nu \to 1$ as $v_\Delta/v_F \to 0$. Then we deduce that $\ell = \ln(1/|r|)$ to leading logarithm accuracy, and so obtain the r dependence of the velocities from Figs. 2.6-2.8. When both T and r are non-zero, we can use $\ell = \ln(\max(|r|, T))$ to leading logarithmic accuracy. Note that this predicts a minimum in v_Δ/v_F as r is tuned across the nematic ordering transition, with the minimum value of order $1/\ln(1/T)$.

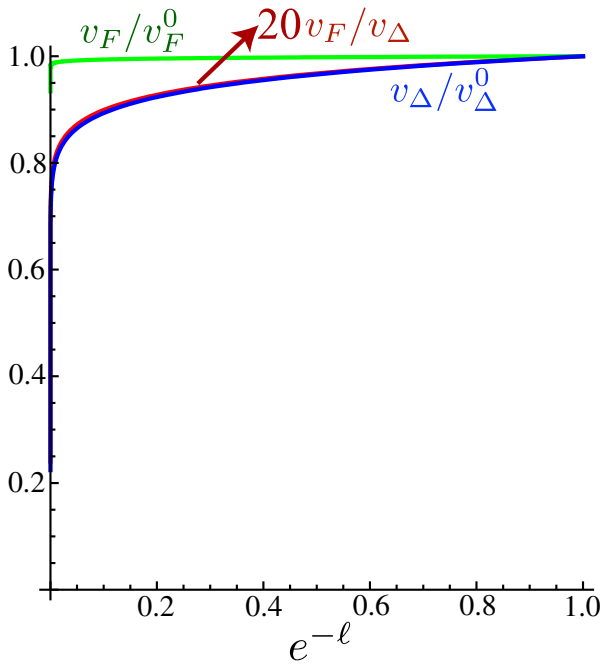

Figure 2.8: As in Fig. 2.6 but for $v_\Delta^0/v_F^0 = 0.05$.

2.4 Theory for small v_Δ/v_F

The RG analysis in Section 2.3 has shown that the β functions at order $1/N_f$ are such that the flow is towards the strong anisotropy limit, $v_\Delta/v_F \to 0$ at large scales. Here we will show that this conclusion holds at all orders in the $1/N_f$ expansion. Indeed, for small v_Δ/v_F we will show that v_Δ/v_F can itself be as the control parameter for the computation, and N_f is not required to be large. In other words, the RG flow equations in Eqs. (2.39-2.41) are asymptotically *exact*, even for the physical value of $N_f = 2$. All corrections to Eq. (2.39-2.41) are higher order in v_Δ/v_F.

Our conclusions follow from an examination of the structure of the action S_ϕ for the nematic order in Eq. (2.6) in the limit of $v_\Delta/v_F \to 0$. As we will shortly verify, the natural scale for the fluctuations of ϕ are at frequency and momenta with $\omega \sim v_F k_x \sim v_F k_y$. Under these conditions, we can just take the $v_\Delta \to 0$ limit of the expressions in Eqs. (2.8), (2.10), and (2.12). This limit exists, and to quadratic order

in ϕ we have the following effective action as $v_\Delta \to 0$ (at criticality, $r = 0$):

$$S_\phi = \frac{N_f}{16 v_F v_\Delta} \int \frac{d^2k}{4\pi^2} \int \frac{d\omega}{2\pi} |\phi(k,\omega)|^2 \left[\sqrt{\omega^2 + v_F^2 k_x^2} + \sqrt{\omega^2 + v_F^2 k_y^2} \right] + \ldots \quad (2.43)$$

Rescaling momenta $k \to k/v_F$, we notice that the prefactor in Eq. (2.43) is proportional to the dimensionless number $N_f v_F / v_\Delta$. Thus each propagator of ϕ will appear with the small prefactor of $v_\Delta/(N_f v_F)$. Further, as claimed above, each propogator has the typical scales $\omega \sim v_F k_x \sim v_F k_y$.

These considerations are easily extended to terms to all orders in ϕ in Eq.(2.6). The full expression for S_ϕ involves the sum of the logarithms of the determinants of the Dirac operators of $\Psi_{1,2}$ fermions in a background ϕ field. The expansion of these determinants in powers of ϕ involves only terms with a single fermion loop. For each Ψ_1 loop we rescale the *fermion* momentum $p_x \to p_x/v_F$ and $p_y \to p_y/v_\Delta$. Similarly for each Ψ_2 loop we rescale the fermion momentum $p_x \to p_x/v_\Delta$ and $p_y \to p_y/v_F$. In both cases, the integral over the fermion loop momentum yields a prefactor of $1/(v_F v_\Delta)$. For the ϕ vertices emerging from the Ψ_1 loops, we have momenta $\omega \sim v_F k_x \sim v_F k_y$, as noted above; when this external momenta enters the fermion loop, we have $k_x \sim p_x$, the typical Ψ_1 x-momentum. However, $k_y \ll p_y \sim 1/v_\Delta$, the typical Ψ_1 y-momentum. Consequently, we may safely set $k_y = 0$ within the fermion loop, and there is no further dependence upon v_Δ in the loop integral. Similarly, in the Ψ_2 loops, we may set $k_x = 0$ within the fermion loop. To summarize, the typical ϕ momenta are $k_x \sim 1/v_F$, $k_y \sim 1/v_F$, the typical Ψ_1 momenta are $p_x \sim 1/v_F$, $p_y \sim 1/v_\Delta$, and typical Ψ_2 momenta are $p_x \sim 1/v_\Delta$, $p_y \sim 1/v_F$. Further, the resulting effective action for ϕ has the form

$$S_\phi = \frac{N_f}{v_F v_\Delta} \mathcal{S}\big[\phi(k,\omega); v_F k_x, v_F k_y, \omega\big] + \text{ terms higher order in } v_\Delta/v_F. \quad (2.44)$$

Here $\mathcal{S}$ is a functional of ϕ which is independent of v_Δ, whose expansion in ϕ has coefficients which depend only upon $v_F k_x$, $v_F k_y$, and ω. It can be verified that Eq. (2.43) and the quartic terms in Eqs. (2.10) and (2.12) are indeed of the form in Eq. (2.44).

From Eq. (2.44), it is evident (after rescaling momenta $k \to k/v_F$ and momentum space fields $\phi \to v_F^2 \phi$) that the natural expansion parameter controlling ϕ fluctuations is $v_\Delta/(N v_F)$. This is the main result of this section.

It remains to understand the $\ln(v_F/v_\Delta)$ factor in Eq. (2.41). If we compute observable ϕ correlations under the reduced effective action $\mathcal{S}$, the resulting expansion in powers of $v_\Delta/(Nv_F)$ leads to Feynman integrals which are not necessarily infrared or ultraviolet finite. Because the action $\mathcal{S}$ is free of any dimensionful coupling constant, the Feynman graph divergences can at most be powers of logarithms. These divergences are cutoff by using the full fermion propagators, including the terms proportional to v_Δ times the momenta of the boson propagators. This leads to factors of $\ln(v_F/v_\Delta)$, as was the case in obtaining Eq. (2.41) from Eq. (2.35).

2.5 Conclusions

This paper has described the RG properties of the field theory (Vojta et al., 2000c,b, 2008) in Eq. (2.5) for nematic ordering. It was previously noted (Kim et al., 2008) that the effective potential for the nematic order, ϕ, remained unrenormalized upon integrating out the nodal fermions $\Psi_{1,2}$. This happens because the ϕ couples to a conserved fermion current, and a spacetime-independent ϕ can be 'gauged away' applying a gauge transformation to the fermions. One consequence of this non-renormalization is that the susceptibility exponent, γ, takes the simple value in Eq. (2.14). However, non-trivial renormalizations of the field scale of both ϕ and $\Psi_{1,2}$ are still possible, along with renormalizations of the velocities, and we have shown here that this leads to an interesting RG flow structure, with non-mean-field exponents.

It is interesting to note here the similarities to the RG flow of supersymmetric field theories (Strassler, 2003). There the effective potential also remains unrenormalized (albeit for very different reasons), but the 'wavefunction renormalizations' lead to many non-trivial RG fixed points.

Our main result was that the transition is described by a fixed point in which the fermion velocities at the nodal points have a ratio which approaches a fixed point with $v_\Delta/v_F \to 0$ logarithmically slowly. However, it is not valid to set the pairing-induced velocity $v_\Delta = 0$ in the computation, and so deal with a metallic Fermi surface. For

the case where the fermion dispersion is $\sim (v_F^2 k_x^2 + v_\Delta^2 k_y^2)^{1/2}$, the typical fermion momenta contributing to the critical theory scale as $k_x \sim 1/v_F$ and $k_y \sim 1/v_\Delta$, and so the full form of the Bogoliubov quasi-particle dispersion is important. The flow of the velocities is described by Eqs. (2.39-2.41) for $v_\Delta/v_F \ll 1$, and these equations are believed to be asymptotically exact.

Unlike the fermions, the fluctuations of the nematic order, ϕ, are isotropic in momenta. These are described asymptotically exactly by Eq. (2.43). Note that the propagator is very different from free field, and has a large anomalous dimension, as was found in the $N_f = \infty$ theory (Kim et al., 2008). Experimental detection of this unusual spectrum in *e.g.* inelastic X-ray scattering would be most interesting.

We thank M. P. A. Fisher, E. Fradkin, E.-A. Kim, S. Kivelson, and M. Lawler for useful discussions.

Chapter 3

Quantum criticality of the kagome antiferromagnet with Dzyaloshinskii-Moriya interactions

3.1 Introduction

The nearest neighbor spin $S = \frac{1}{2}$ antiferromagnet on the kagome lattice has been the focus of extensive theoretical and experimental study because it is a prime candidate for realizing a ground state without antiferromagnetic order.

On the experimental side, much attention has focused on the $S = 1/2$ compound herbertsmithite $ZnCu_3(OH)_6Cl_2$. It has $J \approx 170$ K and no observed ordering or structural distortion. (Helton et al., 2007; Ofer et al., 2006; Mendels et al., 2007; Imai et al., 2008) However, there is an appreciable amount of substitutional disorder between the Zn and Cu sites (believed to be of the order 5-10 %) which affects the low T behavior. (Olariu et al., 2008; Gregor and Motrunich, 2008; Rozenberg and Chitra, 2008; Lee et al., 2007) More importantly, there is an upturn in the susceptibility at $T = 75$ K which has been ascribed to the DM interactions (Rigol and Singh, 2007;

Zorko et al., 2008; Ofer and Keren, 2009).

On the theoretical side, the most recent evidence (Nikolic and Senthil, 2003; Singh and Huse, 2007; Jiang et al., 2008; Evenbly and Vidal, 2010; Poilblanc et al., 2010; Schwandt et al., 2010) on the the nearest-neighbor antiferromagnet points consistently to a ground state with a spin gap of $0.05J$ and valence bond solid (VBS) order. The pattern of the VBS order is quite complex with a large unit cell, but was anticipated by Marston and Zeng (Marston and Zeng, 1991) by an application of the VBS selection mechanism described in the $1/N$ expansion of the SU(N) antiferromagnet. (Read and Sachdev, 1989a)

The influence of the DM interactions has also been studied theoretically (Cépas et al., 2008; Tovar et al., 2009; Hermele et al., 2008). Starting with an "algebraic spin liquid" ground state, Hermele *et al.* (Hermele et al., 2008) argued that the DM coupling, D, was a relevant perturbation, implying that an infinitesimal D would induce long-range magnetic order. In a recent exact diagonalization study, Cepas *et al.* (Cépas et al., 2008) reach a different conclusion: they claim that there is a non-zero critical DM coupling D_c beyond which magnetic order is induced. They estimate $D_c/J \approx 0.1$, quite close to the value measured (Zorko et al., 2008) for $ZnCu_3(OH)_6Cl_2$ which has $D/J \approx 0.08$. This proximity led Cepas *et al.* to suggest that the quantum criticality of the DM-induced transition to magnetic order controls the observable properties of this kagome antiferromagent.

The purpose of this paper is to propose a theory for the quantum critical point discovered by Cepas *et al.* (Cépas et al., 2008). We will compute various observables of this theory, allowing a potential comparison with numerics and experiments.

Given the evidence for VBS order in the model without DM interactions (Nikolic and Senthil, 2003; Singh and Huse, 2007; Jiang et al., 2008; Evenbly and Vidal, 2010), it would appear we need a theory for the transition from the VBS state to the magnetically ordered state. However, the VBS ordering is very weak, and can reasonably be viewed as a small perturbation on some underlying spin-liquid ground state. Schwandt, Mambrini, and Poilblanc (Poilblanc et al., 2010; Schwandt et al., 2010) have recently presented evidence that the kagomé antiferromagnet is proximate

to a Z_2 spin liquid state, and that vison condensation in this state leads to weak VBS ordering. Their dimer representation leads naturally to Z_2 spin liquid states in the same class as that originally described (Sachdev, 1992; Wang and Vishwanath, 2006) by the Schwinger boson method (Arovas and Auerbach, 1988; Auerbach and Arovas, 1988; Sachdev, 2010). We will therefore neglect the complexities associated with the VBS ordering and work with the parent Z_2 spin liquid state. This is equivalent to ignoring the physics of the vison sector, and assumes the magnetic ordering transition can be described in a theory of the spinons alone (Xu and Sachdev, 2009). The main result of this paper will be a theory of the quantum phase transition from the Schwinger boson Z_2 spin liquid to the magnetically ordered state as induced by the DM interactions.

We will begin in Section 3.2 with a description of the mean-field theory of the Z_2 spin liquid and its transition to the magnetically ordered state in the presence of DM interactions. This will be carried using the Sp(N) Schwinger boson formulation (Sachdev, 1992, 2010), for which the mean-field theory becomes exact in the large N limit. We will turn to fluctuation corrections and the nature of the quantum critical point in Section 3.3. Here we will show that the critical theory is the familiar three dimensional XY model. However, its connection to experimental observables is subtle: in particular, the XY field itself is not directly observable.

While this paper was in preparation, a description of the Schwinger boson mean field theory in the presence of DM interactions also appeared in Ref. Messio et al. (2010); they consider mean-field solutions with larger unit cells than we do, but did not analyze the critical field theory. Where they overlap, our results are in agreement with theirs. We also note the recent experimental observations of Helton *et al.* (Helton et al., 2010), who present evidence for quantum criticality in $ZnCu_3(OH)_6Cl_2$.

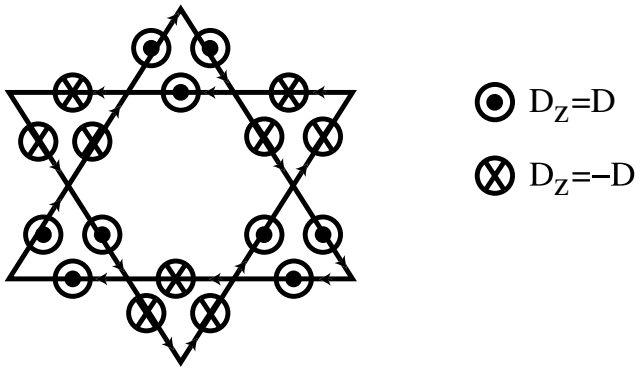

Figure 3.1: Staggered DM interaction from triangle to triangle in z-direction as in Ref. Elhajal et al. (2002). The arrowheads indicate D to come out of the plane, whereas the tails denote D to go into the plane. Note that the triangles are summed clock- and anticlockwise, respectively, indicated by the arrows on the bonds.

3.2 Mean field theory

The model we consider is a standard Heisenberg Hamiltonian supplemented by an additional DM interaction. It assumes the form

$$\mathcal{H} = \frac{1}{2} \sum_{i,j} \left[J_{ij} \mathbf{S_i} \cdot \mathbf{S_j} + \mathbf{D_{ij}} \cdot (\mathbf{S_i} \times \mathbf{S_j}) \right] \ . \tag{3.1}$$

$\mathbf{S_i}$ in this notation denotes the spin operator at site i, J_{ij} is assumed to be uniform and of the nearest neighbor type, and $\mathbf{D}_{ij} = D_{ij}\mathbf{e}_z$ is taken along the z-axis and staggered from triangle to triangle (Elhajal et al., 2002), see Fig. 3.1. This additional term explicitly breaks the spin-rotation symmetry by favoring configurations lying in the x-y plane. Furthermore this term increases the tendency of classical spin ordering. It has been shown in earlier works (Arovas and Auerbach, 1988; Auerbach and Arovas, 1988; Sachdev, 2010) that Schwinger bosons are ideally suited to describe phase transitions between paramagnetic and magnetically ordered phases in spin models. Following Ref. Sachdev (1992) we introduce a Sp(N) generalization of the spin operators, which formally allows to consider a controlled large N limit particularly suited for the study of frustrated spin systems such as kagome or traingular antiferromagnets. In the

Sp(1) case, which is isomorphic to SU(2), one can represent the spin variables as

$$\mathbf{S}_i = b^*_{i\sigma} \frac{\boldsymbol{\tau}_{\sigma\sigma'}}{2} b_{i\sigma'} \tag{3.2}$$

with $\vec{\tau}$ being the Pauli matrices and with

$$b_{i\sigma} = \begin{pmatrix} b_{i\uparrow} \\ b^*_{i\downarrow} \end{pmatrix} \quad \text{and} \quad \sum_\sigma b^*_{i\sigma} b_{i\sigma} = 2S = n_b \; . \tag{3.3}$$

In the case of the large-N generalization the Schwinger bosons acquire another index counting the copies of the system (we drop this index in the following discussions, but display N whenever it is essential). The large-N generalization formally justifies the mean-field, with the saddle point becoming exact in the limit $N \to \infty$. In order to properly reformulate the problem at hand we introduce two decoupling parameters

$$\begin{aligned} Q_{ij} &= \sum_{\sigma\sigma'} \epsilon_{\sigma\sigma'} b_{i\sigma} b_{j\sigma'} \\ P_{ij} &= \sum_{\sigma\sigma'} \tau^x_{\sigma\sigma'} b_{i\sigma} b_{j\sigma'} \end{aligned} \tag{3.4}$$

where $\epsilon_{\sigma\sigma'}$ is the antisymmetric tensor and τ^x is just the standard Pauli matrix. We see from the above expressions that $Q_{ij} = -Q_{ji}$ whereas $P_{ij} = P_{ji}$. This implies that the bond variables P_{ij} do not have a direction.

The constraint Eq. (3.3) is implemented via a Lagrangian multiplier in a standard way. The Hamiltonian of the system formulated in the fields defined in Eq. (3.4) consequently reads

$$\begin{aligned} \frac{\mathcal{H}}{N} = & - \frac{1}{2} \sum_{i,j} J_{ij} Q^*_{ij} Q_{ij} - \frac{i}{4} \sum_{i,j} D_{ij} (P^*_{ij} Q_{ij} - Q^*_{ij} P_{ij}) \\ & + \sum_i \lambda_i \left(b^*_{i\sigma} b_{i\sigma} - \kappa \right) \end{aligned} \tag{3.5}$$

where $\kappa = n_b/N$. We furthermore introduce N_u as the number of unit cells in the systems and N_s as the number of sites within the unit cell. We can write the mean-

field Hamiltonian per flavor and unit cell as

$$\begin{aligned}\frac{H_{MF}}{NN_u} &= \frac{1}{N_u}\sum_{\mathbf{k}}\Psi^*(\mathbf{k})\mathbb{H}(q_{ij},p_{ij},\lambda,\mathbf{k})\Psi(\mathbf{k}) \\ &+ \frac{J}{2}\sum_{(ij)'}|q_{ij}|^2+\frac{iD}{4}\sum_{(ij)'}(p^*_{ij}q_{ij}-q^*_{ij}p_{ij}) \\ &- N_s\lambda(1+\kappa) \end{aligned} \tag{3.6}$$

where $\sum_{(ij)'}$ denotes the sum over bonds belonging to the unit cell,

$$\Psi^*(\mathbf{k}) = (b^*_{1\uparrow}(\mathbf{k}),...,b^*_{N_s\uparrow}(\mathbf{k}),b_{1\downarrow}(-\mathbf{k}),...,b_{N_s\downarrow}(-\mathbf{k}))\ , \tag{3.7}$$

and the matrix

$$\mathbb{H} = \begin{pmatrix} \lambda\mathbb{I} & \mathbb{C}^*(k) \\ \mathbb{C}(k) & \lambda\mathbb{I} \end{pmatrix} \tag{3.8}$$

with the matrices $\mathbb{I}$ (identity) and $\mathbb{C}(k)$ being $N_s \times N_s$ matrices; the explicit form of these matrices is given in Appendix 3.A. As mentioned before, one of the major assets of the Schwinger boson approach is that it can describe magnetically disordered gapped spin liquid phases as well as magnetically ordered states. On a formal level in the large N approach this is achieved by introducing the following notation for the Schwinger bosons

$$b_{i\sigma} = (\sqrt{N}x_i, b_i^{\tilde{m}}) \quad \text{where} \quad \tilde{m} = 2,...,N\ . \tag{3.9}$$

The first component is thus a classical field. If $x \neq 0$ it signals condensation which causes long range order to appear. Following Ref. Arovas and Auerbach (1988); Auerbach and Arovas (1988); Sachdev (1992) we can integrate out the Schwinger

bosons and the zero-temperature mean field energy assumes the following form

$$\begin{aligned}
\frac{E_{MF}}{NN_u} &= \frac{1}{N_u}\sum_{\mathbf{k},\mu=1,..,N_s}\omega_\mu(\mathbf{k}) - N_s\lambda(1+\kappa) + \lambda\sum_{i'\sigma}|x_{i\sigma}|^2 \\
&+ \frac{J}{2}\sum_{(ij)'}\left[|q_{ij}|^2 - \left(q^*_{ij}\epsilon_{\sigma\sigma'}x_{i\sigma}x_{j\sigma'}\right) + \text{h.c.}\right)\Big] \\
&+ \frac{iD}{4}\sum_{(ij)'}(p^*_{ij}q_{ij} - q^*_{ij}p_{ij}) \\
&- \frac{iD}{4}\sum_{(ij)'}(p^*_{ij}\epsilon_{\sigma\sigma'}x_{i\sigma}x_{j\sigma'} + q_{ij}\tau^x_{\sigma\sigma'}x^*_{i\sigma}x^*_{j\sigma'}) \\
&+ \frac{iD}{4}\sum_{(ij)'}(p_{ij}\epsilon_{\sigma\sigma'}x^*_{i\sigma}x^*_{j\sigma'} + q^*_{ij}\tau^x_{\sigma\sigma'}x_{i\sigma}x_{j\sigma'}) \qquad (3.10)
\end{aligned}$$

where $\sum_{i'}$ denotes the sum over all sites within one unit cell. In the following we solve the self-consistency equations according to

$$\begin{aligned}
\kappa &= \langle b^*_{i\sigma}b_{i\sigma}\rangle_{MF} \\
q_{ij} &= \langle Q_{ij}\rangle_{MF}\ , \\
p_{ij} &= \langle P_{ij}\rangle_{MF}\ . \qquad (3.11)
\end{aligned}$$

with the Hamiltonian defined in Eq. (3.6).

Our solution of the mean-field equations follows previous work (Sachdev, 1992; Wang and Vishwanath, 2006), which classified physically different Z_2 spin liquid solutions without the DM interactions. We found that these solutions have a natural generalization in the presence of DM terms, with values of the p_{ij} which reflect the symmetries of the q_{ij}. Two stable solutions were found in previous work, with only two possibly distinct values of q_{ij} as illustrated in Fig. 3.2. Including the DM interactions, these solutions extended to

(*i*) $q_1 = q_2$ real, $p_1 = p_2$ pure imaginary: upon increasing κ, the Schwinger bosons condense at $\mathbf{k} = 0$, with the spins at angles of 120° to each other within the unit cell. This states is therefore called the $\mathbf{k} = 0$ state.

(*ii*) $q_1 = -q_2$ real, $p_1 = -p_2$ pure imaginary: upon increasing κ, the Schwinger bosons condense at wavevector $\mathbf{k} = \pm(2\pi/3, 0)$ into a state which is called the $\sqrt{3}\times\sqrt{3}$ antiferromagnet, characterized by an enlarged unit cell.

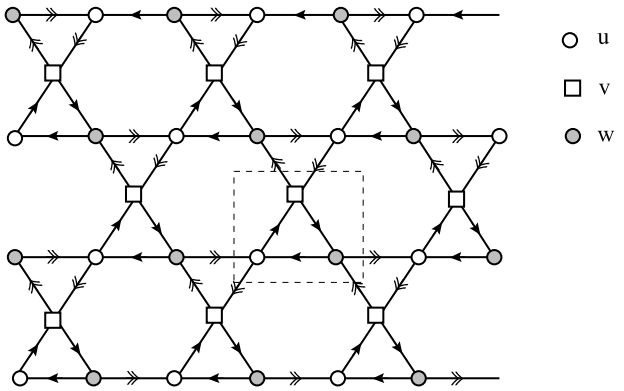

Figure 3.2: We take a unit cell of three sites, labeled u, v, w. The arrows indicate the values of the oriented variables q_{ij}. The links with single arrows have $q_{ij} = q_1$, while those with double arrows have $q_{ij} = q_2$. The P_{ij} are unoriented, and take values p_1 and p_2 on these links respectively.

Solutions with larger unit cells can be present with additional frustrating interactions (Wang and Vishwanath, 2006), but we will not consider them here.

3.2.1 Phase diagram

Our phase diagram is shown in Fig. 3.2.1 as a function of $\kappa = n_b/N$ (which corresponds to the spin size) and the parameter D/J. Our phase diagram is similar to that obtained recently by Messio *et al.* (Messio et al., 2010). They also considered solutions with a larger unit cell which were stable over some portion of the phase diagram.

We start with a discussion of the classical limit. While for $D = 0$ the long-range ordered state of the $\sqrt{3} \times \sqrt{3}$ type is generically preferred (Sachdev, 1992), infinitesimal D favors the so-called $\mathbf{k} = 0$ state. This is reproduced by our mean-field equations in the large spin limit $\kappa \to \infty$. For finite values of κ there is a small slab in which long-range order of the $\sqrt{3} \times \sqrt{3}$ type is favored over the $\mathbf{k} = 0$. These states are separated by a first order transition driven by the ratio D/J.

A similar behavior appears for the corresponding spin liquid states at small κ. The $q_1 = -q_2$ is favored at small D/J, and then undergoes a first order transition to

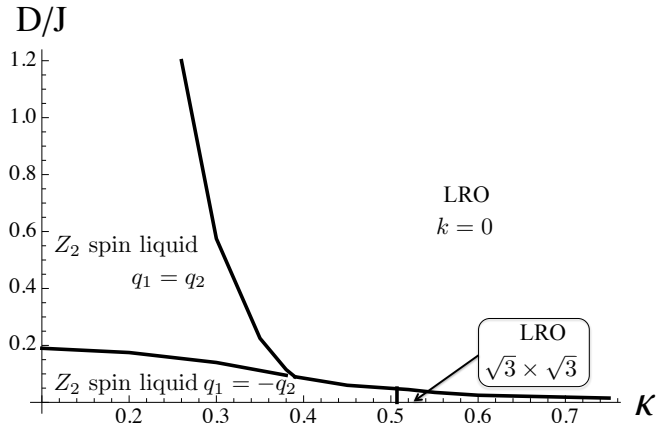

Figure 3.3: Phase diagram in the $N \to \infty$ limit of the Sp(N) theory. The x-axis shows $\kappa = 2S/N$ and the y-axis D/J. The phases have long-range magnetic order type (LRO), or gapped Z_2 spin liquids. The thick line is a first-order transition, while the thin lines are second-order transitions: the transition to the $\mathbf{k} = 0$ LRO state is described in Section 3.3. The limit of $D/J \to 0$ reduces to the results presented in Ref. Sachdev (1992).

the $q_1 = q_2$ state at large D/J.

In exact diagonalization studies of the spin $S = \frac{1}{2}$ kagome antiferromagnet with DM interactions a second order phase transition between a phase with short ranged $\mathbf{k} = 0$ correlations (Jiang et al., 2008; Laeuchli and Lhuillier, 2009) (obtained in the pure Heisenberg case) and phase with $\mathbf{k} = 0$ long range order was found (Messio et al., 2010). Such a transition is also present in our mean-field theory, which therefore can be used for a study of critical properties in Section 3.3.

3.3 Quantum criticality

We will consider only the transition out of the $q_1 = q_2$ spin liquid, because that is what is seen in the numerical studies (Cépas et al., 2008). The corresponding transition out of the $q_1 = -q_2$ spin liquid can be treated in a similar manner. Throughout this section we will consider the physical SU(2) antiferromagnet directly, and not take

the large N limit. The method followed below has been reviewed in a more general context in Ref. Sachdev (2010).

Since we are at $\mathbf{k} = 0$, we can write the effective action for the bosons by making the small momentum expansion of the matrix in Eq. (3.34). We take 3 sites, u, v, w, in each unit cell (see Fig. 3.2), and then take the continuum limit of the saddle-point Lagrangian. We write the boson operators on these sites as $b_{u\sigma} = U_\sigma$, $b_{v\sigma} = V_\sigma$ etc., and set $q_1 = q_2 = q$, and $p_1 = p_2 = ip$ with q and p real. Then, we write the final Lagrangian in the form

$$\mathcal{L} = \mathcal{L}_H + \mathcal{L}_{DM} \tag{3.12}$$

representing the contributions of the Heisenberg exchange and the DM coupling, respectively.

From Eq. (3.34) we obtain the Lagrangian in the absence of a DM term (which describes the $\mathbf{k} = \mathbf{0}$ solution of Ref. Sachdev (1992)):

$$\begin{aligned}
\mathcal{L}_H &= U_\sigma^* \frac{\partial U_\sigma}{\partial \tau} + V_\sigma^* \frac{\partial V_\sigma}{\partial \tau} + W_\sigma^* \frac{\partial W_\sigma}{\partial \tau} \\
&\quad + \lambda \left(|U_\sigma|^2 + |V_\sigma|^2 + |W_\sigma|^2 \right) \\
&\quad - Jq\epsilon_{\sigma\sigma'} \left(U_\sigma V_{\sigma'} + V_\sigma W_{\sigma'} + W_\sigma U_{\sigma'} \right) + \text{c.c.} \\
&+ \frac{Jq}{2} \epsilon_{\sigma\sigma'} \left(\partial_1 U_\sigma \partial_1 V_{\sigma'} + \partial_2 V_\sigma \partial_2 W_{\sigma'} + \partial_3 W_\sigma \partial_3 U_{\sigma'} \right) \\
&\quad + \text{c.c.}
\end{aligned} \tag{3.13}$$

where ∂_i is the gradient along the direction $\mathbf{e}_i$ in Eq. (3.33).

We now perform a unitary transformation to new variables X_σ, Y_σ, Z_σ. These are

chosen to diagonalize only the non-gradient terms in $\mathcal{L}$.

$$\begin{aligned}\begin{pmatrix} U_\sigma \\ V_\sigma \\ W_\sigma \end{pmatrix} &= \frac{Z_\sigma}{\sqrt{6}}\begin{pmatrix} 1 \\ \zeta \\ \zeta^2 \end{pmatrix} + \epsilon_{\sigma\sigma'}\frac{Z^*_{\sigma'}}{\sqrt{6}}\begin{pmatrix} i \\ i\zeta^2 \\ i\zeta \end{pmatrix} \\ &+ \frac{Y_\sigma}{\sqrt{6}}\begin{pmatrix} 1 \\ \zeta \\ \zeta^2 \end{pmatrix} + \epsilon_{\sigma\sigma'}\frac{Y^*_{\sigma'}}{\sqrt{6}}\begin{pmatrix} -i \\ -i\zeta^2 \\ -i\zeta \end{pmatrix} \\ &+ \frac{X_\sigma}{\sqrt{3}}\begin{pmatrix} 1 \\ 1 \\ 1 \end{pmatrix}. \end{aligned} \tag{3.14}$$

where $\zeta \equiv e^{2\pi i/3}$. The tensor structure above makes it clear that this transformation is rotationally invariant, and that X_σ, Y_σ, Z_σ transform as spinors under SU(2) spin rotations. Inserting Eq. (3.14) into $\mathcal{L}_H$ we find

$$\begin{aligned}\mathcal{L}_H &= X^*_\sigma\frac{\partial X_\sigma}{\partial\tau} + Y^*_\sigma\frac{\partial Z_\sigma}{\partial\tau} + Z^*_\sigma\frac{\partial Y_\sigma}{\partial\tau} + (\lambda+\sqrt{3}Jq)|Z_\sigma|^2 \\ &\quad + (\lambda-\sqrt{3}Jq)|Y_\sigma|^2 + \lambda|X_\sigma|^2 \\ &\quad + \frac{Jq\sqrt{3}}{2}\left(|\partial_x Z_\sigma|^2 + |\partial_y Z_\sigma|^2\right) + \ldots \end{aligned} \tag{3.15}$$

The ellipses indicate omitted terms involving spatial gradients in the X_σ and Y_σ which we will not keep track of. This is because the fields Y_σ and X_σ are massive relative to Z_σ (for $q < 0$ which is the case in our mean-field solution), and so can be integrated out. This yields the effective Lagrangian

$$\begin{aligned}\mathcal{L}^Z_H &= \frac{1}{(\lambda-\sqrt{3}Jq)}|\partial_\tau Z_\sigma|^2 + \frac{Jq\sqrt{3}}{2}\left(|\partial_x Z_\sigma|^2 + |\partial_y Z_\sigma|^2\right) \\ &\quad + (\lambda+\sqrt{3}Jq)|Z_\sigma|^2 + \ldots \end{aligned} \tag{3.16}$$

Note that the omitted spatial gradient terms in X_σ, Y_σ do contribute a correction to the spatial gradient term in Eq. (3.16), and we have not accounted for this. This Lagrangian shows that the mean-field theory has a transition to magnetic order at $\lambda = |\sqrt{3}Jq|$, which agrees with earlier results (Sachdev, 1992).

The effective Lagrangian $\mathcal{L}_H^Z$ is almost the complete solution for the critical theory in the system without the DM interactions. However, we also need higher order terms in Eq. (3.16), which will arise from including the fluctuations of the gapped fields Q and λ. Rather than computing these from the microscopic Lagrangian, it is more efficient to deduce their structure from symmetry considerations. The representation in Eq. (3.14), and the connection of the U, V, W to the lattice degrees of freedom, allow us to deduce the following symmetry transformations of the X, Y, Z:

- Under a global spin rotation by the SU(2) matrix $g_{\sigma\sigma'}$, we have $Z_\sigma \to g_{\sigma\sigma'} Z_{\sigma'}$, and similarly for Y, and Z. When DM interactions are included, the global symmetry is reduced to U(1) rotations about the z axis, under which

$$\begin{aligned} Z_\uparrow \to e^{i\theta} Z_\uparrow \quad &, \quad Z_\downarrow \to e^{-i\theta} Z_\downarrow \\ Y_\uparrow \to e^{i\theta} Y_\uparrow \quad &, \quad Y_\downarrow \to e^{-i\theta} Y_\downarrow \\ X_\uparrow \to e^{i\theta} X_\uparrow \quad &, \quad X_\downarrow \to e^{-i\theta} X_\downarrow. \end{aligned} \tag{3.17}$$

- Under a 120° lattice rotation, we have $U_\sigma \to V_\sigma$, $V_\sigma \to W_\sigma$, $W_\sigma \to U_\sigma$. From (3.14), we see that this symmetry is realized by

$$Z_\sigma \to \zeta Z_\sigma \ , \ Y_\sigma \to \zeta Y_\sigma \ , \ X_\sigma \to X_\sigma. \tag{3.18}$$

  Note that this is distinct from the SU(2) rotation because $\det(\zeta) \neq 1$.

- Under time-reversal, we have $U_\sigma \to \epsilon_{\sigma\sigma'} U^*_{\sigma'}$, and similarly for V_σ, W_σ. This is realized in Eq. (3.14) by

$$Z_\sigma \to i Z_\sigma \ , \ Y_\sigma \to -i Y_\sigma \ , \ X_\sigma \to \epsilon_{\sigma\sigma'} X^*_{\sigma'}. \tag{3.19}$$

  In particular, note that $Z_\uparrow$ does not map to $Z_\downarrow$ under time-reversal.

These symmetry operators make it clear that the only allowed quartic term for the Heisenberg Hamiltonian is $\left(\sum_\sigma |Z_\sigma|^2\right)^2$: this implies that the Z_2 spin liquid to antiferromagnetic order transition of this model is in the universality class of the O(4) model (Chubukov et al., 1994b; Chubukova et al., 1994).

Let us now include the DM interactions. From Eq. (3.34), we see that

$$\mathcal{L}_{DM} = i\frac{Dq}{2}\tau^x_{\sigma\sigma'}\left(U_\sigma V_{\sigma'} + V_\sigma W_{\sigma'} + W_\sigma U_{\sigma'}\right) + \text{c.c.}. \tag{3.20}$$

We have dropped a term proportional to Dp which has the same structure as the terms in Eq. (3.15), and ignored spatial gradients. In terms of the fields in Eq. (3.14), this takes the simple form

$$\begin{aligned}\mathcal{L}_{DM} &= \frac{Dq}{2}\Big(i\tau^x_{\sigma\sigma'}X_\sigma X_{\sigma'} + \text{c.c.} \\ &\qquad - Z^*_\sigma\tau^z_{\sigma\sigma'}Z_{\sigma'} + Y^*_\sigma\tau^z_{\sigma\sigma'}Y_{\sigma'}\Big),\end{aligned} \tag{3.21}$$

and it can be verified that these terms are invariant under Eqs. (3.17,3.18,3.19). As before, we now integrate out X_σ and Y_σ from $\mathcal{L}_H + \mathcal{L}_{DM}$ in Eqs. (3.15) and (3.21). We obtain a Lagrangian with the same structure as Eq. (3.16), but all couplings become dependent upon σ; in other words, we have 2 separate XY models for $Z_\uparrow$ and $Z_\downarrow$. Performing a careful analysis of allowed higher order terms as restricted by the symmetry constraints discussed above, and after appropriate rescalings of the spatial, temporal, and field scales, we obtain the field theory with the Lagrangian

$$\begin{aligned}\mathcal{L}_Z &= |\partial_\tau Z_\uparrow|^2 + |\boldsymbol{\nabla} Z_\uparrow|^2 + s_\uparrow|Z_\uparrow|^2 + u_\uparrow|Z_\uparrow|^4 \\ &+ |\partial_\tau Z_\downarrow|^2 + |\boldsymbol{\nabla} Z_\downarrow|^2 + s_\downarrow|Z_\downarrow|^2 + u_\downarrow|Z_\downarrow|^4 \\ &+ v|Z_\uparrow|^2|Z_\downarrow|^2 + w\left((Z_\uparrow Z_\downarrow)^6 + (Z^*_\uparrow Z^*_\downarrow)^6\right).\end{aligned} \tag{3.22}$$

Note that $s_\uparrow \neq s_\downarrow$ in general (and similarly for $u_{\uparrow,\downarrow}$ etc.), and equality is not required by the time-reversal symmetry in Eq (3.19). Time-reversal symmetry does prohibit a term $\sim (Z_\uparrow Z_\downarrow)^3$ which is allowed by the other symmetries. Thus we expect only one of $Z_\uparrow$ or $Z_\downarrow$ to condense at the quantum critical point: as we will see from the analysis of observables in Section 3.3.1, this transition does indeed correspond to the development of spiral magnetic order in the x-y plane. The choice between $Z_\uparrow$ and $Z_\downarrow$ is controlled by the sign of D.

Eq. (3.22) also contains terms which couple the two XY models to each other. The lowest allowed term, v, couples the energy densities and does not have any important effects. More interesting is the w term, which shows that the global symmetry is not

O(2)⊗O(2) but O(2)⊗$\mathbb{Z}_3$. In the magnetically ordered phase with $\langle Z_\uparrow \rangle \neq 0$ (say), this term will induce a small cubic ordering field $\sim Z_\downarrow^6$ in the XY model for $Z_\downarrow$. However, the action for $Z_\downarrow$ has a 'mass' term $s_\downarrow$ with a positive co-efficient, and this sixth order term will not immediately induce ordering in $Z_\downarrow$; *i.e.* a magnetic phase with $\langle Z_\uparrow \rangle \neq 0$ and $\langle Z_\downarrow \rangle = 0$ has a finite range of stability. Thus close to the transition we can neglect the $Z_\downarrow$ field entirely, and transition is in the universality class of the three-dimensional XY model.

The choice above of $Z_\uparrow$ over $Z_\downarrow$ gives the incorrect appearance that we are breaking the spin reflection symmetry $S_z \to -S_z$ of $\mathcal{H}$, suggesting the appearance of a net z ferromagnetic moment. However, notice that the theory of $Z_\uparrow$ is relativistic, and so contains both spinons and anti-spinons which carry $S_z = +1/2$ and $S_z = -1/2$ respectively. The spinon of $Z_\downarrow$ also carries $S_z = -1/2$, and this is degenerate with the anti-spinon of $Z_\uparrow$ in the O(4) invariant theory in Eq. (3.16). It is this latter degeneracy which is lifted by the DM interactions, which induce a vector spin chirality along the z direction (Isakov et al., 2005) (as we will see below). We will also see there is no net ferromagnetic moment, because time-reversal symmetry is preserved.

3.3.1 Observables

To determine the operators corresponding to the ferromagnetic moment, let us couple a uniform external field $\mathbf{h}$ to the lattice Hamiltonian. This adds to the continuum Lagrangian the term

$$\mathcal{L}_h = -\mathbf{h} \cdot \boldsymbol{\tau}_{\sigma\sigma'} \left(U_\sigma^* U_{\sigma'} + V_\sigma^* V_{\sigma'} + W_\sigma^* W_{\sigma'} \right) \tag{3.23}$$

Inserting the parameterization in Eq. (3.14) this becomes

$$\mathcal{L}_h = -\mathbf{h} \cdot \boldsymbol{\tau}_{\sigma\sigma'} \left(X_\sigma^* X_{\sigma'} + Y_\sigma^* Z_{\sigma'} + Z_\sigma^* Y_{\sigma'} \right) \tag{3.24}$$

We now need to integrate out X_σ and Y_σ in the Lagrangian $\mathcal{L}_H + \mathcal{L}_{DM} + \mathcal{L}_h$ defined by the sum of Eqs. (3.15), (3.21), and (3.24), and collect the terms linear in $\mathbf{h}$. Without the DM coupling, we obtain

$$\sim \mathbf{h} \cdot \boldsymbol{\tau}_{\sigma\sigma'} \left(Z_\sigma^* \frac{\partial Z_{\sigma'}}{\partial \tau} - \frac{\partial Z_\sigma^*}{\partial \tau} Z_{\sigma'} \right) \tag{3.25}$$

Comparing with $\mathcal{L}_H^Z$ in Eq. (3.16) we see that this is just the coupling to the conserved SU(2) charges of the O(4) model: this is the usual term which determines the magnetic susceptibility of the Heisenberg antiferromagnet (Chubukov et al., 1994b; Chubukova et al., 1994). Upon including the effects of $\mathcal{L}_{DM}$ we find that the essential structure of Eq. (3.25) does not change: the $\boldsymbol{\tau}$ matrices get multiplied by some σ-dependent factors $\boldsymbol{\tau}_{\sigma\sigma'} \to f_\sigma \boldsymbol{\tau}_{\sigma\sigma'} f_{\sigma'}$ which do not modify the scaling considerations. No term with a new structure is generated by the DM coupling. It can now be seen that these expressions have vanishing expectation values under $\mathcal{L}_Z$ in Eq. (3.22), and so there is no net ferromagnetic moment in the absence of an external field.

We now turn to the antiferromagnetic order parameter; for a coplanar antiferromagnet, this is described by

$$\mathbf{S}_i \propto \mathbf{N}_1 \cos(\mathbf{Q} \cdot \mathbf{r}_i) + \mathbf{N}_2 \sin(\mathbf{Q} \cdot \mathbf{r}_i), \tag{3.26}$$

where $\mathbf{N}_{1,2}$ are 2 orthogonal vectors representing the spiral order, and $\mathbf{Q}$ is wavevector at which the spin structure factor is peaked. For our model, we can see that

$$\mathbf{N}_1 + i\mathbf{N}_2 = \mathbf{S}_u + \zeta \mathbf{S}_v + \zeta^2 \mathbf{S}_w. \tag{3.27}$$

Using Eq. (3.14), and keeping only the lowest order term, we therefore obtain (Chubukov et al., 1994b; Chubukova et al., 1994)

$$\mathbf{N}_1 + i\mathbf{N}_2 = \begin{pmatrix} i(Z_\uparrow^2 - Z_\downarrow^2)/2 \\ -(Z_\uparrow^2 + Z_\downarrow^2)/2 \\ -iZ_\uparrow Z_\downarrow \end{pmatrix}; \tag{3.28}$$

in a notation that makes the rotational invariance evident, this relationship is

$$\mathbf{N}_1 + i\mathbf{N}_2 = \frac{i}{2} \epsilon_{\alpha\beta} \boldsymbol{\tau}_{\beta\sigma} Z_\sigma Z_\alpha. \tag{3.29}$$

Note that a phase with $\langle Z_\uparrow \rangle \neq 0$ and $\langle Z_\downarrow \rangle = 0$ has spiral order in the x-y plane.

To complete the list of operators which are quadratic in the Z_σ, we consider the vector spin chirality (Isakov et al., 2005). This is defined here by

$$\mathbf{S}_u \times \mathbf{S}_v + \mathbf{S}_v \times \mathbf{S}_w + \mathbf{S}_w \times \mathbf{S}_u. \tag{3.30}$$

Using Eq. (3.14) we find that the leading operator mapping to vector spin chirality is (dropping an overall factor of $|Z_\uparrow|^2 + |Z_\downarrow|^2$)

$$Z^*_\sigma \boldsymbol{\tau}_{\sigma\sigma'} Z_{\sigma'}. \tag{3.31}$$

Note that in the presence of the DM term, the couplings in the effective theory (3.22) imply that the z component of the vector spin chirality is always non-zero.

3.3.2 Critical properties

Let us assume the transition to magnetic order proceeds via the condensation of $Z_\uparrow$. The transition is in the XY universality class, and the dimension of the antiferromagnetic order parameter is

$$\dim[\mathbf{N}_1] = \dim[\mathbf{N}_2] = \dim[Z^2_\uparrow] = \frac{1+\overline{\eta}}{2} \, . \tag{3.32}$$

The value of the exponent $\overline{\eta}$ can be read off from results for the three-dimensional XY model (Campostrini et al., 2001; Calabrese et al., 2002), and we obtain $\overline{\eta} \approx 1.474$. The antiferromagnetic susceptibility will diverge at the critical point as $T^{-(2-\overline{\eta})}$. We note the recent work of Ref. Grover and Senthil (2009) in a different context, which also considered a model with an XY critical point at which the physically measurable magnetic order was the square of the XY field.

The behavior of the uniform magnetic susceptibility follows from the scaling dimension of the operators in Eq. (3.25). For $\mathbf{h}$ along the z direction, the magnetization is the just the conserved U(1) charge of the XY model: so (Chubukov et al., 1994a) it has scaling dimension 2, and the susceptibility $\sim T$. For $\mathbf{h}$ along the x or y directions, we have to integrate out $Z_\downarrow$, and then the lowest dimension operator coupling to the square of the field is $|Z_\uparrow|^2$. This means that the susceptibility only has a weak singularity at the quantum critical point given by that in $\langle |Z_\uparrow|^2 \rangle$: at the quantum critical point, there is a non-analytic term $\sim T^{3-1/\nu}$, above an analytic background.

3.4 Conclusion

We have presented a theory for the quantum critical point between a Z_2 spin liquid and an ordered antiferromagnet for the kagomé antiferromagnet in the presence of DM interactions. The critical theory is just the three dimensional XY model. However, the XY order parameter carries a Z_2 gauge charge, and so it is not directly observable. In particular, the antiferromagnetic order parameter is the square of the XY order parameter. Specifically, the theory is given by $\mathcal{L}_Z$ in Eq. (3.22), and its observables are described in Section 3.3.1.

It is interesting to compare our results with recent observations of quantum critical scaling in $ZnCu_3(OH)_6Cl_2$ by Helton *et al.* (Helton et al., 2010). Their neutron scattering measurements show an antiferromagnetic susceptibility which scales as $T^{-0.66}$. This is actually in reasonable agreement with our theory, which has a susceptibility $\sim T^{-0.526}$. However, they also observe a similar divergence in measurements of the uniform magnetization, while our theory only predicts a very weak singularity. We suspect that this difference is due to the present of impurities (Olariu et al., 2008; Gregor and Motrunich, 2008; Rozenberg and Chitra, 2008; Lee et al., 2007), which can mix the uniform and staggered components. A complete study of impurities near the quantum critical point described above is clearly called for.

We thank L. Messio, O. Cépas, C. Lhuillier, and E. Vicari for useful discussions.

3.A Microscopic form of the Hamiltonian

We here give explicit expressions for the Hamiltonian introduced in Sec. 3.2. We introduce the following set of unit vectors

$$\begin{aligned} \mathbf{e}_1 &= a\left(\frac{1}{2}, \frac{\sqrt{3}}{2}\right) \\ \mathbf{e}_2 &= a\left(\frac{1}{2}, -\frac{\sqrt{3}}{2}\right) \\ \mathbf{e}_3 &= a(-1, 0) \end{aligned} \tag{3.33}$$

which allows to express $k_i = \mathbf{k}\cdot\mathbf{e}_i$. In the following we concentrate on the states with 3 sites per unit cell. In that case the vector Ψ introduced in Eq. (3.7) has 6 components and the matrix $\mathbb{C}$ consequently is a 3×3 matrix with the following entries:

$$\begin{aligned}
\mathbb{C}_{uv} &= \frac{J}{2}q_1^* e^{ik_1} + \frac{J}{2}q_2^* e^{-ik_1} + \frac{iD}{4}p_1^* e^{ik_1} + \frac{iD}{4}q_1^* e^{ik_1} + \frac{iD}{4}p_2^* e^{-ik_1} + \frac{iD}{4}q_2^* e^{-ik_1} \\
\mathbb{C}_{uw} &= -\frac{J}{2}q_1^* e^{-ik_3} - \frac{J}{2}q_2^* e^{ik_3} - \frac{iD}{4}p_1^* e^{-ik_3} + \frac{iD}{4}q_1^* e^{-ik_3} - \frac{iD}{4}p_2^* e^{ik_3} + \frac{iD}{4}q_2^* e^{ik_3} \\
\mathbb{C}_{vw} &= \frac{J}{2}q_1^* e^{ik_2} + \frac{J}{2}q_2^* e^{-ik_2} + \frac{iD}{4}p_1^* e^{ik_2} + \frac{iD}{4}q_1^* e^{ik_2} + \frac{iD}{4}p_2^* e^{-ik_2} + \frac{iD}{4}q_2^* e^{-ik_2} \\
\mathbb{C}_{vu} &= -\frac{J}{2}q_1^* e^{-ik_1} - \frac{J}{2}q_2^* e^{ik_1} - \frac{iD}{4}p_1^* e^{-ik_1} + \frac{iD}{4}q_1^* e^{-ik_1} - \frac{iD}{4}p_2^* e^{ik_1} + \frac{iD}{4}q_2^* e^{ik_1} \\
\mathbb{C}_{wv} &= -\frac{J}{2}q_1^* e^{-ik_2} - \frac{J}{2}q_2^* e^{ik_2} - \frac{iD}{4}p_1^* e^{-ik_2} + \frac{iD}{4}q_1^* e^{-ik_2} - \frac{iD}{4}p_2^* e^{ik_2} + \frac{iD}{4}q_2^* e^{ik_2} \\
\mathbb{C}_{wu} &= \frac{J}{2}q_1^* e^{ik_3} + \frac{J}{2}q_2^* e^{-ik_3} + \frac{iD}{4}p_1^* e^{ik_3} + \frac{iD}{4}q_1^* e^{ik_3} + \frac{iD}{4}p_2^* e^{-ik_3} + \frac{iD}{4}q_2^* e^{-ik_3} \,.
\end{aligned} \tag{3.34}$$

3.B Dispersion of the lowest excited spinon state

For $q_1 = q_2$ and $D = 0$, the ground state is doubly degenerate. The degeneracy splits as D moves away from 0. In all cases, the minimum excitation energy occurs at $\mathbf{k} = 0$.

Fig. 3.4 plots the momentum dependence of the energy of the lowest excited spinon at $D/J = 0.3, \kappa = 0.2$ and $D/J = 0.3, \kappa = 0.4$. In the former case, there is a finite energy gap at $\mathbf{k} = 0$ making it a gapped spin liquid. On the other hand, with a larger κ value, it shows long-range magnetic order. The energy gap at $\mathbf{k} = 0$ is closed and condensation occurs at this wave vector.

For $q_1 = -q_2$, there is a unique ground state even for $D = 0$. Energy minima is at $\mathbf{k} = \pm(2\pi/3, 0)$. Fig. 3.5 shows the dispersion of the lowest lying state of the spin liquid with $D/J = 0.03, \kappa = 0.55$ and a case with long range ordering with a higher D/J.

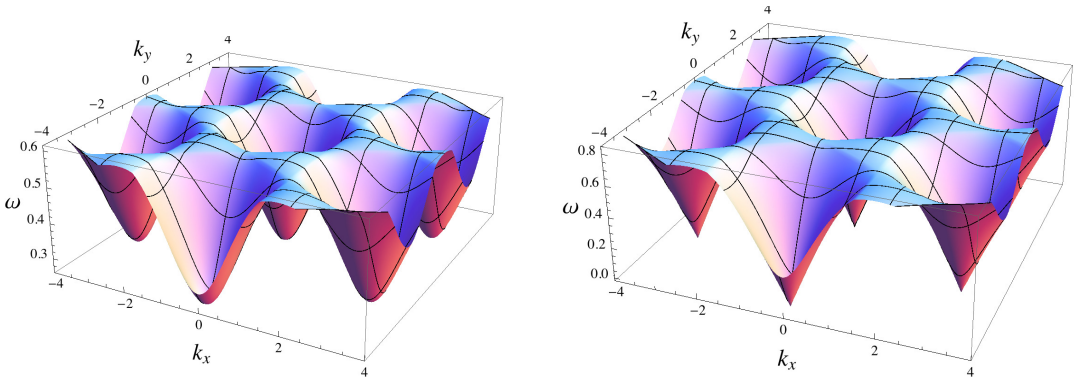

Figure 3.4: Left : Momentum dependence of the energy $\omega(k)$ of the lowest excited spinon state of the kagome-lattice quantum antiferromagnet for the $q_1 = q_2$ state at $D/J = 0.3, \kappa = 0.2$. The minimum excitation energy is at $\mathbf{k} = 0$ and has a finite energy gap. Right : Dispersion of the lowest excited spinon state for the $q_1 = q_2$ state at $D/J = 0.3, \kappa = 0.4$. The energy gap closes at $\mathbf{k} = 0$ and condensation occurs.

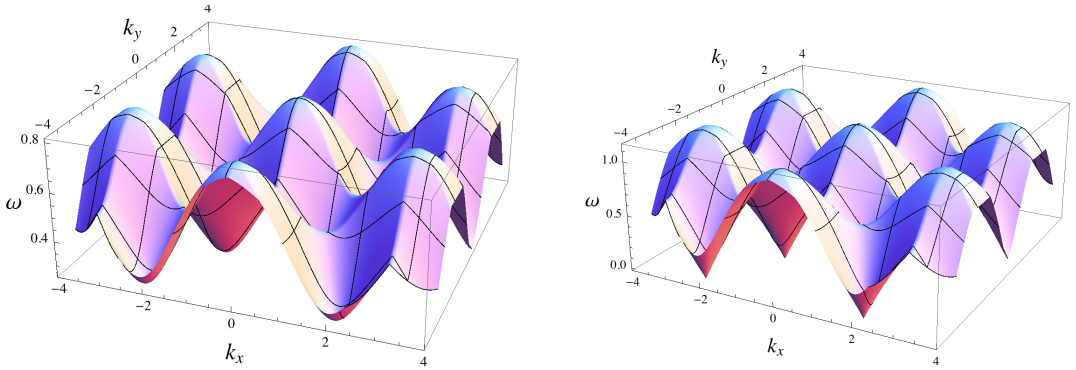

Figure 3.5: Left: disordered $q_1 = -q_2, D/J = 0.05, \kappa = 0.3$ Right : ordered $q_1 = -q_2, D/J = 0.03, \kappa = 0.55$

3.C Condensation

For the $q_1 = q_2$ state Eq. (3.14) leads to the following parametrization of the condensation of $Z_\downarrow$ field at $\mathbf{k} = 0$.

$$\begin{aligned}
\begin{pmatrix} x_u^\uparrow \\ x_u^\downarrow \end{pmatrix} &= \ell \begin{pmatrix} i \\ 1 \end{pmatrix} \\
\begin{pmatrix} x_v^\uparrow \\ x_v^\downarrow \end{pmatrix} &= \ell \begin{pmatrix} i\zeta^2 \\ \zeta \end{pmatrix} \\
\begin{pmatrix} x_w^\uparrow \\ x_w^\downarrow \end{pmatrix} &= \ell \begin{pmatrix} i\zeta \\ \zeta^2 \end{pmatrix}
\end{aligned} \tag{3.35}$$

where ℓ is the size of the condensate. Condensation of $Z_\uparrow$ can be written similarly. For $D > 0$, $Z_\downarrow$ field condensation is energetically favored while the opposite is true for $D < 0$. The two condensations are degenerate for $D = 0$.

For the $q_1 = -q_2$ state, condensation occurs at $\tilde{k} \equiv \vec{k} = (2\pi/3, 0)$ or $\vec{k} = -\tilde{k}$. The two states have identical energies and the condensation is spontaneously chosen. Similar analysis to Eqns. (3.13) and (3.14) gives the eigenvectors corresponding to the lowest lying state. For $\vec{k} = \tilde{k}$ this is $(i, -i, i, 1, -1, 1)$ while for $\vec{k} = -\tilde{k}$ the corresponding eigenvector is $(-i, i, -i, 1, -1, 1)$. Therefore condensations can be parametrized as

$$\begin{aligned}
\begin{pmatrix} x_{k\uparrow}^u \\ x_{-k\downarrow}^u \end{pmatrix} &= \ell \begin{pmatrix} i \\ 1 \end{pmatrix} \\
\begin{pmatrix} x_{k\uparrow}^v \\ x_{-k\downarrow}^v \end{pmatrix} &= \ell \begin{pmatrix} -i \\ -1 \end{pmatrix} \\
\begin{pmatrix} x_{k\uparrow}^w \\ x_{-k\downarrow}^w \end{pmatrix} &= \ell \begin{pmatrix} i \\ 1 \end{pmatrix}
\end{aligned} \tag{3.36}$$

for $\vec{k} = \tilde{k}$, and

$$\begin{aligned}
\begin{pmatrix} x^u_{k\uparrow} \\ x^u_{-k\downarrow} \end{pmatrix} &= \ell \begin{pmatrix} -i \\ 1 \end{pmatrix} \\
\begin{pmatrix} x^v_{k\uparrow} \\ x^v_{-k\downarrow} \end{pmatrix} &= \ell \begin{pmatrix} i \\ -1 \end{pmatrix} \\
\begin{pmatrix} x^w_{k\uparrow} \\ x^w_{-k\downarrow} \end{pmatrix} &= \ell \begin{pmatrix} -i \\ 1 \end{pmatrix}
\end{aligned} \tag{3.37}$$

for $\vec{k} = -\tilde{k}$.

Chapter 4

Vison states and confinement transitions of $\mathbb{Z}_2$ spin liquids on the kagome lattice

4.1 Introduction

The recent DMRG study of Yan *et al.* (Yan et al., 2011) has provided striking evidence for a spin liquid ground state for the $S = 1/2$ Heisenberg antiferromagnet on the kagome lattice. Yan *et al.* found a gap to all excitations, and it is plausible that their ground state realizes a $\mathbb{Z}_2$ spin liquid. (Read and Sachdev, 1991; Wen, 1991; Sachdev, 1992; Wang and Vishwanath, 2009; Tay and Motrunich, 2011; Lu et al., 2011; Iqbal et al., 2011b,a)

The results of Yan *et al.* also indicate the presence of proximate valence bond solid (VBS) states in which the space group symmetry of the kagome lattice is broken, and the fractionalized excitations of the spin liquid are confined into integer spin states. The confinement quantum phase transition should be accessible in extended models with further neighbor exchange interactions, and numerical studies of such transitions can serve as a valuable probe of characteristics of the spin liquid.

This paper shall classify elementary vortex excitations of the $\mathbb{Z}_2$ spin liquid, carry-

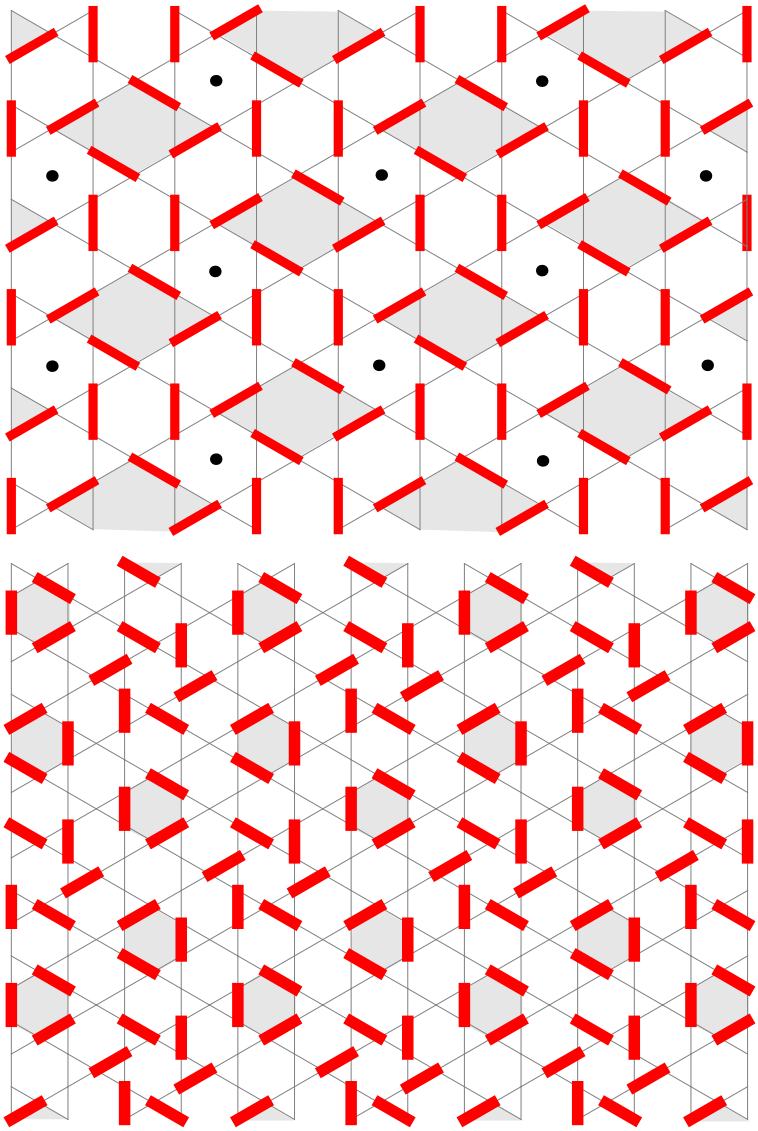

Figure 4.1: Visualization of two different valence bond solid states as dimer coverings of the kagome lattice. Each dimer represents a frustrated bond in the ordered phase of the corresponding Ising model on the dual dice lattice. The left pattern, representing the VBS 1_{F} phase (see text), is a hardcore dimer covering with a 12-site unit cell that maximizes the number of perfectly flippable diamonds (highlighted in gray). Note however, that the choice of diamonds is not unique because the dimer pattern is symmetric with respect to $\pi/3$-rotations around the hexagons marked by a black dot. The pattern on the right represents the VBS 1_{A} phase (see text), has a 36-site unit cell and maximizes the number of perfectly flippable hexagons (highlighted in gray).

ing $\mathbb{Z}_2$ magnetic flux (Read and Chakraborty, 1989; Read and Sachdev, 1991; Senthil and Fisher, 2000), often called 'visons', which are analogous to the Abrikosov vortices of BCS superconductors (Sachdev and Read, 1991) (after electromagnetism is replaced by strong coupling to a compact U(1) gauge theory). We will compute their projective symmetry group (Wen, 2002) (PSG), and their spectrum using an effective frustrated Ising model. (Jalabert and Sachdev, 1991) Note that the Ising 'spin' has nothing to do with the $S = 1/2$ spin of the underlying antiferromagnet, and it is instead the creation or annihliation operator of the vortex excitation which is centered on sites of a lattice dual to that of the antiferromagnet. For the kagome antiferromagnet, the Ising model resides on the dice lattice, and the simplest effective Ising model has a degenerate momentum-independent spectrum. (Nikolic and Senthil, 2003; Sengupta et al., 2006) We shall show how the PSG constraints allow a systematic analysis of further neighbor interactions in the effective Ising model. Such extended interactions must generically be present, (Xu and Balents, 2011) and they lead to well-defined vison states with a finite effective mass. Depending upon the values of these effective interactions, we find 2 possibilities for the vison states: the simplest case has them transforming under the 48 element group $\mathrm{GL}(2, \mathbb{Z}_3)$, the group of 2×2 matrices with non-zero determinant whose matrix elements belong to the field $\mathbb{Z}_3$. The more complex case has visons states of the 288 element group $\mathrm{GL}(2, \mathbb{Z}_3) \times \mathrm{D}_3$.

Armed with this description of the vison states, will propose quantum field theories for the confinement transitions of $\mathbb{Z}_2$ spin liquids on the kagome lattice. These transitions are associated with condensation of visons, (Senthil and Fisher, 2000; Jalabert and Sachdev, 1991; Sachdev and Vojta, 2000; Moessner and Sondhi, 2001b,a; Xu and Sachdev, 2009; Xu and Balents, 2011; Poilblanc et al., 2010; Schwandt et al., 2010) and are expressed in terms of a multi-component 'relativistic' scalar field; the field theory with $\mathrm{GL}(2, \mathbb{Z}_3)$ symmetry appears in Eq. (4.22). These field theories also place constraints on the specific patterns of spatial broken symmetry in the confining VBS states found next to the quantum critical point and we will present phase diagrams illustrating these states. Visualizations of two possible VBS states are shown

in Fig. 4.1. The left VBS pattern in Fig. 4.1 appears for the simplest case of the $\mathrm{GL}(2,\mathbb{Z}_3)$ visons, and it is interesting that it is closely related to the "diamond pattern" which is enhanced in the numerical studies of Yan *et al.* (Yan et al., 2011). The right pattern in Fig. 4.1 is one of many possible VBS states for the $\mathrm{GL}(2,\mathbb{Z}_3) \times \mathrm{D}_3$ visons, and maps to the "honeycomb" VBS states found in earlier studies (Marston and Zeng, 1991; Singh and Huse, 2007; Jiang et al., 2008; Evenbly and Vidal, 2010; Nikolic and Senthil, 2003).

We will begin in Section 4.2 with a review of the basic characteristics of $\mathbb{Z}_2$ spin liquids and of their vison excitations. A key property of a vison is that it picks up a Aharanov-Bohm phase of π upon encircling every $S = 1/2$ spin on the sites of the antiferromagnet; (Jalabert and Sachdev, 1991; Senthil and Fisher, 2000; Sachdev and Vojta, 2000; Moessner and Sondhi, 2001b), as will be described in Section 4.2.

Section 4.3 contains our main new results. We begin with general effective theories of vison motion which incorporate the Aharanov-Bohm phase (Xu and Sachdev, 2009; Xu and Balents, 2011) of π: for the kagome antiferromagnet, these are conveniently expressed in terms of an effective, fully-frustrated Ising model on the dice lattice. A key parameter in this Ising model is the sign of a particular next-nearest-neighbor interaction. A 'ferromagnetic' sign leads to the simpler vison PSG, and is discussed in Section 4.3.1; the more complicated 'antiferromagnetic' case is discussed in Section 4.3.2. In both cases, we use the vison PSG to present quantum field theories for the confinement transitions, and discuss renormalization group analyses of these quantum critical points. The field theories are also used to classify the patterns of lattice symmetry breaking in the confining valence bond solid states.

In Appendix 4.A the explicit calculation of a visons Berry phase can be found. The results of a PSG analysis of visons for different lattice geometries are summarized in Appendix 4.B.

4.2 $\mathbb{Z}_2$ spin liquids and visons

We begin by a review of the basic properties of $\mathbb{Z}_2$ spin liquids, following the description in Ref. Sachdev (1992).

It is convenient to describe the $S = 1/2$ spins $\vec{S}_i$ using Schwinger bosons (Arovas and Auerbach, 1988) $b_{i\alpha}$ ($\alpha = \uparrow, \downarrow$)

$$\vec{S}_i = \frac{1}{2} b^\dagger_{i\alpha} \vec{\sigma}_{\alpha\beta} b_{i\beta}, \tag{4.1}$$

where $\vec{\sigma}$ are the Pauli matrices, and the bosons obey the local constraint

$$\sum_\alpha b^\dagger_{i\alpha} b_{i\alpha} = 1 \tag{4.2}$$

on every site i. Our analysis below can be easily extended to gapped $\mathbb{Z}_2$ spin liquids obtained from the Schwinger fermion formulation, (Wen, 1991; Lu et al., 2011; Iqbal et al., 2011b,a) but we will only consider the Schwinger boson case for brevity.

The $\mathbb{Z}_2$ spin liquid is described by an effective boson Hamiltonian

$$\mathcal{H}_b = -\sum_{i<j} Q_{ij} \varepsilon_{\alpha\beta} b^\dagger_{i\alpha} b^\dagger_{j\beta} + \text{H.c.} + \lambda \sum_i b^\dagger_{i\alpha} b_{i\alpha}, \tag{4.3}$$

where ε is the antisymmetric unit tensor, λ is chosen to satisfy the constraint in Eq. (4.2) on average, and the $Q_{ij} = -Q_{ji}$ are a set of variational parameters chosen to optimize the energy of the spin liquid state. Generally, the Q_{ij} are chosen to be non-zero only on near neighbor links. The '$\mathbb{Z}_2$' character of the spin liquid requires that the links with non-zero Q_{ij} can form closed loops with an odd number of links, (Read and Sachdev, 1991; Wen, 1991; Sachdev, 1992). If the state preserves time-reversal symmetry, all the Q_{ij} can be chosen real.

This effective Hamiltonian also motivates a wavefunction of the spin liquid (Read and Sachdev, 1989b; Tay and Motrunich, 2011)

$$|\text{SL}\rangle = \mathcal{P} \exp\left(\sum_{i<j} f_{ij}\, \varepsilon_{\alpha\beta} b^\dagger_{i\alpha} b^\dagger_{j\beta} \right) |0\rangle, \tag{4.4}$$

where $|0\rangle$ is the boson vaccum, $\mathcal{P}$ is a projection operator which selects only states which obey Eq. (4.2), and the boson pair wavefunction $f_{ij} = -f_{ji}$ is determined

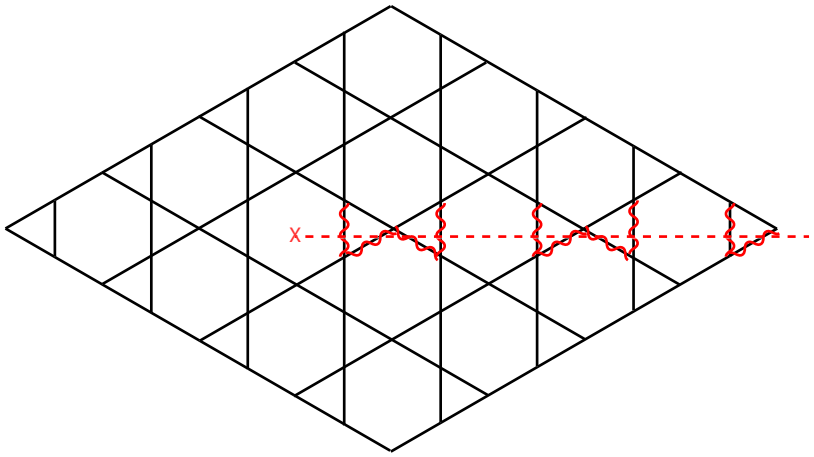

Figure 4.2: A vison on the kagome lattice. The center of the vison is marked by the X. We have $\mathrm{sgn}(Q^v_{ij}) = -\mathrm{sgn}(Q_{ij})$ only on the links marked by the wavy lines.

by diagonalizing Eq. (4.3) by a Bogoliubov transformation (see Eq. (4.35) in Appendix 4.A).

The Schwinger boson approach also allows a description of the vison excited states. (Read and Sachdev, 1991; Sachdev and Read, 1991) We choose the vison state as the ground state of a Hamiltonian, $\mathcal{H}^v_b$, obtained from $\mathcal{H}$ by mapping $Q_{ij} \to Q^v_{ij}$ (see Eq. (4.31)); then the vison state $|\Psi^v\rangle$ has a wavefunction as in Eq. (4.4), but with $f_{ij} \to f^v_{ij}$ (see Eq. (4.34)). Far from the center of the vison, we have $|Q^v_{ij}| = |Q_{ij}|$, while closer to the center there are differences in the magnitudes. However, the key difference is in the signs of the link variables, as illustrated in Fig. 4.2: there is a 'branch-cut' emerging from the vison core along which $\mathrm{sgn}(Q^v_{ij}) = -\mathrm{sgn}(Q_{ij})$. This branch-cut ensures that the $\mathbb{Z}_2$ flux equals -1 on all loops which encircle the vison core, while other loops do not have non-trivial $\mathbb{Z}_2$ flux. Such a configuration of the Q^v_{ij} is expected to be a metastable solution of the Schwinger boson mean-field equations, representing a vison excitation.

The previous solution for the vison state (Sachdev and Read, 1991) was obtained using a continuum field theoretic representation of the Schwinger boson theory, valid

in the limit of a *small* energy gap towards spinful excitations. In principle, such a solution can also be obtained by a complete solution of the Schwinger boson equations on the lattice, but this requires considerable numerical effort. Here, we illustrate the solution obtained in the of a *large* spin gap. In the large spin gap limit, (Tchernyshyov et al., 2006) we can integrate out the Schwinger bosons, and write the energy as a local functional of the Q_{ij}. This functional is strongly constrained by gauge-invariance: for time-independent Q_{ij}, this functional takes the form

$$\begin{aligned} E[\{Q_{ij}\}] &= -\sum_{i<j}\left(\alpha|Q_{ij}|^2+\frac{\beta}{2}|Q_{ij}|^4\right) \\ &\quad +K\sum_{\text{even loops}} Q_{ij}Q^*_{jk}\ldots Q^*_{\ell i} \end{aligned} \tag{4.5}$$

Here α, β, and K are coupling constants determined by the parameters in the Hamiltonian of the antiferromagnet. We have shown them to be site-independent, because we have only displayed terms in which all links/loops are equivalent; they can depend upon links/loops for longer range couplings provided the full lattice symmetry is preserved. We describe the results of a minimization of $E[\{Q_{ij}\}]$ on the simpler case of the triangular lattice in Fig. 4.3. The magnitudes of Q^v_{ij} are suppressed close to the vison, and converge to Q_{ij} as we move away from the vison (modulo the sign change associated with the branch cut), analogous to the Abrikisov vortices. Despite the branchcut breaking the 3-fold rotation symmetry, the gauge-invariant fluxes of Q^v_{ij} preserve the rotation symmetry.

Let us now consider the motion of a single vison. A key ingredient is the Berry phase a vison accumulates while moving through the background spin liquid. The gauge-invariant Berry phases are those associated with a periodic motion, and so let us consider the motion of a vison along a general closed loop $\mathcal{C}$. We illustrate the simple case where $\mathcal{C}$ encloses a single site of the triangular lattice antiferromagnet in Fig. 4.4. The Berry phase for this periodic motion can be computed in a manner analogous to that presented in Section III.A of Ref. Read and Sachdev (1990) for a monopole in a U(1) spin liquid; details appear in Appendix 4.A. The final gauge-invariant Berry phase turns out to be given by the gauge-transformation required

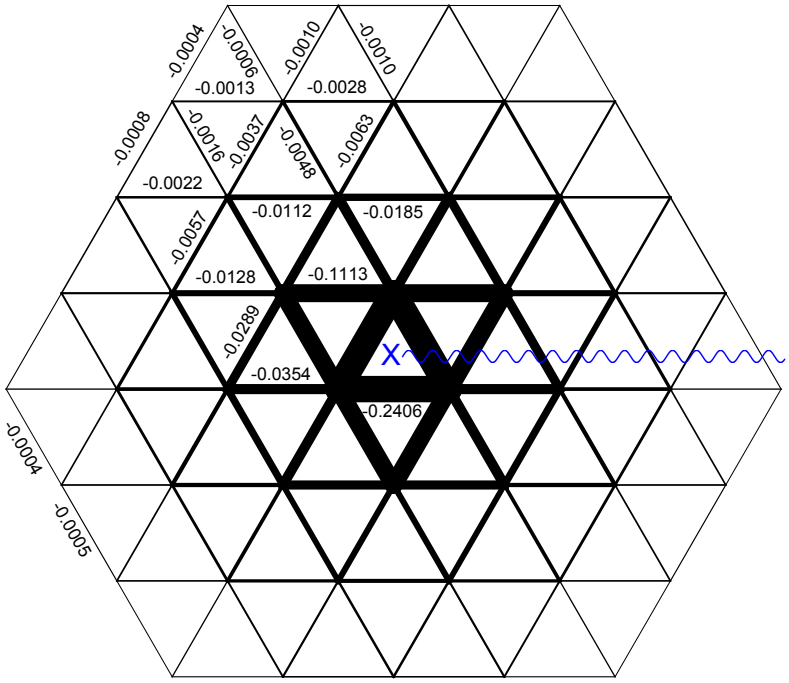

Figure 4.3: A vison on the triangular lattice (a similar solution is expected on the kagome lattice). The center of the vison is marked by the X. The wavy line is the 'branch-cut' where we have $\mathrm{sgn}(Q^v_{ij}) = -\mathrm{sgn}(Q_{ij})$ only on the links crossed by the line. Plotted is the minimization result of $E[\{Q_{ij}\}]$ with $\alpha = 1, \beta = -2, K = -0.5$. Minimization is done with the cluster embedded in a vison-free lattice with all nearest neighbor links Q_{ij}. The numbers are $(Q_{ij} - Q^v_{ij})$ and the thickness of the links are proportional to $(Q^v_{ij} - Q_{ij})^{1/2}$. $K < 0$ gives rise to the zero flux state while $K > 0$ favors the π flux state where the unit cell is doubled. The zero and π flux states without the vison have been studied previously. (Sachdev, 1992; Wang and Vishwanath, 2006)

to map the final state to the initial state. The analysis in Fig. 4.4 shows that the required gauge transformation is

$$\begin{aligned} b_{i\alpha} &\to -b_{i\alpha}, \qquad \text{for } i \text{ inside } \mathcal{C} \\ b_{i\alpha} &\to b_{i\alpha}, \qquad \text{for } i \text{ outside } \mathcal{C}. \end{aligned} \tag{4.6}$$

By Eq. (4.2), each site has one boson, and so the total Berry phase accumulated by

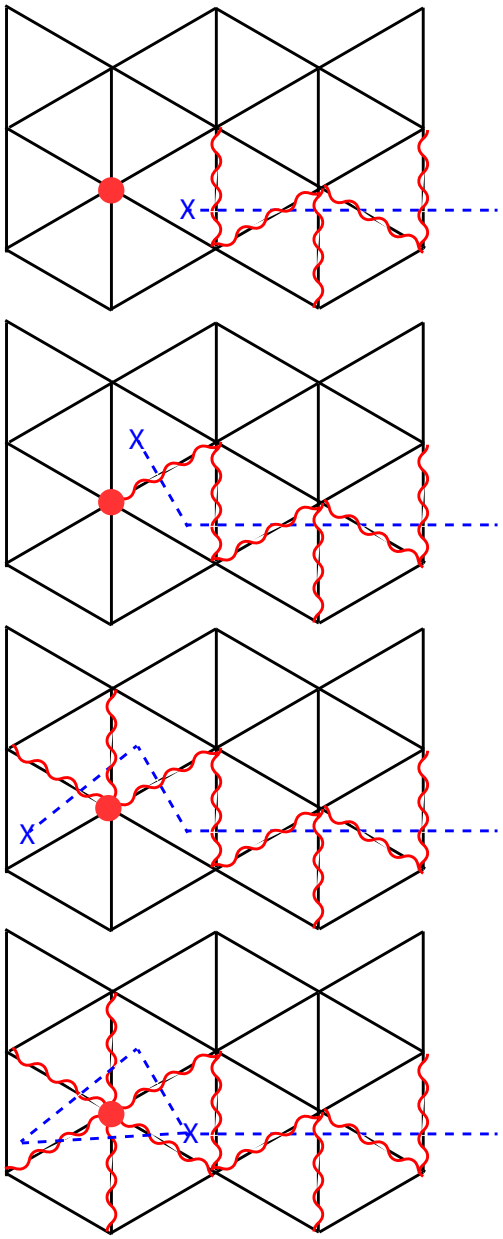

Figure 4.4: Periodic motion of a vison around a closed loop $\mathcal{C}$ on the triangular lattice. Here $\mathcal{C}$ encloses the single site marked by the filled circle. The wavy lines indicate $\mathrm{sgn}(Q^v_{ij}) = -\mathrm{sgn}(Q_{ij})$, as in Fig. 4.2. The bottom state is gauge-equivalent to the top state, after the gauge transformation $b_{i\alpha} \to -b_{i\alpha}$ only for the site i marked by the filled circle.

$|\Psi^v\rangle$ is

$$\pi \times (\text{number of sites enclosed by } \mathcal{C}) \,, \tag{4.7}$$

as recognized in earlier works (Senthil and Fisher, 2000; Jalabert and Sachdev, 1991; Sachdev and Vojta, 2000; Xu and Sachdev, 2009; Xu and Balents, 2011). It is also clear that for a spin S antiferromagnet, the Berry phase would be multiplied by a factor of $2S$.

Finally, let us also mention the spinon states, although these will not play a role in the subsequent analysis of the present paper. These are created by applying the Bogoliubov quasiparticle operator $\gamma^\dagger_{\mu\alpha}$ (Appendix 4.A) on the spin-liquid ground state; in this manner we obtain the spinon state

$$\begin{aligned} |\mu\alpha\rangle &= \sum_\ell \left(U^{-1*}\right)_{\mu\ell} |\ell\alpha\rangle \\ |\ell\alpha\rangle &= \mathcal{P}\, b^\dagger_{\ell\alpha} \exp\left(\sum_{i<j} f_{ij}\, \varepsilon_{\alpha\beta} b^\dagger_{i\alpha} b^\dagger_{j\beta}\right) |0\rangle, \end{aligned} \tag{4.8}$$

where $U_{i\mu}$ is a Bogoliubov rotation matrix defined in Appendix 4.A. We can now also consider a spinon well-separated from a vison, and describe the motion of a vison along a large contour $\mathcal{C}$ which encircles the spinon. First, consider the motion of a vison around the spinon state $|\ell\alpha\rangle$ localized on the site ℓ. Proceeding with the argument as above, the projection onto states which obey Eq. (4.2) now implies that the Berry phase for such a process is $\pi \times ((\text{number of sites enclosed by } \mathcal{C}) - 1)$. The transformation to the spinon state $|\mu\alpha\rangle$ will not change the result, provided the 'wavefunction' $\left(U^{-1*}\right)_{\mu\ell}$ is localized well within the contour $\mathcal{C}$. Thus relative to the Berry phase in the case without a spinon, the vison acquires an additional phase of π upon encircling a spinon *i.e.* the spinons and visons are relative semions. (Read and Chakraborty, 1989)

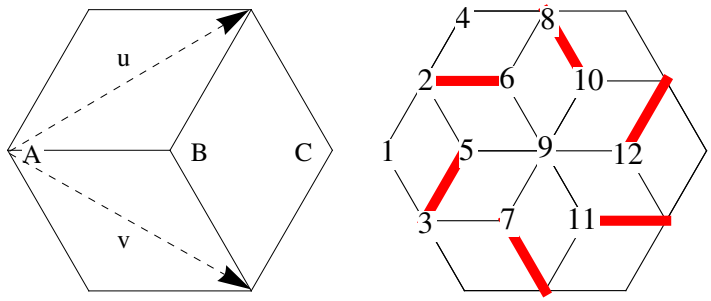

Figure 4.5: Left: unit cell of the dice lattice consisting of the 3 independent sites labeled A, B and C. The A sites are 6-coordinated, whereas the B and C sites are 3-coordinated. The basis vectors $\mathbf{u} = (3/2, \sqrt{3}/2)$ and $\mathbf{v} = (3/2, -\sqrt{3}/2)$ are indicated by dashed arrows. Right: gauge choice for the fully frustrated Ising model on the dice lattice with a 12-site unit cell. Red thick bonds are frustrated, *i.e.* $\mathrm{sgn}(J_{ij}) = -1$.

4.3 PSG analysis of the fully frustrated Ising model on the dice lattice

The analysis of Section 4.2 suggests a simple effective model for the vison fluctuations about the $\mathbb{Z}_2$ spin liquid ground state. In the framework of the path-integral formations of Ref. Sachdev (1992), the visons are saddle-points of the Q_{ij} with π-flux, as shown in Fig. 4.3. Each saddle-point traces a world-line in spacetime, representing the time evolution of the vison. The Berry phase computation in Section 4.2 shows that this world-line picks up π-flux each time it encircles a kagome lattice site. We know further that two such worldlines can annihilate each other, because 2π magnetic flux is equivalent to zero flux. So if we interpret the wordlines as the trajectory of a particle, that particle must be its own anti-particle, and has a real field operator. In this manner, we see that the fluctuations represented as the sum over all vison worldlines is precisely that of a frustrated Ising model in a transverse field (Jalabert and Sachdev, 1991; Sachdev and Vojta, 2000; Senthil and Fisher, 2000):

$$H = -\sum_{i<j} J_{ij}\, \phi_i \phi_j + \dots \ , \tag{4.9}$$

where the product of bonds around each elementary plaquette is negative

$$\prod_{\text{plaq.}} \text{sgn}(J_{ij}) = -1 \ . \tag{4.10}$$

Also, we have not displayed the transverse-field term, because most of our symmetry considerations are restricted to time-independent, static configurations.

In the following we will use a soft-spin formulation where the ϕ_j's take real values. This model is invariant under $\mathbb{Z}_2$ gauge transformations $\phi_j \to \sigma_j \phi_j$, $J_{ij} \to \sigma_i \sigma_j J_{ij}$ with $\sigma_j = \pm 1$. For the case of the $\mathbb{Z}_2$ spin liquid on a kagome lattice the dual Ising model lives on the dice lattice, shown in Fig. 4.5. The dice lattice has three independent sites per hexagonal unit cell, two of them are three-coordinated and one is six-coordinated. Flipping a dual Ising spin changes the flux through a plaquette on the kagome lattice by π, thereby creating or annihilating a vison. The magnetically disordered phase of the Ising model corresponds to a $\mathbb{Z}_2$ spin liquid with deconfined spinon excitations, whereas the ordered phases describe different valence bond solids where the visons are condensed and fractional excitations are confined.

We study the confinement transitions of the spin liquid by constructing a Ginzburg-Landau functional that is consistent with the projective symmetry group (PSG), *i.e.* the combination of lattice-symmetry- and $\mathbb{Z}_2$ gauge-transformations that leave the Hamiltonian (4.9) together with (4.10) invariant. In order to determine the PSG transformations we fix the gauge of nearest neighbor interactions as shown in Fig. 4.5, thereby obtaining a unit cell with twelve sites. The generators of the dice lattice symmetry group are translations by one of the two basis vectors, *e.g.* $\mathbf{u}$, reflections about one axis, *e.g.* the x-axis, and $\pi/3$ rotations about the central 6-coordinated site. Since our gauge choice is already invariant under rotations, we only need to determine the gauge-transformations corresponding to translations and reflections to specify the PSG. These are shown in Fig. 4.6.

The dispersion relations of the soft-spin modes can be obtained directly from the Hamiltonian (4.9). The corresponding action takes the form

$$S = \sum_{\Omega,\mathbf{q}} \phi^{(i)}_{\mathbf{q},\Omega} \big[(\Omega^2 + m^2)\delta_{i,j} - J^{(ij)}_{\mathbf{q}} \big] \phi^{(j)}_{-\mathbf{q},-\Omega} \tag{4.11}$$

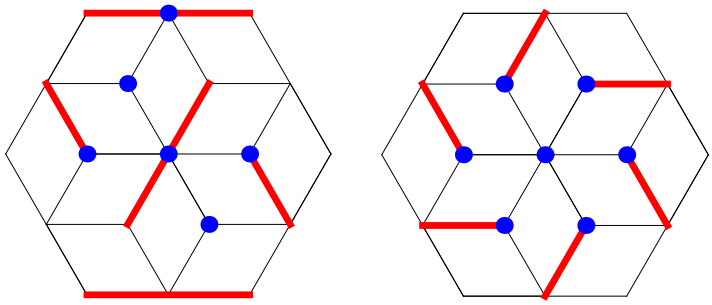

Figure 4.6: Gauge transformations associated with translations by **u** and reflections about the x-axis. Shown is the unit cell of the fully frustrated dice model after a lattice translation by **u** (left) and after a reflection about the x-axis (right). The corresponding gauge-transformations consist of spin flips on the sites marked by blue points, which restore the original gauge pattern as in Fig. 4.5.

where the summation over the sublattice indices $i, j = 1...12$ is implicit, $J_{\mathbf{q}}^{(ij)}$ denotes the Fourier transform of the interaction matrix J_{ij}, and we have included a kinetic energy with frequency Ω (which descends from the transverse field), and a mass term, m. As noted earlier (Nikolic and Senthil, 2003; Sengupta et al., 2006), the frustrated Ising model on the dice lattice with nearest neighbor interactions gives rise to three flat bands (each being four-fold degenerate in our gauge choice with a 12-site unit cell), which would result in infinitely many critical modes. In order to lift this degeneracy we include further interactions beyond nearest neighbors (Xu and Balents, 2011) that are consistent with the PSG. Different masses on the 3- and 6-coordinated sites would be allowed by the PSG, but they don't give rise to a momentum dependence of the modes and thus don't change the picture qualitatively. Out of the five possible additional interactions up to a distance of two times the nearest neighbor bond length only one is consistent with the PSG. This interaction, shown in Fig. 4.7, connects different 3-coordinated lattice sites and gives rise to a non-flat dispersion. The Fourier transform of the interaction matrix J_{ij} takes the form

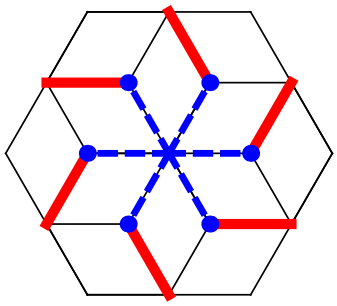

Figure 4.7: Additional next-nearest neighbor interactions between 3-coordinated sites on the dice lattice (shown as dashed blue lines) that are allowed by the PSG. For illustrative clarity not all additional bonds in the unit cell are shown. All other bonds can be obtained from the ones that are shown via translations by the basis vectors $\mathbf{u}$ and/or $\mathbf{v}$.

$$J_{\mathbf{q}}^{(ij)} = \begin{bmatrix} 0 & 1 & 1 & \kappa_1^* & 0 & 0 & 0 & e^{-i2\mathbf{qu}} & 0 & 0 & 0 & 0 \\ 1 & 0 & 0 & 1 & 1 & -1 & 0 & 0 & 0 & 0 & -e^{-i2\mathbf{qv}} & e^{-i2\mathbf{qv}} \\ 1 & 0 & 0 & e^{i2\mathbf{q(v-u)}} & -1 & 0 & 1 & 0 & 0 & e^{-i2\mathbf{qu}} & 0 & -e^{-i2\mathbf{qu}} \\ \kappa_1 & 1 & e^{i2\mathbf{q(u-v)}} & 0 & 0 & 0 & 0 & 1 & 0 & 0 & 0 & 0 \\ 0 & 1 & -1 & 0 & 0 & 0 & 0 & 0 & 1 & 0 & 0 & \kappa_2^* \\ 0 & -1 & 0 & 0 & 0 & 0 & 0 & 1 & 1 & 0 & \kappa_3^* & 0 \\ 0 & 0 & 1 & 0 & 0 & 0 & 0 & -e^{i2\mathbf{q(v-u)}} & 1 & \kappa_1^* & 0 & 0 \\ e^{i2\mathbf{qu}} & 0 & 0 & 1 & 0 & 1 & -e^{i2\mathbf{q(u-v)}} & 0 & 0 & -1 & e^{i2\mathbf{q(u-v)}} & 0 \\ 0 & 0 & 0 & 0 & 1 & 1 & 1 & 0 & 0 & 1 & 1 & 1 \\ 0 & 0 & e^{i2\mathbf{qu}} & 0 & 0 & 0 & \kappa_1 & -1 & 1 & 0 & 0 & 0 \\ 0 & -e^{i2\mathbf{qv}} & 0 & 0 & 0 & \kappa_3 & 0 & e^{i2\mathbf{q(v-u)}} & 1 & 0 & 0 & 0 \\ 0 & e^{i2\mathbf{qv}} & -e^{i2\mathbf{qu}} & 0 & \kappa_2 & 0 & 0 & 0 & 1 & 0 & 0 & 0 \end{bmatrix}. \tag{4.12}$$

Here we have abbreviated $\kappa_1 \equiv t(1 + e^{i2\mathbf{qu}} + e^{i2\mathbf{q(u-v)}})$, $\kappa_2 \equiv t(1 + e^{i2\mathbf{qu}} + e^{i2\mathbf{qv}})$ and $\kappa_3 \equiv t(1 + e^{i2\mathbf{qv}} + e^{i2\mathbf{q(v-u)}})$, which are the additional terms coming from the next nearest neighbor interaction that is allowed by the PSG and t denotes the relative strength of the interaction with respect the the nearest neighbor coupling $J = 1$. Diagonalizing $J_{\mathbf{q}}^{(ij)}$ results in three dispersing bands, each being four-fold degenerate. Depending on the sign of the next-nearest neighbor interaction t, we get different transitions to valence bond solids that we are going to discuss in the following.

4.3.1 Ferromagnetic n.n.n. interactions

For ferromagnetic next-nearest neighbor interactions ($t > 0$) the dispersion minimum of the lowest band is at zero momentum $\mathbf{q} = 0$. The corresponding eigenvalue

of the interaction matrix $J_{\mathbf{0}}^{(ij)}$ is given by $\lambda_+ = (3t + \sqrt{24 + 9t^2})/2$ and one choice for the four degenerate eigenvectors is

$$\begin{aligned}
v^{(1)} &= \left[\lambda_-^{-1} \;\; 1 \;\; 0 \;\; \lambda_-^{-1} \;\; \tfrac{\lambda_+}{6} \;\; -\lambda_-^{-1} \;\; 0 \;\; 0 \;\; 0 \;\; 0 \;\; -\lambda_-^{-1} \;\; \tfrac{\lambda_+}{6}\right] ||v||^{-1} && (4.13)\\
v^{(2)} &= \left[\lambda_-^{-1} \;\; 0 \;\; 1 \;\; \lambda_-^{-1} \;\; -\tfrac{\lambda_+}{6} \;\; 0 \;\; \lambda_-^{-1} \;\; 0 \;\; 0 \;\; \lambda_-^{-1} \;\; 0 \;\; -\tfrac{\lambda_+}{6}\right] ||v||^{-1} && (4.14)\\
v^{(3)} &= \left[\lambda_-^{-1} \;\; 0 \;\; 0 \;\; \lambda_-^{-1} \;\; 0 \;\; \lambda_-^{-1} \;\; -\lambda_-^{-1} \;\; 1 \;\; 0 \;\; -\lambda_-^{-1} \;\; \lambda_-^{-1} \;\; 0\right] ||v||^{-1} && (4.15)\\
v^{(4)} &= \left[0 \;\; 0 \;\; 0 \;\; 0 \;\; \tfrac{\lambda_+}{6} \;\; \tfrac{\lambda_+}{6} \;\; \tfrac{\lambda_+}{6} \;\; 0 \;\; 1 \;\; \tfrac{\lambda_+}{6} \;\; \tfrac{\lambda_+}{6} \;\; \tfrac{\lambda_+}{6}\right] ||v||^{-1} && (4.16)
\end{aligned}$$

with $\lambda_- = (3t - \sqrt{24 + 9t^2})/2$ and $||v|| = \sqrt{(\lambda_+^2 + 6)/6}$. This set of eigenvectors forms an orthonormal basis for the four critical modes at the transition to the confined phase. In the magnetically ordered state the magnetization $\phi_j(\mathbf{R})$ at lattice site $\mathbf{R} = 2n\mathbf{u} + 2m\mathbf{v}$ $(n, m \in \mathbb{N})$ and sublattice site $j \in \{1, ..., 12\}$ is given by

$$\phi_j(\mathbf{R}) = \sum_{n=1...4} \psi_n v_j^{(n)} \tag{4.17}$$

and is independent of the lattice site $\mathbf{R}$ for ferromagnetic n.n.n. interactions, *i.e.* the ordered VBS phases have a 12-site unit cell. The values of the four mode amplitudes ψ_n are obtained by minimizing the Ginzburg-Landau functional, which in turn is given by all homogeneous polynomials in the mode amplitudes ψ_n that are invariant under the PSG transformations. In order construct these polynomials we have to determine how the mode amplitudes transform under the PSG. This can be done by looking at the transformation properties of the eigenvectors $v^{(n)}$. For example, the transformation properties of the mode amplitudes with respect to translations $T_{\mathbf{u}}$ are determined via

$$\begin{aligned}
\hat{T}_{\mathbf{u}}\phi_j &= \sum_n \psi_n \hat{T}_{\mathbf{u}} v_j^{(n)} = \sum_{n,m} (T_{\mathbf{u}})_{mn} \psi_n v_j^{(m)} \\
&= \sum_m (\hat{T}_{\mathbf{u}}\psi)_m v_j^{(m)} \; . && (4.18)
\end{aligned}$$

The resulting PSG transformation matrices for the amplitudes of the four critical modes with respect to translations ($T_{\mathbf{u}}$), reflections (I_x) and rotations (R_6) are given

by

$$T_{\mathbf{u}} = \begin{bmatrix} 0 & 0 & -1 & 0 \\ 0 & 0 & 0 & -1 \\ 1 & 0 & 0 & 0 \\ 0 & 1 & 0 & 0 \end{bmatrix}, \tag{4.19}$$

$$I_x = \begin{bmatrix} 0 & 1 & 0 & 0 \\ 1 & 0 & 0 & 0 \\ 0 & 0 & 1 & 0 \\ 0 & 0 & 0 & -1 \end{bmatrix}, \tag{4.20}$$

$$R_6 = \begin{bmatrix} 0 & 0 & 1 & 0 \\ 1 & 0 & 0 & 0 \\ 0 & 1 & 0 & 0 \\ 0 & 0 & 0 & 1 \end{bmatrix}. \tag{4.21}$$

We used the GAP program (GAP) to show that these three matrices generate a finite, 48 element subgroup of O(4) which is isomorphic to $\mathrm{GL}(2,\mathbb{Z}_3)$. We also determined that this group is isomorphic to the group $\pm\frac{1}{2}[O\times C_2]$ in the classification of Conway and Smith. (Conway and Smith, 2003)

Next we determined the most general Ginzburg-Landau functional of the ψ_n. It turns out that there are three fourth order polynomials that are invariant under this group, thus our functional for the four mode amplitudes depends on the coupling constants, r, u, a and b, and takes the form

$$\begin{aligned} \mathcal{L} = & \sum_{n=1\ldots4} ((\nabla\psi_n)^2 + (\partial_\tau\psi_n)^2 + r\psi_n^2 + u\psi_n^4) \\ & + a\sum_{n<m}\psi_n^2\psi_m^2 + b\big[\psi_1^2(\psi_2\psi_3 - \psi_2\psi_4 + \psi_3\psi_4) \\ & + \psi_2^2(\psi_1\psi_3 + \psi_1\psi_4 - \psi_3\psi_4) + \psi_3^2(\psi_1\psi_2 - \psi_1\psi_4 \\ & + \psi_2\psi_4) - \psi_4^2(\psi_1\psi_2 + \psi_1\psi_3 + \psi_2\psi_3)\big]. \end{aligned} \tag{4.22}$$

At $b = 0$ and $a = 2u$, this is just the well-known ϕ^4 field theory with O(4) symmetry, whose critical properties are described by the extensively studied Wilson-Fisher fixed

point. The b coupling breaks the O(4) symmetry down to $\mathrm{GL}(2,\mathbb{Z}_3)$. Remarkably, the renormalization group (RG) properties of just such a quartic coupling have been studied earlier by Toledano *et al.*; (Toledano et al., 1985) they denoted this symmetry class as $[D_3/C_2; O/D_2]$, following the analysis of Du Val. (Du Val, 1964) Toledano *et al.* found that the O(4) fixed point was unstable, but were unable to find a stable critical fixed point at two-loop order. It would be interesting to extend the analysis of Eq. (4.22) to higher loop order, and search for a suitable fixed point by the methods reviewed in Ref. Vicari (2007).

Despite the difficulty in finding a suitable critical fixed point, we can assume the existence of a second-order quantum phase transition, and use Eq. (4.22) to determine the structures of possible confining phases. Minimizing this functional for the magnetically ordered phase $r < 0$ gives rise to two possible phases, depending on the values of the two parameters a and b in the GL-functional (4.22). The phase diagram is shown in Fig. 4.8.

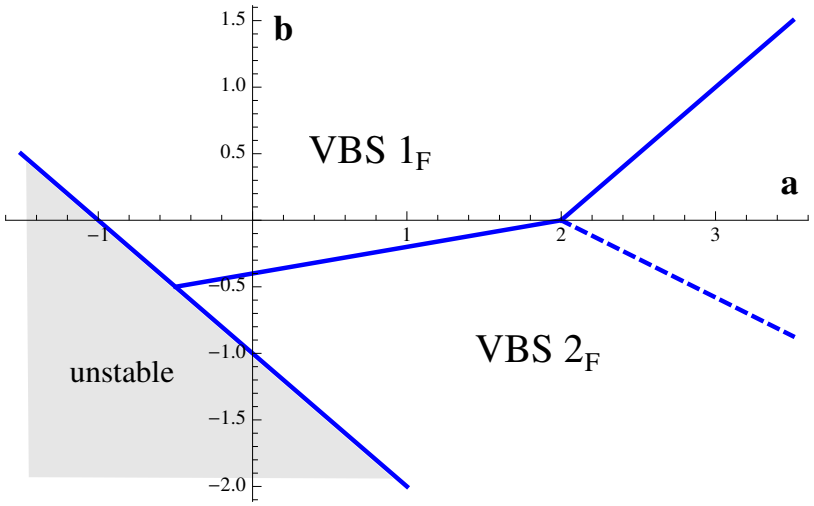

Figure 4.8: Phase diagram of Eqn. (4.22) as a function of the two couplings a and b (here we have set $u = 1$). The VBS 1_F phase is not reflection symmetric, whereas the VBS 2_F phase is reflection symmetric. In the VBS 2_F phase there is a crossover (indicated by the dashed line) from a phase where one of the ψ_n's is zero (left of the dashed line) to a phase where three of the ψ_n's are zero (right of the dashed line).

In the VBS 1_F phase the GL-functional (4.22) has 16 degenerate minima corre-

sponding to different magnetization patterns. Note, however, that the magnetization itself is not a gauge invariant quantity. In fact, all degenerate minima give rise to the same bond patterns, which are related by simple lattice symmetry transformations. The bond pattern in the VBS 1_{F} phase is symmetric under rotations by $\pi/3$, translations by $2\mathbf{u}$ and $2\mathbf{v}$ but it is not reflection symmetric. The 16 minima thus correspond to 8 different bond patterns that are related by translations by $\mathbf{u}$ and $\mathbf{v}$ as well as by a reflection about the x-axis (the factor of two arises from a global spin flip symmetry). In Fig. 4.9 we show the bond pattern in the VBS 1_{F} phase, *i.e.* we plot the gauge-invariant value of the bond-strength $J_{ij}\phi_i\phi_j$ for every nearest neighbor bond. In this figure we mapped the bond pattern from the dice lattice back to the kagome lattice by assigning the value of the bond-strength on the dice lattice to the bond on the kagome lattice that intersects the dice lattice bond. Deep in the confined phase the bonds plotted in Fig. 4.9 thus represent the expectation value $\langle\sigma^x_{ij}\rangle$ of the $\mathbb{Z}_2$ gauge field on the kagome bonds in the transverse field direction.

One way to relate the symmetries of valence bond solid phases on the kagome lattice to the ordered phases of the frustrated Ising model is to make use of the mapping between hardcore dimer models and frustrated Ising models (Moessner et al., 2001), *i.e.* by putting a dimer on every bond of the kagome lattice that intersects a frustrated bond on the dual dice lattice. The dimer covering that is obtained in this way for the VBS 1_{F} phase is shown in Fig. 4.1. In comparison to previously obtained dimer coverings of the kagome lattice (Nikolic and Senthil, 2003; Poilblanc et al., 2010; Schwandt et al., 2010) which maximize the number of perfectly flippable hexagons on a 36-site unit cell, this dimer covering maximizes the number of perfect flippable diamonds on a 12-site unit cell. Note that this bond pattern is similar to the diamond pattern observed by Yan *et al.* (Yan et al., 2011).

We note that the VBS 1_{F} state has recently been identified as the ground state of the deformed kagome lattice spin-1/2 antiferromagnet $Rb_2Cu_3SnF_{12}$. (Matan et al., 2010) It is possible that the spin physics being discussed here played a role in the lattice distortion observed in this experiment. (Yang and Kim, 2009) Also in Zn-paratacamite, $Zn_xCu_{4-x}(OH)_6Cl_2$, there is a transition (Lee et al., 2007) between a

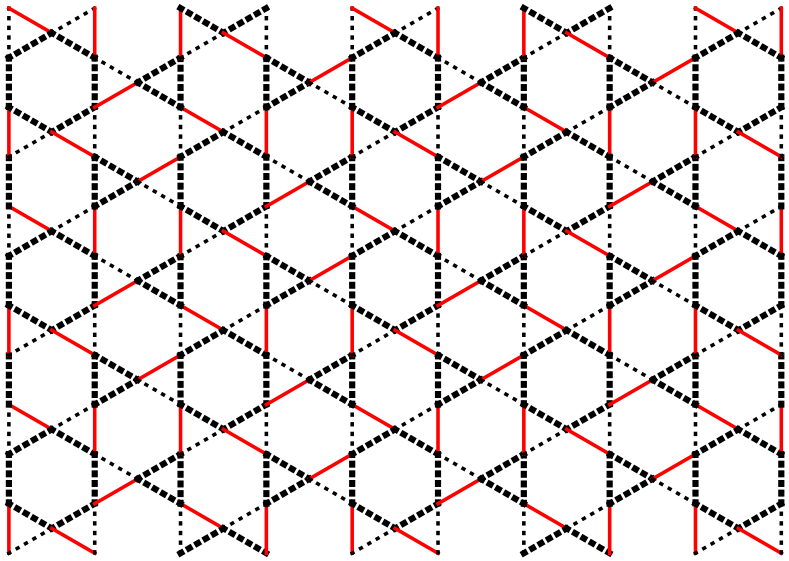

Figure 4.9: Bond pattern in the VBS 1_{F} phase. Plotted is the gauge invariant bond-strength $J_{ij}\phi_i\phi_j$ for nearest neighbor bonds on the dice-lattice at $a = b = 1$, which has been assigned to each respective kagome bond. Black dashed lines indicate satisfied bonds ($-J_{ij}\phi_i\phi_j < 0$), red solid lines are frustrated bonds ($-J_{ij}\phi_i\phi_j > 0$). The thickness of the bonds is proportional to the bond-strength.

spin-liquid phase near $x = 1$ to a distorted kagome lattice near $x = 0$, and it has been argued (Lawler et al., 2008) that a 'pinwheel' VBS state, which is identical in symmetry to our VBS 1_{F} state, plays a role in the latter case.

In the VBS 2_{F} phase the GL-functional (4.22) has 8 degenerate minima and the corresponding bond-patterns have an additional reflection symmetry as compared to the VBS 1_{F} phase. Moreover, there is a crossover from a phase where one of the ψ_n's is zero to a phase where three of the ψ_n's are zero, indicated by the dashed line in Fig. 4.8. The bond patterns are shown in Fig. 4.10.

4.3.2 Antiferromagnetic n.n.n. interactions

If the additional next-nearest neighbor interactions are antiferromagnetic ($t < 0$) and smaller than a critical value $|t| < t_c \sim 1$, the dispersion-minimum of the lowest band lies at the edges of the Brillouin zone, *i.e.* at $\mathbf{q} = \pm\mathbf{Q}_1 = \left(0,\ \pm\frac{2\pi}{3\sqrt{3}}\right)$

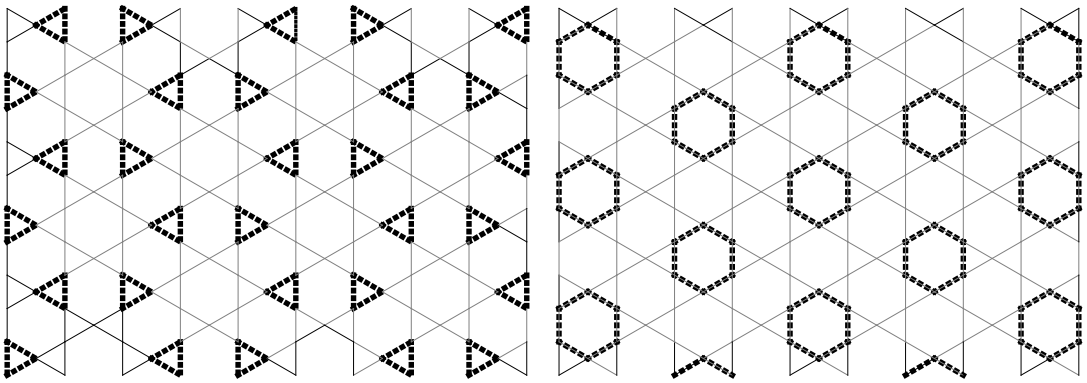

Figure 4.10: Bond patterns in the VBS 2_{F} phase. Plotted is the gauge invariant bond-strength $J_{ij}\phi_i\phi_j$ for nearest neighbor bonds on the dice lattice, shown on the corresponding kagome bonds. Black dashed lines represent satisfied bonds ($-J_{ij}\phi_i\phi_j < 0$). In this phase there are no frustrated bonds at all. The thickness of the bonds is proportional to the bond-strength.

for our gauge choice with a hexagonal 12-site unit cell. In this case eight modes become critical at the confinement transition and the resulting unit cell has 36 sites. The corresponding eigenvalue of the interaction matrix $J^{(ij)}_{\pm\mathbf{Q}_1}$ is $\sqrt{6}$ and the eight eigenvectors occur in complex conjugate pairs

$$\begin{aligned}
v^{(1)}_{Q_1} = v^{(1)*}_{-Q_1} &= \left[\tfrac{1}{\sqrt{12}} \quad \tfrac{1}{\sqrt{2}} \quad 0 \quad \tfrac{1}{\sqrt{12}} \quad \tfrac{1}{\sqrt{12}} \quad \tfrac{-1}{\sqrt{12}} \quad 0 \quad 0 \quad 0 \quad 0 \quad \tfrac{e^{i\pi/3}}{\sqrt{12}} \quad \tfrac{-e^{i\pi/3}}{\sqrt{12}}\right] \\
v^{(2)}_{Q_1} = v^{(2)*}_{-Q_1} &= \left[\tfrac{1}{\sqrt{12}} \quad 0 \quad \tfrac{1}{\sqrt{2}} \quad \tfrac{-e^{i\pi/3}}{\sqrt{12}} \quad \tfrac{-1}{\sqrt{12}} \quad 0 \quad \tfrac{1}{\sqrt{12}} \quad 0 \quad 0 \quad \tfrac{-e^{-i\pi/3}}{\sqrt{12}} \quad 0 \quad \tfrac{e^{-i\pi/3}}{\sqrt{12}}\right] \\
v^{(3)}_{Q_1} = v^{(3)*}_{-Q_1} &= \left[\tfrac{-e^{i\pi/3}}{\sqrt{12}} \quad 0 \quad 0 \quad \tfrac{1}{\sqrt{12}} \quad 0 \quad \tfrac{1}{\sqrt{12}} \quad \tfrac{e^{-i\pi/3}}{\sqrt{12}} \quad \tfrac{1}{\sqrt{2}} \quad 0 \quad -\tfrac{1}{\sqrt{12}} \quad \tfrac{-e^{-i\pi/3}}{\sqrt{12}} \quad 0\right] \\
v^{(4)}_{Q_1} = v^{(4)*}_{-Q_1} &= \left[0 \quad 0 \quad 0 \quad 0 \quad \tfrac{1}{\sqrt{12}} \quad \tfrac{1}{\sqrt{12}} \quad \tfrac{1}{\sqrt{12}} \quad 0 \quad \tfrac{1}{\sqrt{2}} \quad \tfrac{1}{\sqrt{12}} \quad \tfrac{1}{\sqrt{12}} \quad \tfrac{1}{\sqrt{12}}\right]
\end{aligned} \tag{4.23}$$

Note that in this case the magnetization at lattice site $\mathbf{R} = 2n\mathbf{u} + 2m\mathbf{v}$ and sublattice site j is given by

$$\phi_j(\mathbf{R}) = e^{i\mathbf{Q}_1\cdot\mathbf{R}} \sum_{n=1\ldots4} \psi_n v^{(n)}_{\mathbf{Q}_1,j} + \text{c.c.} \tag{4.24}$$

The PSG transformations of the four complex mode amplitudes ψ_n can be determined similarly to the ferromagnetic case. Quite generally they are defined by

$$\begin{aligned} \hat{\mathcal{O}}\phi_j(\mathbf{R}) &= \mathrm{Re}\Big[e^{i\mathbf{Q}_1\cdot(\hat{\mathcal{O}}\mathbf{R})}\sum_{n=1\ldots4}\psi_n\,\hat{\mathcal{O}}v^{(n)}_{\mathbf{Q}_1,j}\Big] \\ &\doteq \mathrm{Re}\Big[e^{i\mathbf{Q}_1\cdot\mathbf{R}}\sum_{n=1\ldots4}(\hat{\mathcal{O}}\psi)_n\,v^{(n)}_{\mathbf{Q}_1,j}\Big] \end{aligned} \tag{4.25}$$

If we define the vector $\Psi = \left(\psi_1,..,\psi_4,\psi_1^*,..,\psi_4^*\right)$, the PSG transformation matrices corresponding to translations by $\mathbf{u}$, reflections about the x-axis and rotations by $\pi/3$ around the central site, that act on the vector Ψ take the form

$$T_{\mathbf{u}} = \begin{bmatrix} 0 & 0 & -1 & 0 & 0 & 0 & 0 & 0 \\ 0 & 0 & 0 & -1 & 0 & 0 & 0 & 0 \\ e^{i2\pi/3} & 0 & 0 & 0 & 0 & 0 & 0 & 0 \\ 0 & e^{i2\pi/3} & 0 & 0 & 0 & 0 & 0 & 0 \\ 0 & 0 & 0 & 0 & 0 & 0 & -1 & 0 \\ 0 & 0 & 0 & 0 & 0 & 0 & 0 & -1 \\ 0 & 0 & 0 & 0 & e^{-i2\pi/3} & 0 & 0 & 0 \\ 0 & 0 & 0 & 0 & 0 & e^{-i2\pi/3} & 0 & 0 \end{bmatrix}, \tag{4.26}$$

$$I_x = \begin{bmatrix} 0 & 0 & 0 & 0 & 0 & 1 & 0 & 0 \\ 0 & 0 & 0 & 0 & 1 & 0 & 0 & 0 \\ 0 & 0 & 0 & 0 & 0 & 0 & e^{-i2\pi/3} & 0 \\ 0 & 0 & 0 & 0 & 0 & 0 & 0 & -1 \\ 0 & 1 & 0 & 0 & 0 & 0 & 0 & 0 \\ 1 & 0 & 0 & 0 & 0 & 0 & 0 & 0 \\ 0 & 0 & e^{i2\pi/3} & 0 & 0 & 0 & 0 & 0 \\ 0 & 0 & 0 & -1 & 0 & 0 & 0 & 0 \end{bmatrix}, \tag{4.27}$$

$$R_6 = \begin{bmatrix} 0 & 0 & 0 & 0 & 0 & 1 & 0 & 0 \\ 0 & 0 & 0 & 0 & 0 & 0 & e^{-i2\pi/3} & 0 \\ 0 & 0 & 0 & 0 & 1 & 0 & 0 & 0 \\ 0 & 0 & 0 & 0 & 0 & 0 & 0 & 1 \\ 0 & 1 & 0 & 0 & 0 & 0 & 0 & 0 \\ 0 & 0 & e^{i2\pi/3} & 0 & 0 & 0 & 0 & 0 \\ 1 & 0 & 0 & 0 & 0 & 0 & 0 & 0 \\ 0 & 0 & 0 & 1 & 0 & 0 & 0 & 0 \end{bmatrix}. \tag{4.28}$$

As in the previous subsection, we used the GAP program to determine that these three matrices generate a 288 element subgroup of O(8) which is isomorphic to $\mathrm{GL}(2,\mathbb{Z}_3) \times \mathrm{D}_3$ The Ginzburg-Landau functional is again given by all homogeneous polynomials that are invariant under this group. At fourth order there are five such polynomials, thus the GL-functional depends on the coupling constants $r, u, a_1, ..., a_4$ and is given

by

$$
\begin{aligned}
\mathcal{L}_4 \;=\; & \sum_{n=1..4} \left(r\psi_n^2 + u\psi_n^4\right) + \psi_2^2\psi_3^2\Big[a_1 - 2a_4\cos(2(\theta_2-\theta_3))\Big] \\
& +\psi_1^2\psi_2^2\Big[a_1 + a_4\cos(2(\theta_1-\theta_2)) + \sqrt{3}a_4\sin(2(\theta_1-\theta_2))\Big] \\
& +\psi_1^2\psi_3^2\Big[a_1 + a_4\cos(2(\theta_1-\theta_3)) + \sqrt{3}a_4\sin(2(\theta_1-\theta_3))\Big] \\
& +\psi_1^2\psi_4^2\Big[a_1 + a_4\cos(2(\theta_1-\theta_4)) - \sqrt{3}a_4\sin(2(\theta_1-\theta_4))\Big] \\
& +\psi_2^2\psi_4^2\Big[a_1 + a_4\cos(2(\theta_2-\theta_4)) + \sqrt{3}a_4\sin(2(\theta_2-\theta_4))\Big] \\
& +\psi_3^2\psi_4^2\Big[a_1 + a_4\cos(2(\theta_3-\theta_4)) + \sqrt{3}a_4\sin(2(\theta_3-\theta_4))\Big] \\
& +\psi_1\psi_2^2\psi_4\Big[- a_2\cos(\theta_1-\theta_4) - 2a_3\cos(\theta_1-2\theta_2+\theta_4) - \sqrt{3}a_2\sin(\theta_1-\theta_4)\Big] \\
& +\psi_1\psi_3^2\psi_4\Big[a_2\cos(\theta_1-\theta_4) + 2a_3\cos(\theta_1-2\theta_3+\theta_4) + \sqrt{3}a_2\sin(\theta_1-\theta_4)\Big] \\
& +\psi_1\psi_2\psi_4^2\Big[a_2\cos(\theta_1-\theta_2) + 2a_3\cos(\theta_1+\theta_2-2\theta_4) - \sqrt{3}a_2\sin(\theta_1-\theta_2)\Big] \\
& +\psi_1^2\psi_2\psi_4\Big[2a_3\cos(2\theta_1-\theta_2-\theta_4) + a_2\cos(\theta_2-\theta_4) - \sqrt{3}a_2\sin(\theta_2-\theta_4)\Big] \\
& +\psi_2\psi_3^2\psi_4\Big[- a_2\cos(\theta_2-\theta_4) + a_3\cos(\theta_2-2\theta_3+\theta_4) + \sqrt{3}a_2\sin(\theta_2-\theta_4) \\
& \qquad +\sqrt{3}a_3\sin(\theta_2-2\theta_3+\theta_4)\Big] \\
& +\psi_1\psi_2\psi_3^2\Big[- a_2\cos(\theta_1-\theta_2) + a_3\cos(\theta_1+\theta_2-2\theta_3) + \sqrt{3}a_2\sin(\theta_1-\theta_2) \\
& \qquad -\sqrt{3}a_3\sin(\theta_1+\theta_2-2\theta_3)\Big] \\
& +\psi_1\psi_3\psi_4^2\Big[a_2\cos(\theta_1-\theta_3) + 2a_3\cos(\theta_1+\theta_3-2\theta_4) - \sqrt{3}a_2\sin(\theta_1-\theta_3)\Big] \\
& +\psi_1^2\psi_2\psi_3\Big[a_3\cos(2\theta_1-\theta_2-\theta_3) + 2a_2\cos(\theta_2-\theta_3) + \sqrt{3}a_3\sin(2\theta_1-\theta_2-\theta_3)\Big] \\
& +\psi_2^2\psi_3\psi_4\Big[- a_3\cos(2\theta_2-\theta_3-\theta_4) + a_2\cos(\theta_3-\theta_4) + \sqrt{3}a_3\sin(2\theta_2-\theta_3-\theta_4) \\
& \qquad -\sqrt{3}a_2\sin(\theta_3-\theta_4)\Big] \\
& +\psi_1^2\psi_3\psi_4\Big[- 2a_3\cos(2\theta_1-\theta_3-\theta_4) - a_2\cos(\theta_3-\theta_4) + \sqrt{3}a_2\sin(\theta_3-\theta_4)\Big] \\
& +\psi_1\psi_2^2\psi_3\Big[- a_2\cos(\theta_1-\theta_3) + a_3\cos(\theta_1-2\theta_2+\theta_3) + \sqrt{3}a_2\sin(\theta_1-\theta_3) \\
& \qquad -\sqrt{3}a_3\sin(\theta_1-2\theta_2+\theta_3)\Big] \\
& +\psi_2\psi_3\psi_4^2\Big[- 2a_2\cos(\theta_2-\theta_3) - a_3\cos(\theta_2+\theta_3) - \sqrt{3}a_3\sin(\theta_2+\theta_3)\Big] \;. \qquad (4.29)
\end{aligned}
$$

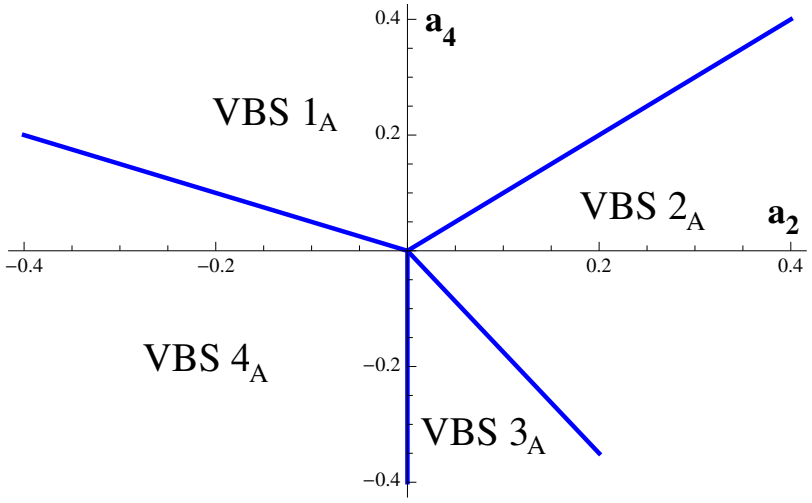

Figure 4.11: Phase diagram obtained from the GL-functional (4.30) as a function of the couplings a_2 and a_4. The other parameters are fixed at $u = 1$, $a_1 = 1/2$, $a_3 = a_2$, $a_5 = 1/20$ and $a_6 = -1/25$. The different phases are described in the text.

Here we have expressed the complex mode amplitudes in terms of their absolute value and phase $\psi_n e^{i\theta_n}$. Note that this fourth order Ginzburg-Landau functional has a remaining continuous $U(1)$ symmetry, since it is invariant under a change of all phases $\theta_n \to \theta_n + \chi$. The "magnetization" (4.24) is not invariant under this $U(1)$ transformation, however. In order to break this continuous degeneracy we need to include higher order terms in the Ginzburg-Landau functional. Among the invariant sixth order polynomials there are five which break the $U(1)$ symmetry. A full analysis of the invariant GL-functional at sixth order is beyond the scope of this paper, and we restrict ourselves to the simplest $U(1)$-breaking sixth order term. The $U(1)$-invariant sixth order terms are not expected to qualitatively change our results at the confinement transition.

In the remainder of this section we are going to consider the following fourth order GL-functional, including the simplest invariant sixth order $U(1)$-breaking polynomial, which takes the form

$$\mathcal{L} = \mathcal{L}_4 + \sum_{n=1\ldots4} \psi_n^6 \big(a_5 + a_6 \cos[6\theta_n]\big) \ . \tag{4.30}$$

In total our simplified GL-functional thus has seven coupling constants. Again, a complete analysis of the phase diagram as a function of these seven couplings is hardly feasible. A representative slice of the phase diagram is shown in Fig. 4.11, where we have fixed the values $u = 1$, $a_1 = 1/2$, $a_3 = a_2$, $a_5 = 1/20$ and $a_6 = -1/25$ and show the different phases as function of the two remaining parameters a_2 and a_4. All phases have a 36-site unit cell and are invariant with respect to translations by $4\mathbf{u} - 2\mathbf{v}$ and $4\mathbf{v} - 2\mathbf{u}$. In the above mentioned parameter regime there are four different ordered phases. VBS 1_A has a $\pi/3$ rotational symmetry, but is not reflection symmetric. A dimer representation of this state is shown in Fig. 4.1, which was obtained by putting a dimer on every kagome bond that intersects a frustrated bond on the dice lattice. This dimer covering suggests that our VBS 1_A state is identical to previously found valence bond solid states on the kagome lattice which maximize the number of perfectly flippable hexagons (Nikolic and Senthil, 2003; Poilblanc et al., 2010; Schwandt et al., 2010). The VBS 2_A phase is symmetric under $2\pi/3$ rotations and has a reflection symmetry. No rotational symmetry is present in the VBS 3_A and 4_A phases. The 3_A phase has a reflection symmetry, however, which is not present in the 4_A phase. Bond patterns of all four phases are shown in Fig. 4.12.

We performed a one-loop RG calculation for (4.29) and found six additional fixed points besides the Gaussian one, but all of them turned out to be unstable. Again it would be useful to revisit this issue using higher loop methods. (Vicari, 2007)

4.4 Conclusions

We have studied confinement transitions of $\mathbb{Z}_2$ spin liquids of Heisenberg antiferromagnets on the kagome lattice by constructing field theories that are consistent with the projective symmetry group of the vison excitations. Depending on the sign of the next-nearest neighbor interaction between the visons, we found that the visons transformed under the group $\mathrm{GL}(2, \mathbb{Z}_3)$ for the simpler case, and under $\mathrm{GL}(2, \mathbb{Z}_3) \times \mathrm{D}_3$ for the other case. Our analysis shows that possible VBS phases close to the confinement transition are strongly constrained by the vison PSG. We found VBS states

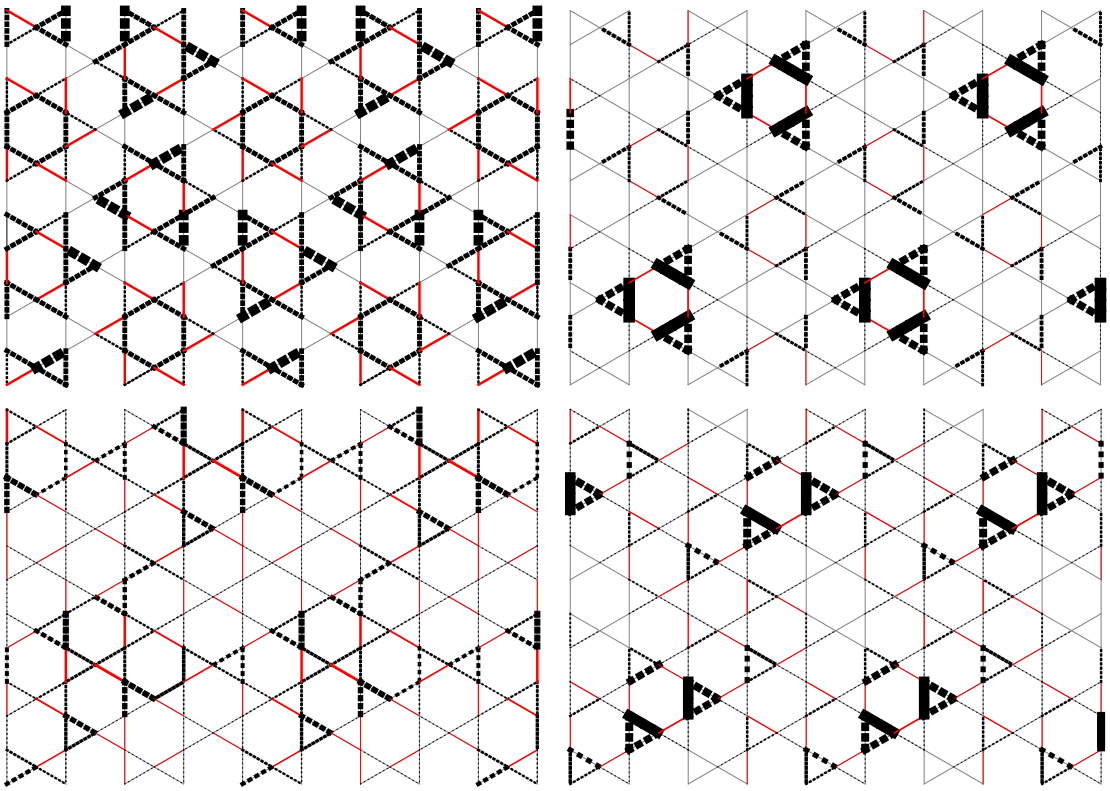

Figure 4.12: Bond patterns in the VBS 1_A, 2_A, 3_A and 4_A phase (clockwise, starting from the upper left). Again we plot the gauge invariant bond-strength $J_{ij}\phi_i\phi_j$ for nearest neighbor bonds on the dice lattice, mapped to the corresponding kagome bonds. Black dashed lines represent satisfied bonds ($-J_{ij}\phi_i\phi_j < 0$), red lines are frustrated bonds. The thickness of the lines is proportional to the bond strength.

that break the translational symmetry of the kagome lattice with either 12- or 36-site unit cells, for the two vison PSGs respectively. The two possible VBS states with 12-site unit cells do not break the rotation symmetry of the kagome lattice but one of them breaks the reflection symmetry; this state is closely connected to the "diamond pattern" enhancement observed in the recent numerical study of Yan *et al.* (Yan et al., 2011) As far as possible VBS states with 36-site unit cells are concerned, our analysis is not exhaustive. Nevertheless, we found different VBS states with either full, reduced or no rotation symmetry, as well as states that do or do not break the reflection symmetry of the kagome lattice. Our results should be useful in more completely characterizing spin liquids in numerical or experimental studies of the kagome antiferromagnet.

Analogous analyses for Z_2 spin liquids on other lattices have been carried out in other cases (see Appendix 4.B). In all other cases, the effective theory for confining transition has an emergent continuous symmetry, and the criticality can be computed using properties of the Wilson-Fisher fixed point; reduction to the discrete lattice symmetry appears only upon including higher-order couplings which are formally "irrelevant" at the critical fixed point. The kagome lattice is therefore the unique case (so far) in which the reduction to discrete lattice symmetry appears already in the critical theory: these is the theory in Eqs. (4.22), and its relevant quartic couplings are invariant only under discrete symmetries. This suggests that the numerical studies of confinement transitions may be easier on the kagome lattice.

We thank Steve White for sharing the results of Ref. Yan et al. (2011) prior to publication, and for valuable discussions. We are also grateful to M. Lawler and C. Xu for discussions.

4.A Berry phase of a vison

This appendix will compute the Berry phase of a vison moving around a $S = 1/2$ spin of the antiferromagnet, as illustrated in Fig. 4.4. We will follow the method of Section III.A of Ref. Read and Sachdev (1990), generalized to a $\mathbb{Z}_2$ spin liquid as in

Ref. Sachdev (1992).

We consider the time-dependent Schwinger boson Hamiltonian

$$\mathcal{H}_b^v(\tau) = -\sum_{i<j} Q_{ij}^v(\tau)\varepsilon_{\alpha\beta} b_{i\alpha}^\dagger b_{j\beta}^\dagger + \text{H.c.} + \sum_i \lambda_i^v(\tau) b_{i\alpha}^\dagger b_{i\alpha}, \tag{4.31}$$

where the τ dependence of Q_{ij}^v and λ_i^v is chosen so that the vison executes the motion shown in Fig. 4.4, while always maintaining the constraint in Eq. (4.2).

We compute the Berry phase by working with the instantaneous ground state of $\mathcal{H}_b(\tau)$. This is facilitated by a diagonalization of the Hamiltonian by performing a Bogoliubov transformation to a set of canonical Bose operators, $\gamma_{\mu\alpha}$, where the index $\mu = 1 \ldots N_s$, where N_s is the number of lattice sites. These are related to the $b_{i\alpha}$ by

$$b_{i\alpha} = \sum_\mu \left(U_{i\mu}(\tau)\gamma_{\mu\alpha} - V_{i\mu}^*(\tau)\varepsilon_{\alpha\beta}\gamma_{\mu\beta}^\dagger \right). \tag{4.32}$$

The $N_s \times N_s$ matrices $U_{i\mu}(\tau), V_{i\mu}(\tau)$ perform the Bogoliubov transformation, and obey the following identities: (Sachdev, 1992)

$$\begin{aligned}
\begin{pmatrix} \lambda^v & -Q^v \\ -Q^{v*} & -\lambda^v \end{pmatrix} \begin{pmatrix} U \\ V \end{pmatrix} &= \hat{\omega} \begin{pmatrix} U \\ V \end{pmatrix} \\
U^\dagger U - V^\dagger V &= 1 \\
U U^\dagger - V^* V^T &= 1 \\
V^T U + U^T V &= 0 \\
U V^\dagger + V^* U^T &= 0,
\end{aligned} \tag{4.33}$$

where $\hat{\omega}$ is a diagonal matrix containing the excitation energies of the Bogoliubov quasiparticles, and all quantities in Eq. (4.33) have an implicit τ dependence.

We can use the above transformations to write down the instantaneous (unnormalized) wavefunction of the vison as the unique state which obeys $\gamma_{\mu\alpha}|\Psi^v\rangle = 0$ for all μ, α:

$$|\Psi^v\rangle = \exp\left(\sum_{i<j} f_{ij}^v \, \varepsilon_{\alpha\beta} b_{i\alpha}^\dagger b_{j\beta}^\dagger \right) |0\rangle, \tag{4.34}$$

where

$$f_{ij}^v = \sum_\mu \left(U^{-1\dagger}\right)_{i\mu} \left(V^\dagger\right)_{\mu j}. \tag{4.35}$$

Then the Berry phase accumulated during the τ variation of $\mathcal{H}_b(\tau)$ is

$$\frac{i \,\mathrm{Im}\, \langle \Psi^v | \, \frac{d}{d\tau} \, | \Psi^v \rangle}{\langle \Psi^v | \Psi^v \rangle} = i \,\mathrm{Im}\, \mathrm{Tr} \left[V^\dagger V \left(U^{-1} \frac{dU}{d\tau} - V^{-1} \frac{dV}{d\tau} \right) \right]. \tag{4.36}$$

We now assume that the Hamiltonian in Eq. (4.31) preserves time-reversal symmetry. Then, we can always choose a gauge in which the Q_{ij}, $U_{i\mu}$ and $V_{i\mu}$ are all real. Under these conditions, the expression in Eq. (4.36) vanishes identically. It is clear that this argument generalizes to the case where we project the wavefunction to boson states which obey the constraint in Eq. (4.2).

We have now shown that no instantaneous Berry phase is accumulated during the vison motion of Fig. 4.4. Under these conditions, the total gauge-invariant Berry phase is simply equal to the phase difference between the wavefunctions in the initial and final states. (Read and Sachdev, 1991) As shown in Fig. 4.4, this phase difference is π.

4.B Effective Ising models for visons on various other lattice geometries

In this Appendix we summarize the results of a Ginzburg-Landau analysis of frustrated transverse field Ising models (TIMs) on various lattice geometries. These models describe the low energy properties of different frustrated Heisenberg antiferromagnets in terms of their vison exciations. Some of these results have been discussed previously in the literature.

4.B.1 Triangular lattice

The vison excitations of a Heisenberg antiferromagnet on the triangular lattice are described by a frustrated TIM on the dual honeycomb lattice, which has been studied previously by Moessner and Sondhi (Moessner and Sondhi, 2001b). A Ginzburg-Landau analysis reveals four critical modes and the corresponding PSG transformation matrices generate a 288 element subgroup of O(4) which is isomorphic to

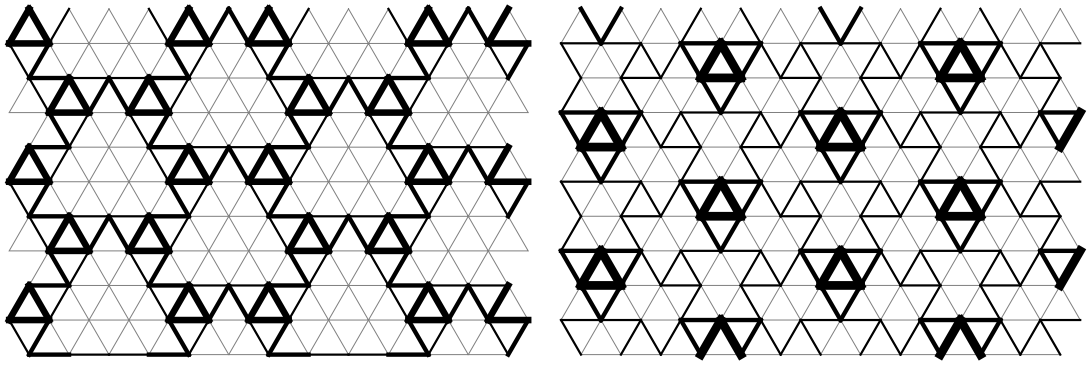

Figure 4.13: Confining phase on the triangular lattice. Plotted is the gauge invariant bond-strength $J_{ij}\phi_i\phi_j$ for nearest neighbor bonds on the frustrated honeycomb lattice, shown on the corresponding triangular lattice bonds. Black lines represent satisfied bonds ($-J_{ij}\phi_i\phi_j < 0$). There are no frustrated bonds in the confining phase. The thickness of the bonds is proportional to the bond-strength. The two different patterns arise due to a crossover when the sign of the O(4)-breaking term in the GL-functional changes.

$(C_3 \times GL(2,\mathbb{Z}_3)) \ltimes C_2$, (GAP) where C_n denotes the cyclic group of order n. PSG matrices for a specific gauge choice can be found in Ref. Moessner and Sondhi (2001b). An O(4)-breaking term appears at sixth order in the GL-functional, the minimization of which gives rise to a single confined phase with a 24-site unit cell (*i.e.* a 12-site unit cell on the triangular lattice) that is symmetric under $2\pi/3$-rotations and reflections. Bond patterns of this phase are shown in Fig. 4.13. Note that there is a transition when the sign of the O(4)-breaking term changes.

4.B.2 Honeycomb lattice

For the frustrated honeycomb lattice antiferromagnet the visons are described by an antiferromagnetic TIM on the dual triangular lattice. There are two critical modes at the Brillouin zone edges $\mathbf{Q} = \pm(4\pi/3, 0)$ and the PSG matrices corresponding to translations T by any basis vector, rotations R_6 and reflections I_y about the y-axis of the two mode amplitudes are given by

$$T = -\big(\mathbb{1}_2 + i\sqrt{3}\,\sigma_z\big)/2\ , \qquad R_6 = I_y = \sigma_x \tag{4.37}$$

where σ_i denote the Pauli matrices. These PSG matrices generate the 6 element dihedral group D_3, *i.e.* the symmetry group of the equilateral triangle. The invariant Ginzburg-Landau functional has been discussed previously by Blankenschtein *et al.* (Blankschtein et al., 1984b), who showed that an O(2) symmetry breaking term appears at sixth order. (Xu and Balents, 2011) Minimizing the GL functional gives rise to only one possible confining phase which breaks the translational symmetry. For a particular sign of the sixth order term, (Xu and Balents, 2011) the confining phase has a three-site unit cell (*i.e.* six sites per unit cell on the honeycomb lattice) and is symmetric both with respect to rotations and reflections; the corresponding dimer pattern on the honeycomb lattice has the maximal number of one perfectly flippable hexagon per six-site unit cell (Moessner and Sondhi, 2001b) and is identical to the VBS state found in Ref. Read and Sachdev (1990). A plaquette-like phase is obtained for the other sign of the sixth-order term. (Xu and Balents, 2011) More complex minima structure for the vison dispersion have also been considered in Ref. Xu and Balents (2011).

4.B.3 Square lattice

The effective vison model for the frustrated square lattice Heisenberg antiferromagnet is a frustrated TIM on the dual square lattice. (Jalabert and Sachdev, 1991; Balents et al., 2005) In an appropriate gauge the two critical modes appear at zero momentum and the corresponding (gauge-dependent) PSG-matrices for translations T_x, rotations R_4 and reflections I_x take the form

$$T_x = \big(\sigma_x + \sigma_z\big)/\sqrt{2}\ , \quad R_4 = \sigma_z\ , \quad I_x = \mathbb{1}_2\ . \tag{4.38}$$

These matrices generate the 16 element dihedral group D_8. An invariant GL-polynomial that breaks the O(2) symmetry appears only at eight order, as discussed by Blankenschtein *et al.* (Blankschtein et al., 1984a). Depending on the sign of this eight order term, two different confining phases are possible. Both phases are reflection symmetric, break the translational symmetries and have a four-site unit cell. One of the two phases is invariant under $\pi/2$-rotations, whereas the other one has a reduced

rotational symmetry and is only invariant with respect to π-rotations. These are the familiar 'plaquette' and 'columnar' VBS states. (Senthil et al., 2004b,a)

More complex vison dispersion structures, with further-neighbor couplings, have been described recently in Ref. Xu and Balents (2011).

Bibliography

Affleck, I. and Marston, J., 1988. *Large-n limit of the Heisenberg-Hubbard model: Implications for high-Tc superconductors.* Physical Review B, 37:3774.

Anderson, P., 1973. *Resonating valence bonds: a new kind of insulator?* Materials Research Bulletin, 8(2):153.

Arovas, D. P. and Auerbach, A., 1988. *Functional integral theories of low-dimensional quantum Heisenberg models.* Phys. Rev. B, 38(1):316.

Auerbach, A. and Arovas, D. P., 1988. *Spin Dynamics in the Square-Lattice Antiferromagnet.* Phys. Rev. Lett., 61(5):617.

Balents, L., Bartosch, L., Burkov, A., et al., 2005. *Putting competing orders in their place near the Mott transition.* Phys. Rev. B, 71(14):144508.

Balents, L., Fisher, M. P. A., and Nayak, C., 1998. *Nodal Liquid Theory of the Pseudo-Gap Phase of High-T_c Superconductors.* International Journal of Modern Physics B, 12:1033.

Blankschtein, D., Ma, M., and Berker, A. N., 1984a. *Fully and partially frustrated simple-cubic Ising models: Landau-Ginzburg-Wilson theory.* Phys. Rev. B, 30(3):1362.

Blankschtein, D., Ma, M., Berker, A. N., et al., 1984b. *Orderings of a stacked frustrated triangular system in three dimensions.* Phys. Rev. B, 29(9):5250.

Brézin, E., Guillou, J. C. L., and Zinn-Justin, J., 1976. In Domb, C. and Green, M. S., eds., *Phase Transitions and Critical Phenomena*, volume 6 (Academic, London).

Calabrese, P., Pelissetto, A., and Vicari, E., 2002. *Critical structure factors of bilinear fields in $O(N)$ vector models.* Phys. Rev. E, 65(4):046115.

Campostrini, M., Hasenbusch, M., Pelissetto, A., et al., 2001. *Critical behavior of the three-dimensional XY universality class.* Phys. Rev. B, 63(21):214503.

Cépas, O., Fong, C. M., Leung, P. W., and Lhuillier, C., 2008. *Quantum phase transition induced by Dzyaloshinskii-Moriya interactions in the kagome antiferromagnet.* Phys. Rev. B, 78(14):140405.

Chubukov, A. V., Sachdev, S., and Ye, J., 1994a. *Theory of two-dimensional quantum Heisenberg antiferromagnets with a nearly critical ground state.* Phys. Rev. B, 49(17):11919.

Chubukov, A. V., Senthil, T., and Sachdev, S., 1994b. *Universal magnetic properties of frustrated quantum antiferromagnets in two dimensions.* Phys. Rev. Lett., 72(13):2089.

Chubukova, A. V., Sachdevb, S., and Senthilb, T., 1994. *Quantum phase transitions in frustrated quantum antiferromagnets.* Nuclear Physics B, 3:601.

Conway, J. and Smith, D., 2003. *On quaternions and octonions: their geometry, arithmetic, and symmetry* (AK Peters / CRC Press).

Du Val, P., 1964. *Homographies, quaternions, and rotations* (Clarendon Press Oxford).

Elhajal, M., Canals, B., and Lacroix, C., 2002. *Symmetry breaking due to Dzyaloshinsky-Moriya interactions in the kagomé lattice.* Phys. Rev. B, 66(1):014422.

Evenbly, G. and Vidal, G., 2010. *Frustrated Antiferromagnets with Entanglement Renormalization: Ground State of the Spin-*12 *Heisenberg Model on a Kagome Lattice.* Phys. Rev. Lett., 104(18):187203.

GAP, 2008. *GAP – Groups, Algorithms, and Programming, Version 4.4.12.* The GAP Group.

Gregor, K. and Motrunich, O. I., 2008. *Nonmagnetic impurities in the spin-* 1?2 *kagome antiferromagnet.* Phys. Rev. B, 77(18):184423.

Grover, T. and Senthil, T., 2009. *Quantum phase transition from an antiferromagnet to a spin liquid in a metal.* ArXiv:0910.1277v1.

Helton, J. S., Matan, K., Shores, M. P., et al., 2007. *Spin Dynamics of the Spin-*1/2 *Kagome Lattice Antiferromagnet* $ZnCu_3(OH)_6Cl_2$. Phys. Rev. Lett., 98(10):107204.

Helton, J. S., Matan, K., Shores, M. P., et al., 2010. *Dynamic Scaling in the Susceptibility of the Spin-*12 *Kagome Lattice Antiferromagnet Herbertsmithite.* Phys. Rev. Lett., 104(14):147201.

Hermele, M., Ran, Y., Lee, P. A., and Wen, X.-G., 2008. *Properties of an algebraic spin liquid on the kagome lattice*. Phys. Rev. B, 77(22):224413.

Hinkov, V., Bourges, P., Pailhés, S., et al., 2007. *Spin dynamics in the pseudogap state of a high-temperature superconductor*. Nature Physics, 3:780.

Hinkov, V., Haug, D., Fauqué, B., et al., 2008. *Electronic Liquid Crystal State in the High-Temperature Superconductor* $YBa_2Cu_3O_{6.45}$. Science, 319(5863):597.

Hinkov, V., Pailhés, S., Bourges, P., et al., 2004. *Two-dimensional geometry of spin excitations in the high-transition-temperature superconductor* $YBa_2Cu_3O_{6+x}$. Nature, 430:650.

Imai, T., Nytko, E. A., Bartlett, B. M., et al., 2008. Cu^{63}, Cl^{35}, *and* H^1 *NMR in the* $S = 12$ *Kagome Lattice* $ZnCu_3(OH)_6Cl_2$. Phys. Rev. Lett., 100(7):077203.

Iqbal, Y., Becca, F., and Poilblanc, D., 2011a. *Projected wave function study of Z2 spin liquids on the kagome lattice for spin-1/2 quantum Heisenberg antiferromagnet*. Arxiv preprint arXiv:1105.0341.

Iqbal, Y., Becca, F., and Poilblanc, D., 2011b. *Valence-bond crystal in the extended kagome spin-1/2 quantum Heisenberg antiferromagnet: A variational Monte Carlo approach*. Physical Review B, 83(10):100404.

Isakov, S. V., Senthil, T., and Kim, Y. B., 2005. *Ordering in* Cs_2CuCl_4 *: Possibility of a proximate spin liquid*. Phys. Rev. B, 72(17):174417.

Jalabert, R. A. and Sachdev, S., 1991. *Spontaneous alignment of frustrated bonds in an anisotropic, three-dimensional Ising model*. Phys. Rev. B, 44(2):686.

Jiang, H. C., Weng, Z. Y., and Sheng, D. N., 2008. *Density Matrix Renormalization Group Numerical Study of the Kagome Antiferromagnet*. Phys. Rev. Lett., 101(11):117203.

Kim, E.-A., Lawler, M. J., Oreto, P., et al., 2008. *Theory of the nodal nematic quantum phase transition in superconductors*. Phys. Rev. B, 77(18):184514.

Kivelson, S. A., Fradkin, E., and Emery, V. J., 1998. *Electronic liquid-crystal phases of a doped Mott insulator*. Nature, 393:550.

Kogut, J., 1979. *An introduction to lattice gauge theory and spin systems*. Reviews of Modern Physics, 51(4):659.

Laeuchli, A. and Lhuillier, C., 2009. *Dynamical Correlations of the Kagome* $S = 1/2$ *Heisenberg Quantum Antiferromagnet*. ArXiv:0901.1065v1.

Lawler, M. J., Fritz, L., Kim, Y. B., and Sachdev, S., 2008. *Theory of Néel and Valence-Bond Solid Phases on the Kagome Lattice of Zn Paratacamite*. Phys. Rev. Lett., 100(18):187201.

Lee, S.-H., Kikuchi, H., Qiu, Y., et al., 2007. *Quantum-spin-liquid states in the two-dimensional kagome antiferromagnets* $Zn_xCu_{4-x}(OD)_6Cl_2$. Nature Materials, 6:853.

Lu, Y.-M., Ran, Y., and Lee, P. A., 2011. *Z_2 spin liquids in the $S = 12$ Heisenberg model on the kagome lattice: A projective symmetry-group study of Schwinger fermion mean-field states*. Phys. Rev. B, 83(22):224413.

Marston, J. and Zeng, C., 1991. *Spin-Peierls and spin-liquid phases of Kagomé quantum antiferromagnets*. Journal of Applied Physics, 69(8):5962.

Matan, K., Ono, T., Fukumoto, Y., et al., 2010. *Pinwheel valence-bond solid and triplet excitations in the two-dimensional deformed kagome lattice*. Nature Physics, 6:865.

Mendels, P., Bert, F., de Vries, M. A., et al., 2007. *Quantum Magnetism in the Paratacamite Family: Towards an Ideal Kagomé Lattice*. Phys. Rev. Lett., 98(7):077204.

Messio, L., Cépas, O., and Lhuillier, C., 2010. *Schwinger-boson approach to the kagome antiferromagnet with Dzyaloshinskii-Moriya interactions: Phase diagram and dynamical structure factors*. Phys. Rev. B, 81(6):064428.

Moessner, R. and Sondhi, S. L., 2001a. *Ising models of quantum frustration*. Phys. Rev. B, 63(22):224401.

Moessner, R. and Sondhi, S. L., 2001b. *Resonating Valence Bond Phase in the Triangular Lattice Quantum Dimer Model*. Phys. Rev. Lett., 86(9):1881.

Moessner, R., Sondhi, S. L., and Fradkin, E., 2001. *Short-ranged resonating valence bond physics, quantum dimer models, and Ising gauge theories*. Phys. Rev. B, 65(2):024504.

Nikolic, P. and Senthil, T., 2003. *Physics of low-energy singlet states of the Kagome lattice quantum Heisenberg antiferromagnet*. Phys. Rev. B, 68(21):214415.

Ofer, O. and Keren, A., 2009. *Symmetry of the spin Hamiltonian for herbertsmithite: A spin- 12 kagome lattice*. Phys. Rev. B, 79(13):134424.

Ofer, O., Keren, A., Nytko, E. A., et al., 2006. *Ground state and excitation properties of the quantum kagom system* $ZnCu_3(OH)_6Cl_2$ *investigated by local probes*. ArXiv:cond-mat/0610540v2.

Olariu, A., Mendels, P., Bert, F., et al., 2008. *O17 NMR Study of the Intrinsic Magnetic Susceptibility and Spin Dynamics of the Quantum Kagome Antiferromagnet $ZnCu3(OH)6Cl2$.* Phys. Rev. Lett., 100(8):087202.

Poilblanc, D., Mambrini, M., and Schwandt, D., 2010. *Effective quantum dimer model for the kagome Heisenberg antiferromagnet: Nearby quantum critical point and hidden degeneracy.* Phys. Rev. B, 81(18):180402.

Read, N. and Chakraborty, B., 1989. *Statistics of the excitations of the resonating-valence-bond state.* Phys. Rev. B, 40(10):7133.

Read, N. and Sachdev, S., 1989a. *Some features of the phase diagram of the square lattice SU(N) antiferromagnet.* Nuclear Physics B, 316:609.

Read, N. and Sachdev, S., 1989b. *Valence-bond and spin-Peierls ground states of low-dimensional quantum antiferromagnets.* Phys. Rev. Lett., 62(14):1694.

Read, N. and Sachdev, S., 1990. *Spin-Peierls, valence-bond solid, and Néel ground states of low-dimensional quantum antiferromagnets.* Phys. Rev. B, 42(7):4568.

Read, N. and Sachdev, S., 1991. *Large-N expansion for frustrated quantum antiferromagnets.* Physical review letters, 66(13):1773.

Rigol, M. and Singh, R. R. P., 2007. *Magnetic Susceptibility of the Kagome Antiferromagnet $ZnCu_3(OH)_6Cl_2$.* Phys. Rev. Lett., 98(20):207204.

Rokhsar, D. and Kivelson, S., 1988. *Superconductivity and the quantum hard-core dimer gas.* Physical review letters, 61(20):2376.

Rozenberg, M. J. and Chitra, R., 2008. *Disorder effects in the quantum kagome antiferromagnet $ZnCu3(OH)6Cl2$.* Phys. Rev. B, 78(13):132406.

Sachdev, S., 1992. *Kagomé-and triangular-lattice Heisenberg antiferromagnets: Ordering from quantum fluctuations and quantum-disordered ground states with unconfined bosonic spinons.* Physical Review B, 45(21):12377.

Sachdev, S., 1999. *Quantum Phase Transitions* (Cambridge University Press).

Sachdev, S., 2010. *Quantum phase transitions of antiferromagnets and the cuprate superconductors [Lectures at the Les Houches School on* Modern theories of correlated electron systems*].* ArXiv:1002.3823v3.

Sachdev, S. and Read, N., 1991. *Large N Expansion for Frustrated and Doped Quantum Antiferromagnets.* International Journal of Modern Physics B, 5:219. Cond-mat/0402109.

Sachdev, S. and Vojta, M., 2000. *Translational symmetry breaking in two-dimensional antiferromagnets and superconductors.* J Phys Soc Jpn, 69(Supplement B):1.

Schwandt, D., Mambrini, M., and Poilblanc, D., 2010. *Generalized hard-core dimer model approach to low-energy Heisenberg frustrated antiferromagnets: General properties and application to the kagome antiferromagnet.* Phys. Rev. B, 81(21):214413.

Sengupta, K., Isakov, S. V., and Kim, Y. B., 2006. *Superfluid-insulator transitions of bosons on the kagome lattice at noninteger fillings.* Phys. Rev. B, 73(24):245103.

Senthil, T., Balents, L., Sachdev, S., et al., 2004a. *Quantum criticality beyond the Landau-Ginzburg-Wilson paradigm.* Physical Review B, 70(14):144407.

Senthil, T. and Fisher, M. P. A., 2000. *$Z2$ gauge theory of electron fractionalization in strongly correlated systems.* Phys. Rev. B, 62(12):7850.

Senthil, T., Vishwanath, A., Balents, L., et al., 2004b. *Deconfined quantum critical points.* Science, 303(5663):1490.

Singh, R. R. P. and Huse, D. A., 2007. *Ground state of the spin-1/2 kagome-lattice Heisenberg antiferromagnet.* Phys. Rev. B, 76(18):180407.

Strassler, M. J., 2003. *An Unorthodox Introduction to Supersymmetric Gauge Theory.* ArXiv:hep-th/0309149v1.

Tay, T. and Motrunich, O., 2011. *Variational study of J1-J2 Heisenberg model on Kagome lattice using projected Schwinger boson wave functions.* Arxiv preprint arXiv:1103.4429.

Tchernyshyov, O., Moessner, R., and Sondhi, S., 2006. *Flux expulsion and greedy bosons: Frustrated magnets at large N.* EPL (Europhysics Letters), 73:278.

Toledano, J.-C., Michel, L., Toledano, P., and Brezin, E., 1985. *Renormalization-group study of the fixed points and of their stability for phase transitions with four-component order parameters.* Phys. Rev. B, 31(11):7171.

Tovar, M., Raman, K. S., and Shtengel, K., 2009. *Dzyaloshinskii-Moriya interactions in valence-bond systems.* Phys. Rev. B, 79(2):024405.

Vicari, E., 2007. *Critical phenomena and renormalization-group flow of multi-parameter Φ^4 field theories.* Arxiv preprint arXiv:0709.1014.

Vojta, M., Zhang, Y., and Sachdev, S., 2000a. *Competing orders and quantum criticality in doped antiferromagnets.* Phys. Rev. B, 62(10):6721.

Vojta, M., Zhang, Y., and Sachdev, S., 2000b. *Quantum Phase Transitions in d-Wave Superconductors*. Phys. Rev. Lett., 85(23):4940.

Vojta, M., Zhang, Y., and Sachdev, S., 2000c. *Renormalization group analysis of quantum critical points in d-wave superconductors*. International Journal of Modern Physics B, 14:3719.

Vojta, M., Zhang, Y., and Sachdev, S., 2008. *Erratum: Quantum Phase Transitions in d-Wave Superconductors [Phys. Rev. Lett. 85, 4940 (2000)]*. Phys. Rev. Lett., 100(8):089904.

Wang, F. and Vishwanath, A., 2006. *Spin-liquid states on the triangular and Kagomé lattices: A projective-symmetry-group analysis of Schwinger boson states*. Phys. Rev. B, 74(17):174423.

Wang, F. and Vishwanath, A., 2009. *Z2 spin-orbital liquid state in the square lattice Kugel-Khomskii model*. Phys. Rev. B, 80(6):064413.

Wen, X., 1991. *Mean-field theory of spin-liquid states with finite energy gap and topological orders*. Physical Review B, 44(6):2664.

Wen, X.-G., 2002. *Quantum orders and symmetric spin liquids*. Phys. Rev. B, 65(16):165113.

Xu, C. and Balents, L., 2011. *Quantum Phase Transitions around the Staggered Valence Bond Solid*. Arxiv preprint arXiv:1103.1638.

Xu, C. and Sachdev, S., 2009. *Global phase diagrams of frustrated quantum antiferromagnets in two dimensions: Doubled Chern-Simons theory*. Phys. Rev. B, 79(6):064405.

Yan, S., Huse, D., and White, S., 2011. *Spin-Liquid Ground State of the S= 1/2 Kagome Heisenberg Antiferromagnet*. Science, 332(6034):1173.

Yang, B.-J. and Kim, Y. B., 2009. *Valence bond solid phases on deformed kagome lattices: Application to* $Rb_2Cu_3SnF_{12}$. Phys. Rev. B, 79(22):224417.

Zorko, A., Nellutla, S., van Tol, J., et al., 2008. *Dzyaloshinsky-Moriya Anisotropy in the Spin-1/2 Kagome Compound* $ZnCu_3(OH)_6Cl_2$. Phys. Rev. Lett., 101(2):026405.